1976

COMPUTATIONAL STUDIES OF VOLUME DOMINATED PLASMA PROCESSES IN THE CARBON-MONOXIDE LASER AND CALCULATION OF THE RELATIVISTIC FORM FACTOR FOR ELECTRON IMPACT IONIZATION OF ARGON.

WILLIAM LOWELL. MORGAN
University of Windsor

Follow this and additional works at: https://scholar.uwindsor.ca/etd

INFORMATION TO USERS

THIS DISSERTATION HAS BEEN
MICROFILMED EXACTLY AS RECEIVED

This copy was produced from a micro-
fiche copy of the original document.
The quality of the copy is heavily
dependent upon the quality of the
original thesis submitted for
microfilming. Every effort has
been made to ensure the highest
quality of reproduction possible.

PLEASE NOTE: Some pages may have
indistinct print. Filmed as
received.

Canadian Theses Division
Cataloguing Branch
National Library of Canada
Ottawa, Canada   K1A ON4

AVIS AUX USAGERS

LA THESE A ETE MICROFILMEE
TELLE QUE NOUS L'AVONS RECUE

Cette copie a été faite à partir
d'une microfiche du document
original. La qualité de la copie
dépend grandement de la qualité
de la thèse soumise pour le
microfilmage. Nous avons tout
fait pour assurer une qualité
supérieure de reproduction.

NOTA BENE: La qualité d'impression
de certaines pages peut laisser à
désirer. Microfilmée telle que
nous l'avons reçue.

Division des thèses canadiennes
Direction du catalogage
Bibliothèque nationale du Canada
Ottawa, Canada   K1A ON4

COMPUTATIONAL STUDIES OF VOLUME DOMINATED PLASMA

PROCESSES IN THE CARBON MONOXIDE LASER

AND

CALCULATION OF THE RELATIVISTIC FORM FACTOR.

FOR ELECTRON IMPACT IONIZATION OF ARGON

by

William Lowell Morgan

A Dissertation
submitted to the Faculty of Graduate Studies
through the Department of
Physics in Partial Fulfillment
of the requirements for the Degree
of Doctor of Philosophy at
The University of Windsor

Windsor, Ontario, Canada

1976

ABSTRACT

COMPUTATIONAL SUTDIES OF VOLUME DOMINATED PLASMA PRO-
CESSES IN THE CARBON MONOXIDE LASER/CALCULATION OF THE
RELATIVISTIC FORM FACTOR FOR ELECTRON IMPACT IONIZATION
OF ARGON

by

William Lowell Morgan

PART I

   The theory and methodology for the solution of the elec-
tron energy distribution function in a molecular laser dis-
charge plasma is detailed. The steady state Boltzmann equa-
tion is solved numerically for mixtures of N_2 and CO includ-
ing all the important inelastic and elastic collision proces-
ses. Predictions on the drift velocity for both N_2 and CO
show good agreement with experiment. Some differences with
past predictions are noted in the drift velocity of N_2/CO
mixtures depending on the excitation cross sections used. In
contrast to past calculations, we find that the presence of
N_2 does not enhance the electron-CO excitation rate at room
temperature. Results of chemical kinetics calculations on
the CO-He laser with O_2 as an additive are also presented.
In these calculations, the electron energy distribution func-
tion is used to compute realistic rate coefficients for
electron impact processes that include the effects of col-
lisions of the second kind. The calculations predict, in
agreement with experiment, that, due to charge transfer re-
actions, O_2^+ replaces $C_2O_2^+$ as the dominant ion in the

plasma when O_2 is added to a CO-He discharge. In a constant current discharge this results in a lowering of the electric field in the positive column which, in turn, is responsible for more efficient coupling between the electrons and the CO vibrational levels. In addition, we find that for higher partial pressures of O_2 in the discharge, there is substantial dissociation into oxygen atoms which has a deleterious effect upon laser performance due to V-T relaxation of the CO laser levels.

PART II

Calculations in the Bethe-Born approximation of the Bethe surface and total cross section for ionization of the Argon M_{III} shell by relativistic electrons are presented. They were performed using Dirac-Hartree-Fock-Slater bound state wavefunctions and numerical continuum wavefunctions, computed from the DHFS potential. In addition, photoionization cross sections were computed in the relativistic dipole approximation. The photoionization results are in agreement with previous calculations in the single particle central field approximation. The computed electron impact ionization cross sections are in good agreement with experiment for electron energies up to 100 keV. For higher impact energies the computed cross sections deviate greatly from the measured ones. This is shown to be due to inaccuracies in the differential cross section in the small momentum transfer (photoionization) limit which can be traced to

inadequacies in the single particle model. It is shown that these problems can be overcome by use of an approximate formulation, due to Fano, incorporating empirical photoionization data and the computed non-relativistic form factor.

To Joyce, without whose love and caring this work would not have been accomplished.

ACKNOWLEDGEMENTS

TABLE OF CONTENTS

PART I: COMPUTATIONAL STUDIES OF VOLUME DOMINATED PLASMA
          PROCESSES IN THE CARBON MONOXIDE LASER

LIST OF TABLES

LIST OF FIGURES

List of Figures, continued.

PART I

COMPUTATIONAL STUDIES OF VOLUME DOMINATED PLASMA

PROCESSES IN THE CARBON MONOXIDE LASER

I. Introduction

The prediction of the operating characteristics of
an electric discharge molecular gas laser requires a de-
tailed knowledge of neutral chemistry and energy transfer
processes as well as the excitation, attachment, and
recombination processes occurring in the discharge plasma.
Although considerable effort in the past has concentrated
on developing sophisticated models for the energy transfer
processes in molecular lasers[1,2,3], only recently has a
similar extensive effort been aimed at an understanding
of the important plasma processes[4,5,6]. This understanding
encompasses a predictive capability to model the transient
electron density in CW molecular lasers but more im-
portantly to characterize the electron energy distribution
function in molecular systems where significant electron
energy loss processes are present. These loss processes
include excitation of vibrational, rotational and electro-
nic levels, ionization, recombination, and dissociation and
attachment processes.

The rate coefficient characterizing these various
processes is calculated from

$$K_j = \left[\frac{2e}{m}\right]^{1/2} \int_0^\infty Q_j(\varepsilon) f(\varepsilon) \varepsilon \, d\varepsilon \qquad \frac{cm^3}{sec} \qquad (1)$$

where ε = relative collision energy (eV)

m = electron mass (g)

Q_j = electron impact cross section for j^{th} state (cm^2)

$f(\varepsilon)$ = distribution function (probability function) for

relative collision energies ε. $\qquad$ e = electronic

charge, 1.602^{-19} coul.; this is also the conversion be-

tween electron volts (eV) and joules of energy since 1 eV=

1.602^{-19} joule. The energy dependent excitation cross section

comes from a wide variety of experimental and theoretical

sources[7].

Recent calculations on the characteristics of pulsed

CO/N_2 molecular laser systems have assumed that the elec-

tron energy distribution function was Maxwell-Boltzmann[1,2].

In terms of the distribution of electron energy, this as-

sumption means

$$f(\varepsilon) = \frac{2}{\pi^{1/2}} \left[\frac{e}{kT}\right]^{3/2} \exp[-\varepsilon/(kT/e)] \qquad (2)$$

where ε = electron energy (eV)

and T = electron temperature ($^\circ$K); defined in terms of

the mean electron energy, $\bar{\varepsilon}$, where $\bar{\varepsilon} = (3/2)kT$

For preliminary calculations on molecular laser pheno-

menology where the total electron density is unknown,

this Boltzmann assumption appears justified[1]; however, as

more detailed and precise information on the optimum

operating characteristics of molecular laser systems is required, particularly regarding the role of additive species, considerable improvement in the above plasma description is needed. Nighan has shown, for example, that the actual electron distribution is far from Boltzmann[4,5]; showing regions of underpopulation in the electron energy distribution corresponding to strong coupling to the molecular energy levels. These non-Boltzmann energy distributions are a function of E/N, the electric field divided by the total number density, the partial pressure of the gas species present and the state of excitation of the molecular gases (superelastic processes).

In order to incorporate realistic electron energy distribution functions into the molecular laser modeling codes, and to investigate the effects of additives on laser efficiency and power output, a program was initiated to develop a reliable and fast method for the solution to the Boltzmann equation including the coupling to the many available energy states in the gases present in the laser discharge.

A description of the calculation of the electron energy distribution function is given in sections II and III. In the later sections are discussed the applications of this calculation to the study of excitation processes in carbon monoxide lasers with particular emphasis on

the effects that additive gases have on these processes.

It is clear from several past studies on discharge sustained CO molecular lasers[1,2,3,34] that the primary energy input to the CO vibrational levels is direct electron impact excitation. This excitation occurs via the unstable negative ion, CO^-[1,23], and thus the excitation rates are sensitive to both the electron density (resulting from ionization and recombination processes in the plasma) and the electron energy distribution. This latter sensitivity necessitates that reliable modelling of CO laser performance accurately account for superelastic and inelastic processes which lead to non-Boltzmann electron energy distributions and subsequently alter calculated excitation rate coefficients. Once the vibrational energy is input by the electrons, rapid vibration-vibration energy exchange processes rearrange the vibrational energy until sufficient gain to lase is obtained on individual vibration-rotation-lines of the fundamental sequence in CO. The latter processes are well documented elsewhere[1,2,3,31-34]. This study focuses on the plasma chemistry and plasma electron processes critical to laser operation and, in particular, the role of trace additive species.

II. Application of the Boltzman Equation to the Electric Discharge

In order to find the distribution in electron energy (or velocity) in a laser plasma we need to start with the kinetic equation describing the dependence of the distribution function upon the electric field strength, particle density, and the various elastic and inelastic collision processes. This kinetic equation, the Boltzmann equation, can be written[8]:

$$\left[\frac{\partial}{\partial t} + \vec{v} \cdot \vec{\nabla}_r + \frac{\vec{F}}{m} \cdot \vec{\nabla}_v \right] f(\vec{r}, \vec{v}, t) = \left(\frac{\partial f}{\partial t}\right)_{collisions} \quad (3)$$

where the LHS is the usual hydrodynamic derivative. The form of the RHS depends upon the details of the collision processes being considered. The distribution function, f, is defined such that $f(\vec{r}, \vec{v}, t) d\vec{r} d\vec{v} dt$ represents the probability of a particle being in the differential volume element $d\vec{r}$ around $\vec{r}$ with velocity in the range $(\vec{v}, \vec{v} + d\vec{v})$ in the time interval $(t, t+dt)$.

We assume that the laser plasma is placed in a uniform dc-electric field (i.e., $\vec{F} = e\vec{E}$). If the system is in a steady state, the partial time derivative can be eliminated from equation (3). The steady state assumption implies that the time scale for the relaxation of the electron energy distribution[9] is much shorter than the time scale characterizing the change in the populations of the various molecular states. This electron energy relaxation time is

5

determined by the electron-molecule collision frequency which is given by:

$$\nu = NQv$$

where N = molecular density (cm^{-3})

Q = total elastic collision cross section (cm^2)

and   v = electron speed (cm/sec).

The relaxation time, τ, is defined as $1/\nu$. The elastic collision cross sections for the major species CO and N_2 lie in the range between 10^{-15} cm^2 and 10^{-14} cm^2[7], while the molecular number densities in appropriate laser systems are between about 10^{17} cm^{-3} and 10^{20} cm^{-3}. /Average electron energies are in the range of .5 eV to 2 eV with corresponding speeds between 4×10^8 cm/sec and 8×10^8 cm/sec. These values of N, Q, and v give the following approximate limits on the electron distribution relaxation time:

$$10^{-15} \text{ sec} \lesssim \tau \lesssim 3 \times 10^{-11} \text{ sec.}$$

Since the inelastic cross sections are smaller than the elastic cross sections by from one to four orders of magnitude (depending on the particular level) the characteristic time for electron impact excitation of these states will be correspondingly longer. Hence, on this longer time scale the electron distribution will always be in a quasi-steady state. Notice that in discharges possessing a large concentration of a neutral gas, such as He, the

difference between characteristic times will be further enhanced due to the increased elastic collision frequency.

If we assume further that the electron distribution is uniform in space, the spatial gradient term may be eliminated from equation (3). This is the case if the collisional mean free path (MFP) in the gas is much smaller than the characteristic dimension of the discharge tube. Since the mean free path is equal to 1/NQ, the values of N and Q used above give:

$$10^{-5} \text{ cm} \lesssim \text{MFP} \lesssim 10^{-1} \text{ cm}$$

Since the discharge tube is generally much larger than 1 mm in diameter, this should also be a good assumption.

With these assumptions the Boltzmann equation is reduced to:

$$\frac{e\vec{E}}{m} \cdot \vec{\nabla}_v f(\vec{v}) = \left(\frac{\partial f}{\partial t}\right) \text{coll.} \tag{4}$$

The usual treatment[10] of the LHS involves expanding the distribution function in spherical harmonics. The first two terms would be:

$$f(\vec{v}) \simeq f_0(v) + \frac{\vec{v}}{v} \cdot \vec{f}_1(v) \tag{5}$$

The rationale behind this expansion procedure involves the assumption that the electric field, $\vec{E}$, is weak enough that the directed speed of the electrons due to the field (drift velocity) is much smaller than their random ("thermal")

speed. A spherical harmonic expansion gives us what is needed, a function having a directional part that amounts to just a perturbation on a spherically symmetric part. For a typical glow discharge, drift speeds are on the order of 10^6-10^7 cm/sec and the random speeds might be about ten to twenty times greater. For this case the first two terms in the expansion are expected to be adequate.

If the expansion (5) is substituted into the equation (4) and the resulting equation is separated into its scalar and vector parts, the following two equations result:

$$\frac{e\vec{E}}{3mv^2} \cdot \frac{d}{dv}\left[v^2\vec{f}_1(v)\right] = \left(\frac{\partial f_o}{\partial t}\right)_{coll.} \tag{6a}$$

$$\frac{-e\vec{E}}{m} \quad \frac{df_o(v)}{dv} = \left(\frac{\partial \vec{f}_1}{\partial t}\right)_{coll.} \tag{6b}$$

Under the above assumptions the RHS of (6b) is simple,

$$\left[\frac{\partial \vec{f}_1}{\partial t}\right]_{coll.} = \sum_s \nu_{ms}\vec{f}_1 \tag{7}$$

where ν_{ms} is the frequency for elastic collisions between electrons and molecular species, and the sum is over the molecular species labelled by s.

Substitution of (7) into (6a) gives the equation for the spherically symmetric (random motion) part of the distribution function, f_o:

$$-\frac{1}{3}\left(\frac{eE}{m}\right)^2 \frac{1}{v^2} \frac{d}{dv}\left[\frac{v^2}{\sum_s \nu_{ms}} \frac{df_o}{dv}\right] = \left(\frac{\partial f_o}{\partial t}\right) \text{coll.} \quad (8)$$

In (8),

$$\sum_s \nu_{ms} = N\sum_s \delta_s Q_{ms} v$$

where δ_s = mole fraction of species s.

Q_{ms} = elastic momentum transfer collision cross section (cm^2) for species s

and N = total number density of molecules (cm^{-3}).

Inserting $E = |\vec{E}|$, and changing the variable to energy, $u = mv^2/2$, gives,

$$-\frac{1}{3} \frac{(eE)^2}{N} \frac{d}{du}\left[\frac{u}{\sum_s \delta_s Q_{ms}} \frac{df_o}{du}\right] = \left(\frac{\partial f_o}{\partial t}\right)_{\text{coll.}} \cdot \sqrt{2mu} \quad (9)$$

The form of $\left(\frac{\partial f_o}{\partial t}\right)_{\text{coll.}}$ depends upon the specific interactions that we want to consider. In the most general case it would involve integrals of n-particle correlation functions. The two assumptions usually made to simplify the collision integral are:

i) binary collisions

ii) molecular chaos.

The first of these assumptions is valid if the gas density is sufficiently small. An additional criterion is that the interaction forces be short range. If the interaction is long range, Coulomb forces for example, each particle then interacts with many others simultaneously. A different approach, the Fokker-Planck equation[8], is needed to treat

this problem.

The second assumption, molecular chaos, simply means that the velocities of two colliding particles are uncorrelated before their collision. This is valid if the gas density is low enough that the mean free path between collisions is much greater than the range of the interaction force.

With these assumptions the collision integral in the Boltzmann equation for $f(v_1)$ becomes[12],

$$\left[\frac{\partial f(v_1)}{\partial t}\right]_{coll.} = \int d\Omega \int d^3 v_2 \sigma(\Omega) |\vec{v}_1 - \vec{v}_2| \qquad (10)$$

$$\cdot \left[f(\vec{v}'_2) f(\vec{v}'_1) - f(\vec{v}_2) f(\vec{v}_1) \right]$$

where $\sigma(\Omega)$ = the differential collision cross section in the center-of-mass reference frame,

$\vec{v}_1 - \vec{v}_2$ = the relative speed of the colliding particles, and

$\vec{v}_1$, $\vec{v}_2$, $\vec{v}'_1$, $\vec{v}'_2$ are the velocities of the colliding particles and the product particles, respectively.

For the molecular laser plasma of interest here, the detailed form of $\left[\frac{\partial f_o}{\partial t}\right]_{coll.}$ is[13]:

$$\sqrt{2mu} \left[\frac{\partial f_o}{\partial t}\right]_{coll.} = \frac{-d}{du}\left[(N \sum_s \frac{2m}{M_s} \delta_s Q_{ms}) u^2 (f_o + kT \frac{df_o}{du}) \right]$$

$$-N \sum_{s,j} \delta_s [(u+u_{sj})Q_{sj}(u+u_{sj})f_0(u+u_{sj}) - uQ_{sj}(u)f_0(u)]$$

$$-N \sum_{s,j} \delta_s [(u-u_{sj})Q_{s,-j}(u-u_{sj})f_0(u-u_{sj}) - uQ_{s,-j}f_0(u)]$$

$$\tag{11}$$

where M_s = mass of molecular species s

T = gas temperature (^{O}K)

u_{sj} = energy of the jth level of molecular species s

and $Q_{s,\pm j}$ = collision cross section for excitation (+j),
or de-excitation (-j) of the jth level of species s.
The distribution function $f_0(u)$ is normalized such that

$$_0\int^\infty f_0(u) \ u^{1/2} \ du = 1. \tag{12}$$

On the RHS of equation (11) the first term represents
the energy lost by electrons in elastic collisions with
molecules, the second term represents the energy gained by
electrons in collisions with fast molecules, the third
term accounts for the energy lost by electrons in
inelastic (molecular excitation) collisions, and the fourth
term represents the energy gained by electrons in super-
elastic (molecular de-excitation) collisions.

The superelastic cross sections are related to the
inelastic cross sections by a detailed balance relation
giving:[14]

$$uQ_{s,-j}(u) = \frac{N_{sj}}{N_{so}} (u+u_{sj}) Q_{s,j} (u+u_{sj}) \qquad (13)$$

where N_{so} and N_{sj} are the populations of the ground and j^{th} states, respectively, of species s. Applying detailed balance and combining (11) and (9) gives:

$$\frac{1}{3}\left(\frac{eE}{N}\right)^2 \frac{d}{du}\left[\frac{u}{\Sigma_s \delta_s Q_{ms}} \frac{df}{du}\right] + \frac{d}{du}\left[\left(\sum_s \frac{2m}{M_s}\delta_s Q_{ms}\right)\right.$$

$$u^2\left(f(u) + kT\frac{df}{du}\right)\bigg]$$

$$+ \sum_{s,j}\delta_s\left[(u+u_{sj})Q_{sj}(u+u_{sj})f(u+u_{sj})\right.$$

$$\left. -uQ_{sj}(u)f(u)\right]$$

$$-\sum_{s,j}\delta_s\frac{N_{sj}}{N_{so}}\bigg[(u+u_{sj})Q_{sj}(u+u_{sj})f(u)$$

$$\left. -uQ_{sj}(u)f(u-u_{sj})\right] = 0 \qquad (14)$$

Note that integrating this once over energy gives the equivalent integro-differential equation:

$$\frac{1}{3}\left(\frac{eE}{N}\right)^2 \frac{u}{\Sigma_s \delta_s Q_{ms}}\cdot\frac{df}{du} + \left(\sum_s \frac{2m}{M_s}\delta_s Q_{ms}\right)u^2$$

$$\left(f(u) + kT\frac{df}{du}\right)$$

$$+ \sum_{s,j}\delta_s \int_u^{u+u_{sj}} du'u'Q_{sj}(u')$$

$$\left[f(u') - \frac{N_{sj}}{N_{so}}f(u'-u_{sj})\right] = 0 \qquad (15)$$

In these equations we have dropped the subscript from f_o. From here, unless noted otherwise, $f_o(u)$ will be called

the distribution function and will be denoted simply by
f(u). Boundary conditions on these equations are that.
f(u) be finite at u = 0 and f(u) →0 as u → ∞. The
population factor, $\frac{N_{sj}}{N_{so}}$, is related to the vibration temp-
erature, T_{sj}, defined with respect to the ground state by
the relation:

$$\frac{N_{sj}}{N_{so}} = e^{-u_{sj}/kT_{sj}}$$

Hence, when $T_{sj} = T_s$ for all levels, we have the Boltzmann
population distribution that would exist if the molecules
of species s were in thermal equilibrium at temperature T_s.
This vibrational temperature is a commonly used method of
describing the relative populations of vibrational levels.

Frost and Phelps[15]; Carleton and Megill[16]; Gibson[17];
Rockwood, Brau, Proctor, and Canavan[3]; and Lowke, Phelps
and Irwin[19] solved equation (14) in their respective works.
Nighan[5] used equation (15) in his calculations. Both ap-
proaches have been used in the CO_2 calculations of Elliot,
Judd, Lockett, and Rockwood[18].

If they are important, terms for rotational excita-
tion[15,16,17], and long range interactions[20] can be included
in $\left(\frac{\delta f_o}{\delta t}\right)_{coll.}$. In order to neglect electron-electron
(Coulomb) collisions, we assume that the plasma is weakly
ionized. Rotational excitation can be neglected if the
electron mean energy is much greater than the energy as-

sociated with rotational excitation.

As they stand, these equations are independent of electron density. As long as the fractional ionization is small, allowing us to neglect electron-electron interactions this will be valid. For highly ionized gases the electrons will interact with each other, tending to push the distribution function, now electron density dependent, toward the Maxwell-Boltzmann distribution. The effects of electron-electron collisions on the distribution function have been investigated by Rockwood[19]. He found that the effects were negligible for fractional ionization less than about 4×10^{-4} in calculations on Hg discharges. Lasers typically have fractional ionizations of less than 10^{-5}. Hence electron-electron collisions can probably be safely neglected.

Equations (14) and (15) relate the energy gained by electrons from the electric field and the energy gained by de-excitation of higher molecular states to the energy lost by elastic collisions with molecules and by inelastic collisions which excite molecules. This can be more easily seen if equation (14) is integrated over the energy range $(0, \infty)$. The result is:

$$\frac{1}{3} \left(\frac{eE}{N} \right)^2 \int_0^\infty \frac{u}{\sum_s \delta_s Q_{ms}} \frac{df}{du} \, du$$

$$= \int_0^\infty \left(\frac{2m}{\sum_s M_s} \delta_s Q_{ms} \right) u^2 \left(f(u) + kT \frac{df}{du} \right) du$$

$$+ \sum_{s,j} \delta_s u_{sj} \int_0^\infty du\, u Q_{sj}(u) \left[f(u) - \frac{N_{sj}}{N_{so}} f(u-u_{sj}) \right]$$

$$(16)$$

Recalling that here $f(u) = f_o(u)$ and noting the relation between $f_1(u)$ and $\frac{df_o}{du}$ expressed by equations (6b) and (7) we see that the LHS of (16) is proportional to the mean particle velocity for the distribution f_1. This is, of course, the drift velocity. More precisely,

$$\frac{1}{3} \left(\frac{eE}{N} \right)^2 \int_0^\infty \frac{u}{\sum_s \delta_s Q_{ms}} \frac{df_o}{du} du$$

$$= \left(e \cdot \frac{eE}{N} \right) \left(\frac{m}{2e} \right)^{1/2} v_D \tag{17}$$

Now, looking at the second term on the RHS of (16) we note the similarity between it and equation (1) which defines the rate constants. Simplification of this term, using (1), gives:

$$\left(\frac{m}{2e} \right)^{1/2} \sum_{s,j} \delta_s u_{sj} \left[k_{sj} - \frac{N_{sj}}{N_{so}} k_{s-j} \right] \tag{18}$$

Combining (16), (17), and (18), we get an energy balance equation relating all of the various processes:

$$\left(\frac{eE}{N} \right) v_D = \int_0^\infty \left[\sum_s \frac{2m}{M_s} \delta_s Q_{ms} \right] u^2 \left[f(u) + kT \frac{df}{du} \right] du$$

$$+ e \left(\frac{m}{2e} \right)^{1/2} \int_0^\infty \sum_{s,j} \delta_s u_{sj} \left[k_{sj} - \frac{N_{sj}}{N_{so}} k_{s,-j} \right] \tag{19}$$

III. The Numerical Solution of the Boltzmann Equation

Examination of equation (14) will show that in order to compute $f(u)$ at some energy u, the values of f at higher energies, $u+u_{sj}$ must be known. This characteristic makes the computation of $f(u)$ difficult. Note, however, that if superelastic collisions can be neglected (i.e., the excited molecular levels are not highly populated) $f(u)$ only depends upon terms of the form $f(u+u_{sj})$. Sherman[22] showed that there exists a unique solution to equation (14), in the absence of superelastic processes, subject to the following conditions:

    i) $f(u) \geq 0$

    ii) $\int_0^\infty f(u) u^{1/2} du = 1$ (normalization)

    iii) $\int_0^\infty f(u) u\, du < \infty$.

Since $\lim f(u) = 0$ as $u \to \infty$, it is possible to start at some high energy, u_0, where the value of the distribution function $f(u)$ is small, and integrate equation (14) in toward zero energy, a process which Sherman[22] calls "backward prolongation". Another alternative involves the standard finite difference technique of superposing an N point grid on the interval $(0,u_0)$ and solving the resulting N simultaneous equations.

When the population of excited molecules is small (i.e., low vibrational temperature) we solve equation (14)

16

by backward prolongation. This is done by separating equation (14), which is a second order differential equation, into two coupled first order equations:

$$\frac{1}{3}\left[\left[\frac{eE}{N}\right]^2 \frac{u}{\sum_s \delta_s Q_{ms}} + \left[\sum_s \frac{2m}{M_s} \delta_s Q_{ms}\right] u^2 kT\right] \frac{df}{du} \qquad (20)$$

$$= -\left[\sum_s \frac{2m}{M_s} \delta_s Q_{ms}\right] u^2 \, f(u) - g(u)$$

$$\frac{dg}{du} = \sum_{s,j} \delta_s \left[(u+u_{sj}) \, Q_{sj} \, (u+u_{sj}) f(u+u_{sj}) \right.$$

$$\left. - u Q_{sj}(u) f(u) \right] - \sum_{s,j} \delta_s \frac{N_{sj}}{N_{so}}$$

$$\left[(u+u_{sj}) \, Q_{sj} \, (u+u_{sj}) f(u) - u Q_{sj}(u) f(u-u_{sj}) \right]$$

These equations are solved numerically using a modified fourth order Hamming Predictor-corrector scheme[23].

The initial values $f(u_0)$ and $g(u_0)$ are obtained using an approximate solution to the Boltzmann equation given by Holstein[10].

When the superelastic terms cannot be neglected, the integration is performed as before until the energy range of non-zero vibrational cross sections is reached (generally 1-3 eV) where a simple polynomial extrapolation technique is then used for the terms containing $f(u-u_{sj})$. When these superelastic terms are large (high vibrational temperatures) the polynomial extrapolation causes the numerical integration to become unstable. If the extrapolated value is too low the calculated distribution function is too

high, and if it is too high, the computed distribution is too low. In both cases the instability rapidly grows. When instability sets in, the integration is stopped and the standard finite difference technique is used over the remainder of the energy range.

Our solution is an iterative one in that the distribution function calculated on the first run through the above procedure is used for the extrapolation on the next iteration. On higher iterations, if they are needed, a logarithmic average of the previous two distribution functions is used in the extrapolation procedure.

Some Additions to the Formalism

The solution of equation (14) is difficult due to the high vibrational temperatures that we normally deal with in modeling molecular lasers. Because we must treat systems characterized by large excited state populations, it is desirable to include in the calculations transitions between all molecular vibrational levels rather than just between the ground level and the other levels. The cross sections $Q_{sj}(u)$ in the equations represent transitions between the ground level (j=0) and the jth vibrational level or electronic level. With the exception of theoretical calculations on N_2[24], the cross sections

$$Q_{j \rightarrow j + \Delta j}$$

are generally unavailable. In order to do the calculations

allowing for transitions between arbitrary vibrational levels we assume that:

$$Q_{j \to j+\Delta j} = Q_{0 \to \Delta j}$$

This approximation appears reasonable from the calculations on N_2 [25] and is also applied to CO which couples to electrons by a similar mechanism.

With this assumption equation (20b) becomes:

$$\frac{dg}{du} = \sum_{s,j} \delta_s \left(1 + \sum_{i=1}^{j_{max}-j} \frac{N_{si}}{N_{so}} \right)$$
$$\left[(u+u_{sj})Q_{sj}(u+u_{sj})f(u+u_{sj}) - uQ_{sj}(u)f(u) \right] \qquad (21)$$
$$- \sum_{s,j} \delta_s \left(\frac{N_{si}}{N_{so}} + \sum_{i=j+i}^{j_{max}} \frac{N_{si}}{N_{so}} \right)$$
$$\left[(u+u_{sj})Q_{sj}(u+u_{sj})f(u) - uQ_{sj}(u)f(u-u_{sj}) \right] .$$

In equation (21), j_{max} is the number of vibrational levels used in the calculation. In calculations involving CO or N_2, we generally use eight vibrational levels. The vibrational states higher than $v=8$ have very small cross sections which have only recently been measured[26].

Ionization processes are included in the calculations using the formulation given by Holstein[10]. Let $Q_u^i(u,u')$ be the cross section for an electron of energy u producing an electron in the energy range $(u',u'+du')$ in an ionizing collision with a molecule of species s having an ioniza-

tion potential u_s^i. Then as an additional term in equations (14), (20b), and (21) we have:

$$\left.\frac{dg}{du}\right|_{ion} = \Sigma \delta_s \left[\int^{\infty} du'uQ_s^i(u',u)f(u') \right. \tag{22}$$
$$\left. - uf(u)\ \frac{u-u_s^i}{-2} \int_0^{u+u_s^i} Q_s^i(u,u')du' \right]$$

The first term on the RHS of (22) represents the addition of electrons to the energy range (u,u+du) due to ionizing collisions. The second term represents the loss of electrons from the range (u,u+du).

We generally have no information on ionization cross sections with regard to how the energy remaining after ionization is divided between the resulting electrons. Since we are dealing with low energies we assume that one of the electrons has zero energy after an ionizing collision. This is a good assumption when the primary electron energy is relatively low   , when ionizing collisions are infrequent compared to the other elastic and inelastic collisions, and when there is an electric field to drive the secondary electrons from zero energy so that they relax into the distribution in a short time consistent with the steady state assumption. All of these assumptions are expected to be valid for most molecular gas discharge lasers of interest. In this case, equation (22) becomes:

$$\frac{dg}{du}\bigg|_{ion} = \sum_s \delta s \left[(u+u_s^i Q_s^i (u+u_s^i) \right. \tag{23}$$

$$\left. - uQ_s^i (u) f(u) \right]$$

where $Q_s^i(u)$ = the total cross section for ionization of molecular species s by an electron of incident energy u.

If the calculation were to be dependent upon electron density we would need to include the electrons produced by ionization in a balance of electron number density, as is done by Rockwood[20]. Since our calculation is steady state, we treat the electron density as a parameter and assume that the new electrons (the ones produced at zero energy) relax into the distribution on a time scale that is short compared to the time scale of interest to us. This assumption is consistent with our previous arguments concerning the steady state approximation.

Calculated Distribution Functions for Electrons in Carbon Monoxide

In Figure III-1 are shown some computed energy distribution functions for electrons in CO. These calculations, which contain no superelastic contributions, illustrate the dependence of the distribution function on E/N. A discussion of the cross sections used will appear in Section IV. The dip in the distribution in the 1-4 eV range is due to strong vibrational coupling of the CO
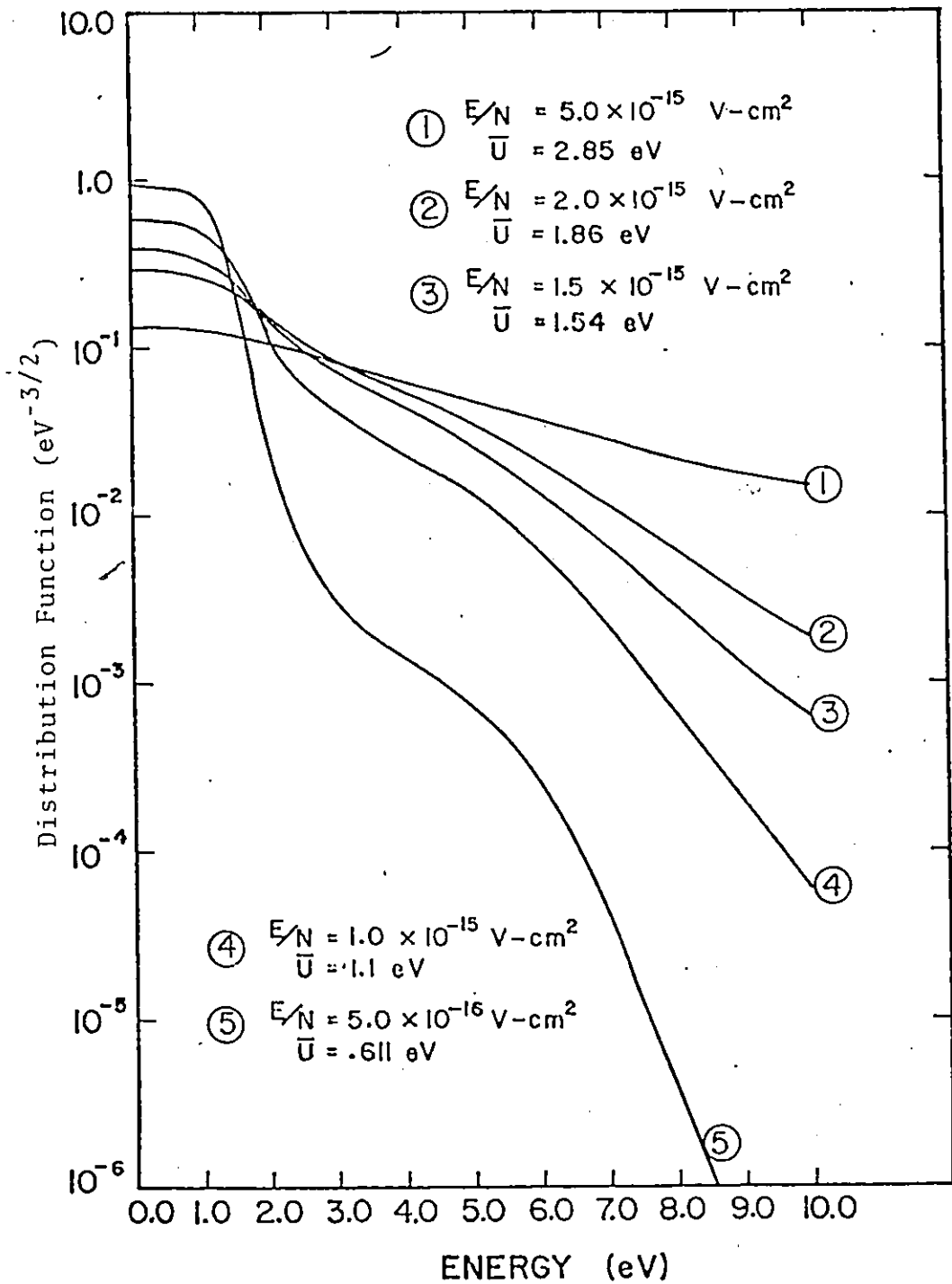
Figure III-1:   Electron Energy Distribution Functions in CO
                vs. Energy for Various E/N Using the Cross
                Sections of Ehrhardt, et al.

with the electrons. At high E/N the distribution function
is controlled by the electric field and this structure is
washed out. At high E/N the distribution function ap-
proaches, as a limiting form, the Dryvesteyn distribu-
tion[8,10] which has an EXP(-const. $\cdot$ u^2) energy dependence.
The effects due to superelastic processes are shown in
Figure III-2 for a CO vibrational temperature of 4000K.
Here electrons in the 1-4 eV energy range gain quanta
of energy from the vibration levels, ranging from .27 eV
for V = 1 to 2.03 eV for V = 8, increasing the mean energy
of the distribution.

The quantity $\bar{u}$ shown along with these calculations
is a "reduced" average energy[5] for the distribution which is
related to the effective "electron temperature", T_e,
and mean energy, E_m, of the distribution by

$$\bar{u} = kT_e = \frac{2}{3} E_m$$

where

$$E_m = \frac{_0\int^\infty f(u)u^{3/2}du}{_0\int^\infty f(u)u^{1/2}du}$$

In Figure III-3 is shown the fractional energy balance,
that is the fraction of the electron energy which is trans-
ferred to the internal states of CO, for two values of E/N.
As E/N is increased the fraction of energy going into
electronic excitation increases at the expense of vibra-
tional excitation, leading to decreased inversion efficiency.
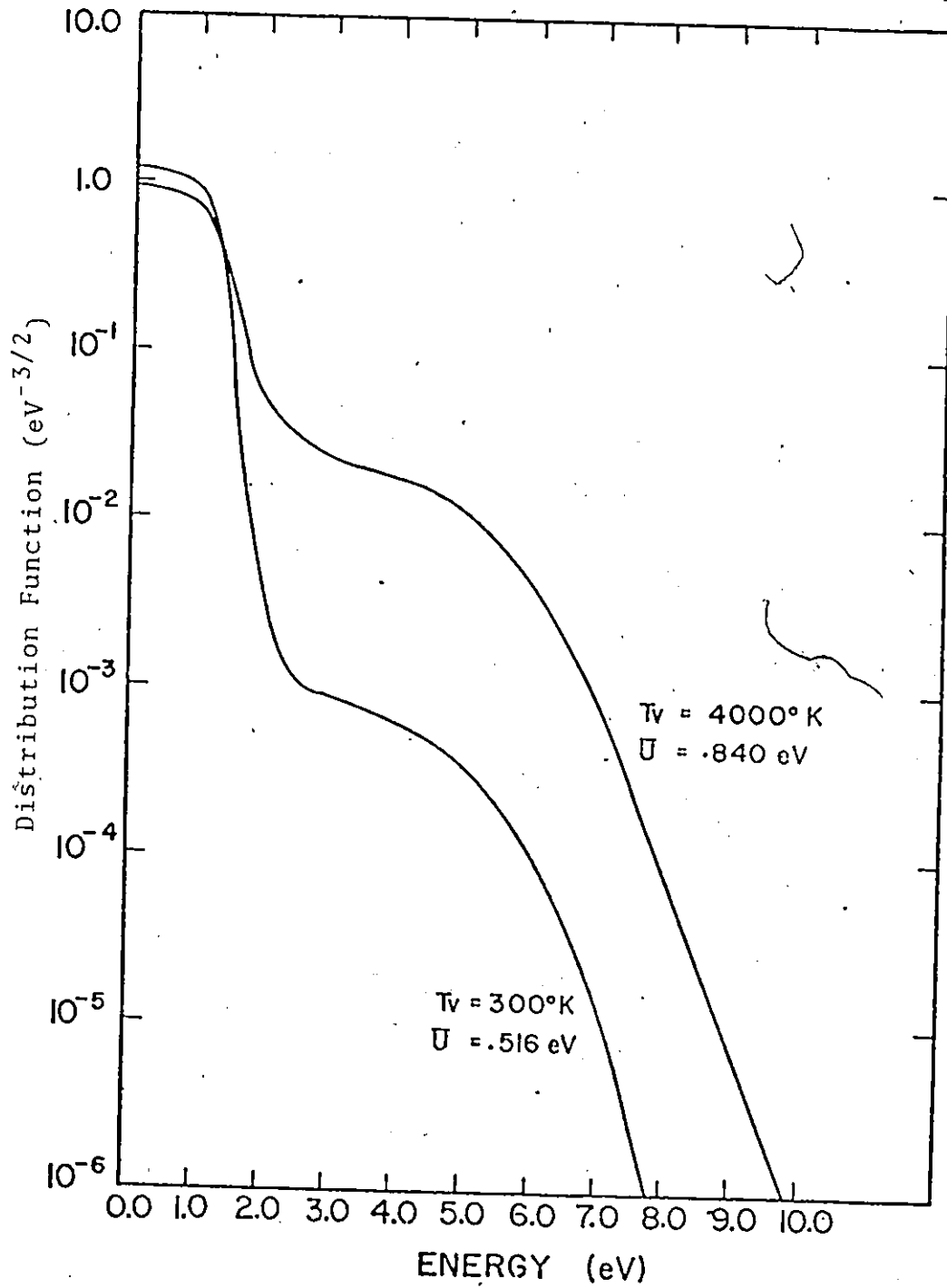
Figure III-2: Effect of Superelastic Collisions on the Electron Energy Distribution Function in CO vs. Energy for an $E/N = 4 \times 10^{-16}$ v-cm^2 Using the Hake and Phelps Cross Sections.
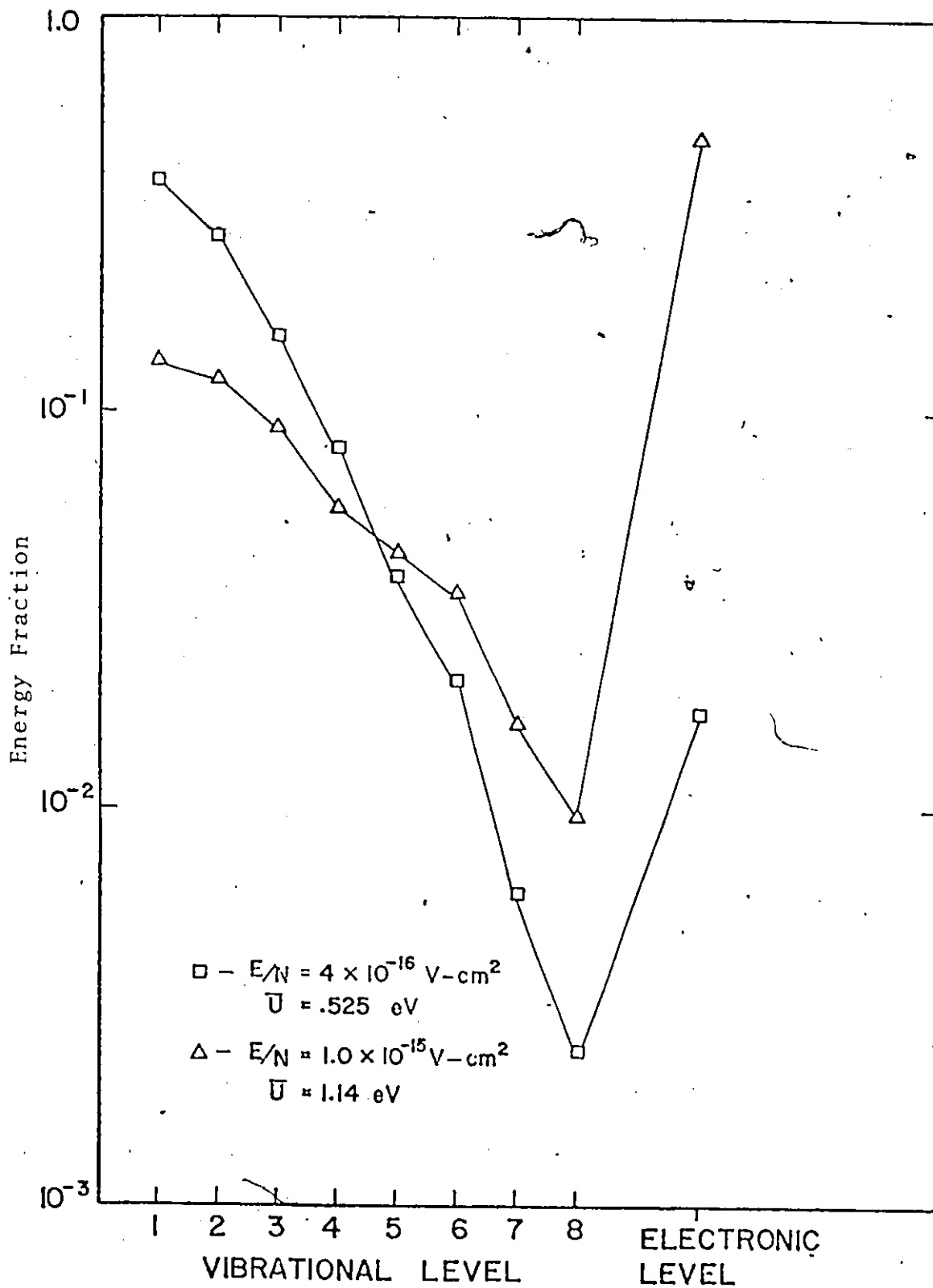
Figure III-3:   Fractional Energy Balance in CO for Two
               Values of E/N Using the Cross Sections
               of Hake and Phelps.

This suggests that CO laser operation at low E/N is desirable except that this means low ionization rates and low electron densities unless appropriate additives or external ionization sources are used. The use of low ionization potential additives to overcome this problem will be discussed later

IV. Vibrational Excitation Processes in CO/N$_2$ Mixtures

This electron energy distribution analysis has been applied to the study of CO/N$_2$ discharges. N$_2$ is used in carbon monoxide lasers to increase the pumping efficiency of the CO. N$_2$ is vibrationally excited by electrons just as is CO but cannot radiate the energy away because it lacks a dipole moment. Since the vibrational spacing of N$_2$ is slightly larger than that of CO it exchanges vibrational energy with the CO and thereby assists in pumping the laser. Nitrogen also affects the electron energy distribution function and, consequently, has an effect upon vibrational excitation rate coefficients, electron temperature, and the partition of electron energy into the various states of excitation. These effects will be discussed in this section.

Vibrational Excitation Cross Sections Used In CO/N$_2$ Calculations

As will be evident from the results discussed in this study, even the qualitative characteristics of CO laser systems are affected by the set of input cross sections used in the calculation. This is particularly true in CO where the vibrational excitation cross sections are large and, consequently, the power output or gain is sensitive to the shape of the vibrational distribution curve.

Table IV-1 lists the cross section data used in the current calculations to solve equation (20) for the electron energy distribution f(u). All data from these references has

27

	<u>CO</u>	<u>N</u>$_2$
momentum transfer (elastic)	Hake & Phelps[27] (1967)	Engelhardt, Phelps, & Risk (1964)[28]
vibrational excitation	Hake & Phelps (1967) or Ehrhardt, et al.[26] (1968)	"
electronic excitation	Hake & Phelps[†] (1967)	"

[†] see section V

Table IV-1: References to cross sections
used in the calculations

been taken from the recent compilation of Kieffer[7]. Two sets of data appear in the literature for the vibrational excitation cross sections of CO by electrons. Although the shapes of the excitation cross sections from these sources are similar as shown in Figure IV-1, the quantitative differences are important in assessing the role of N_2 in CO laser plasmas (vide infra). The CO and N_2 excitation cross sections for levels v=9 and v=10 for N_2 and CO are also available[26] but were not included in the calculations which follow because they are very small and have a negligible effect on the computed distribution function.

Calculation of the Distribution for CO/N$_2$ Mixtures

Figure IV-2 shows the effect on the electron energy distribution calculated without superelastic contributions by the addition of N_2 to a CO discharge. The presence of N_2 appears to increase the number of electrons in the energy region 1-3 eV which results in both increased mean electron energy as well as enhanced CO excitation rate coefficients. This result suggests, as found previously by Rockwood[29], that the presence of N_2 in the laser plasma might enhance the power output from the CO laser independently of the N_2-CO pumping process via vibrational-vibrational energy exchange known to occur in this mixture[1,3,32-35]. However, actual calculations performed on the CO/N_2 system are found to be strongly dependent on the CO vibrational cross section set used and generally do not show this enhanced CO pumping as will be discussed later.
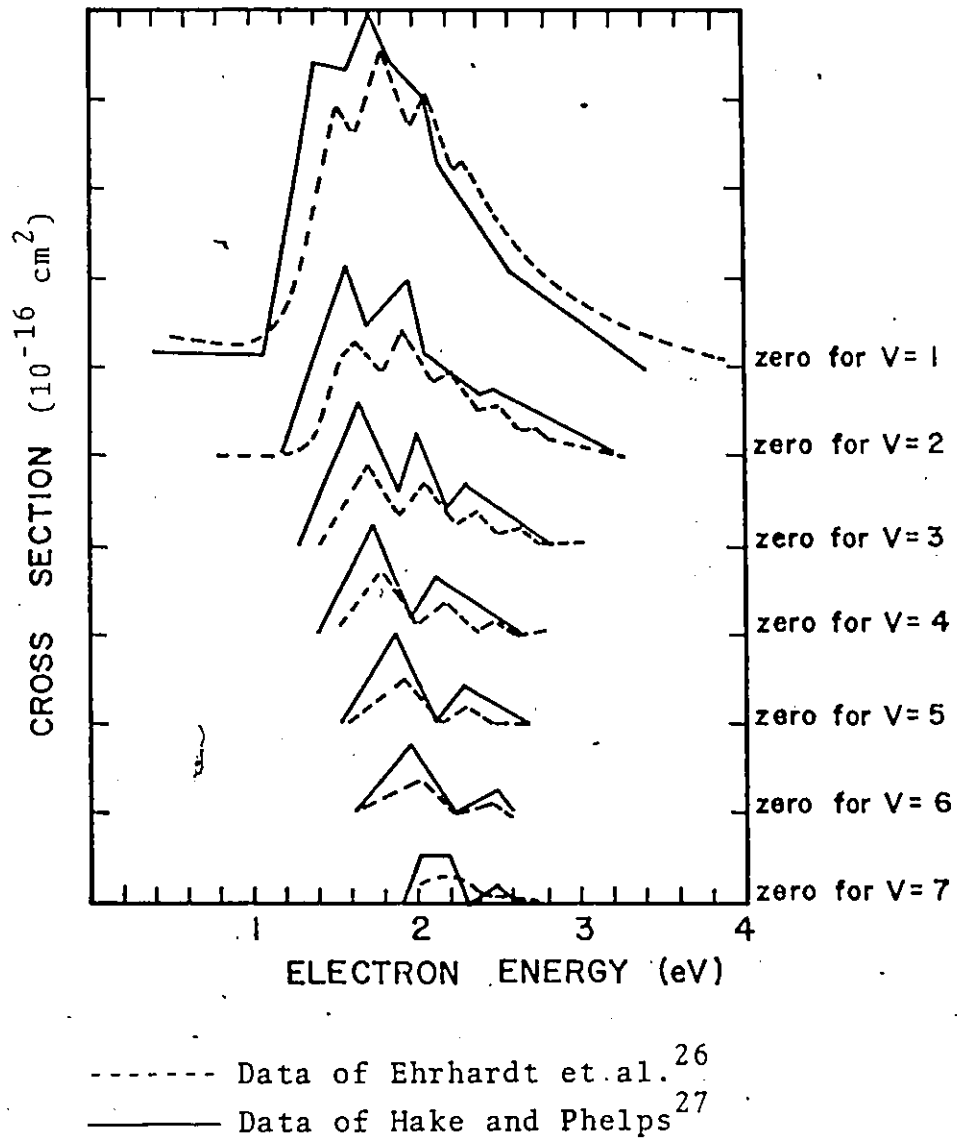
Figure IV-1: CO Vibrational Excitation Cross Sections
Taken from the Compilation of Kieffer (7).
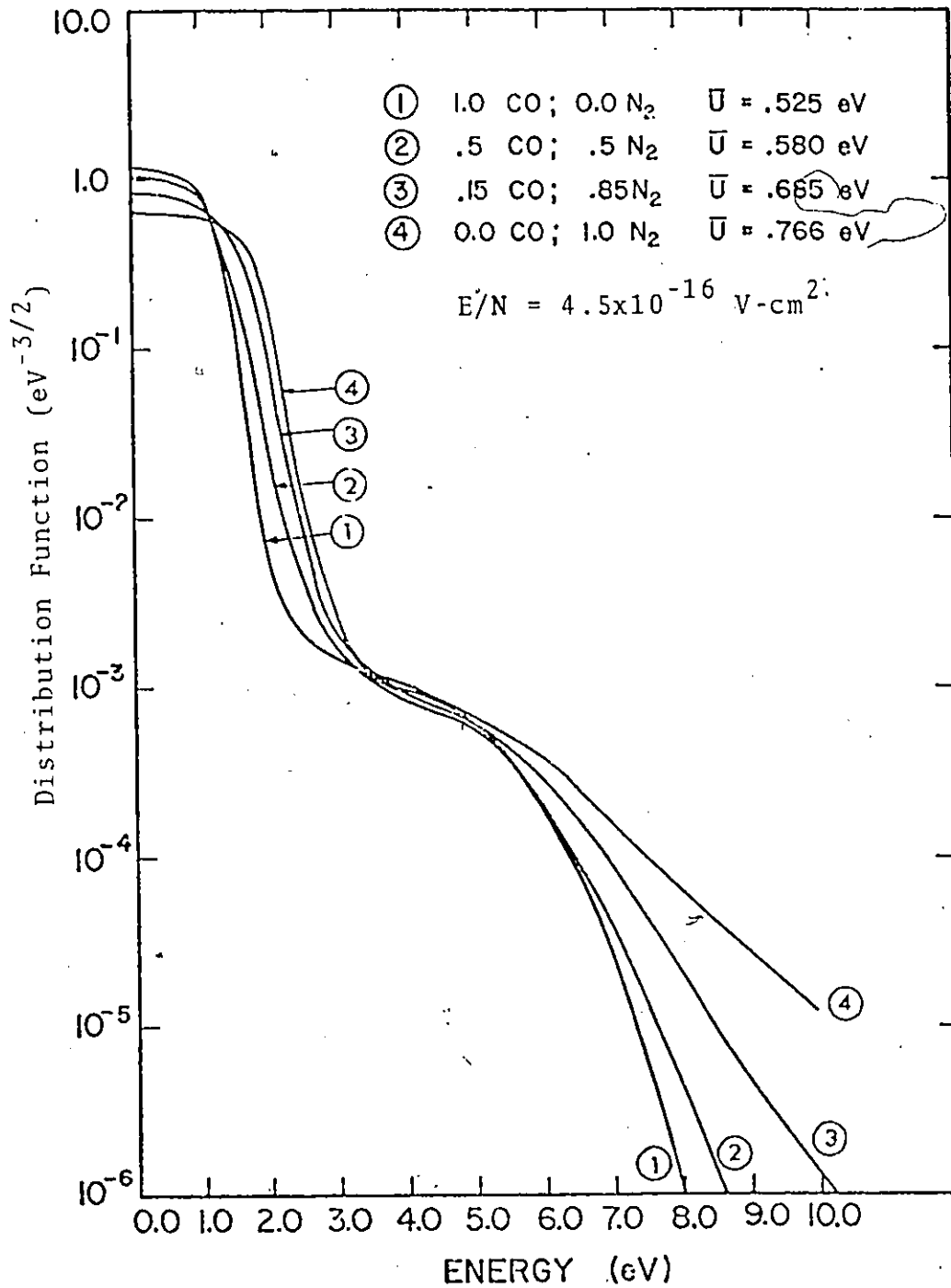
Figure IV-2: Effect of N_2 on the Electron Energy Distribution Function in CO/N_2 Mixtures Using the Cross Sections of Hake and Phelps.

The addition of N_2 to the discharge will have an additional effect that may lead to greater efficiency in vibrational excitation. Because its cross sections for vibrational excitation are smaller, the addition of N_2 at constant value of E/N increases the mean electron energy as shown in Figure IV-2. This raises the high energy "tail" of the distribution function causing an increase in the rate coefficient for ionization which, in turn, results in increased electron density in the plasma. The addition of N_2 will, then, via this sequence of events, cause an increase in the vibrational excitation rates and thereby increase the efficiency of a CO laser.

Plasma Drift Velocities

One measure of the successful operation of a molecular plasma code is agreement between predicted and measured transport properties. In this context, drift velocity measurements in N_2 and CO are available and are herein presented in comparison with predicted values from the laser plasma code. Figure IV-3 shows the drift velocity versus E/N for both CO and N_2 in comparision to literature values. Note that the two sets of cross section data for CO shown in Table IV-2 are used and are so labeled in the figure.

The N_2 drift velocities and the CO drift velocities using the Hake and Phelps cross sections agree well with the measured values from Massey and Burhop[30]. Both sets of cross sections give results that are substantially different from the experimental results at low E/N. Both
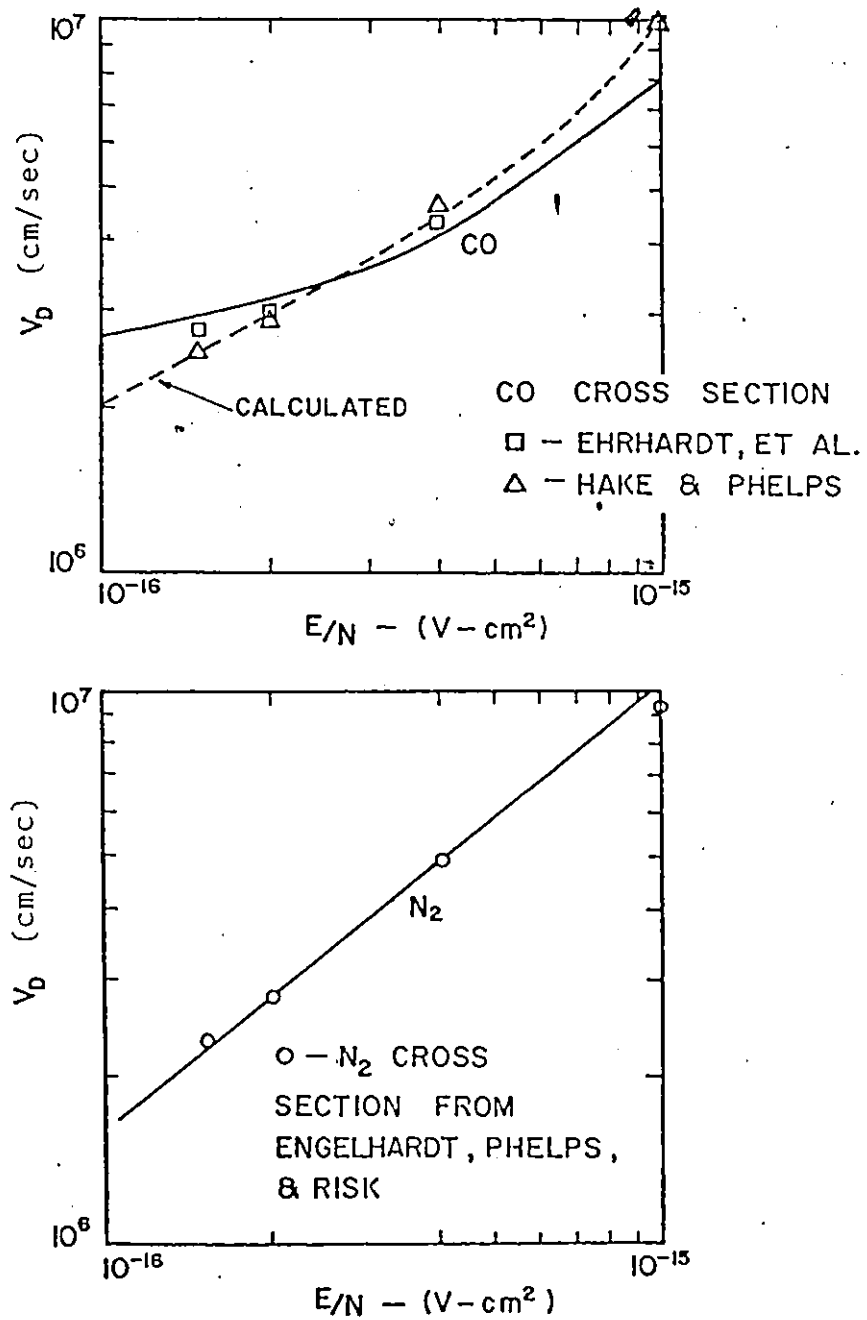
Figure IV-3: Calculated Drift Velocities vs. E/N for CO and N_2 Compared to Data from Massey and Burhop (30).

sets of CO cross sections give good agreement at high E/N (i.e. above about 2×10^{-16} V-cm^2).

The predictions for the CO/N$_2$ mixture drift velocities versus mole fraction of CO for various E/N are shown in Figure IV-4 in comparison to the earlier predictions of Rockwood[29]. The velocities predicted using the cross sections of Hake and Phelps are in substantial agreement with the Rockwood predictions while the Ehrhardt cross sections give rise to a somewhat different mixture dependence. These differences become more dramatic when we look at electron excitation rates in CO/N$_2$ mixtures which are given in the next section.

The Effect of CO/N$_2$ Mixtures on Electron Excitation Rates

Of major interest in laser plasma predictions is the total rate at which energy flows into the vibrational modes of CO due to hot electrons. In Figure IV-2 we noted that the presence of N$_2$ causes a favorable shift in the electron energy distribution function, increasing the mean electron energy at fixed E/N and reducing the dip in the electron energy distribution associated with coupling to the CO vibrational modes. To investigate the direct effect on the CO excitation rates as a function mixture ratio, we calculated the total excitation rate for CO, $f_{CO}Q$,

$$f_{CO}Q \equiv \delta_{CO} \sum_j \{k_j - k_{-j} \exp(-u_j/kT_j)\}$$
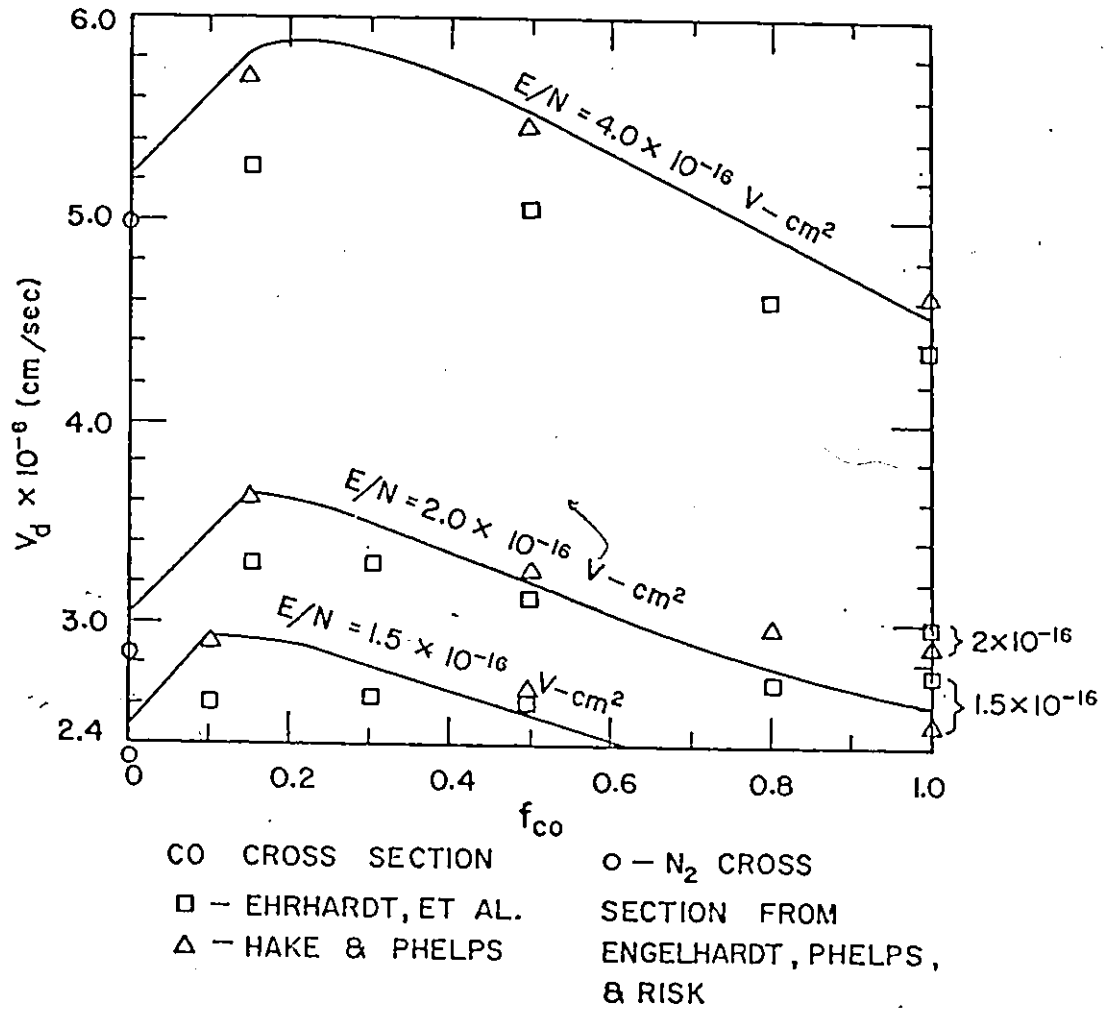
Figure IV-4: Calculated CO/N$_2$ Mixture Drift Velocities for Several E/N Compared to the Calculations of Rockwood (Solid Lines).

where δ_{CO} = fraction of CO

u_j = energy of jth level

k_j = inelastic rate constant

k_{-j} = superelastic rate constant

and T_j = vibrational temperature of jth level.

Figure IV-5 shows the results for the total CO excitation rate versus fraction of N_2 for various E/N in comparision with the previous calculations of Rockwood[29]. Three effects are particularly important to note. When the Hake and Phelps cross sections are used we find rather good agreement with Rockwood's predictions for high E/N but poor agreement at low E/N. The inclusion of a superelastic contribution, however, (arbitrarily chosen as T_V = 4000 $^{\circ}$K for illustrative purposes) leads to a disagreement even at high E/N.

The conclusions reached by Rockwood that an optimum N_2/CO mixture ratio exists as shown by Rockwood's curves in Figure IV-5 appears questionable when another cross section set is used as well as when superelastic processes are included. These calculations, though, do not take into account other processes due to the addition of N_2 that may affect these results. One effect, an increase in electron density, has been discussed above. In addition, there will be other molecular species, atomic species, and negative ions produced in the discharge that, although in small concentrations will not alter the distribution function appreciably, may affect the vibrational excitation via a variety of energy transfer processes. In order to assess the
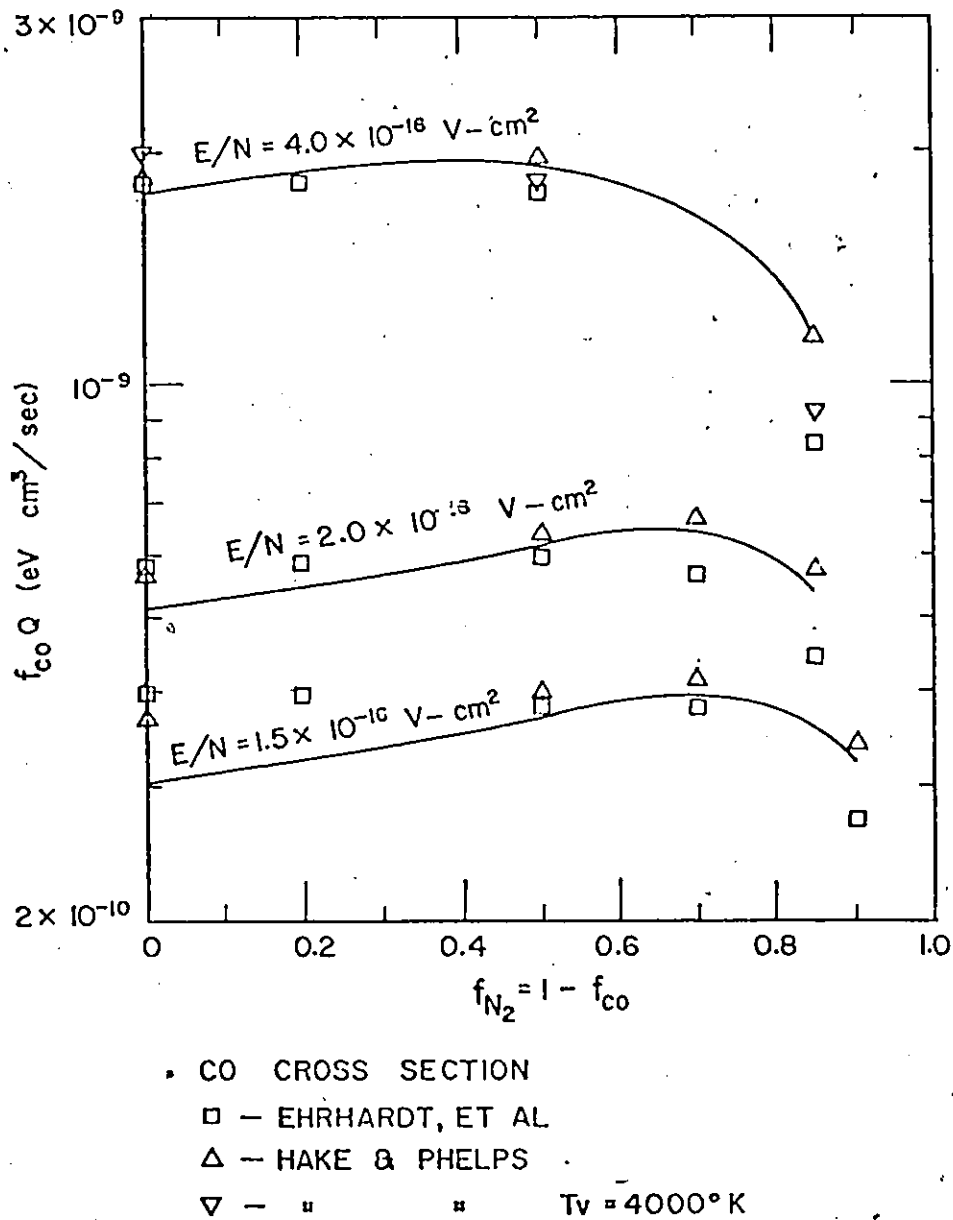
Figure IV-5:   Total Electron Energy Flow into Vibrational Modes of CO as a Function of N_2/CO Mole Fraction for Several E/N. (——— calculations of Rockwood)

importance of these processes a study of the plasma
chemistry of the discharge is needed. Because the $CO-N_2$
system would be an extremely difficult one for which to model the
chemistry, since it would involve neutral and ionic re-
actions of molecules composed of C, O, and N atoms, the
simpler $CO-O_2$ laser was chosen for study. This system
is important because it is known that O_2 as an additive
enhances the power output of a CO laser. The plasma chem-
istry of the $CO-O_2$ laser is discussed in the next section.

V. The Plasma Chemistry of the CO-O_2-He Discharge

A number of experimenters[35-39] have found that a small amount of O_2 added to a CW CO laser plasma has a pronounced effect upon the operation of the laser. Bhaumik, et al.[36] have found that small amounts of O_2 (approximately 5% of the CO partial pressure) enhanced the power output by a factor of 10%-20% and reduced carbon deposits on the walls of the laser tube. They suggested that the O_2 affected the dissociation reaction $CO \rightleftharpoons C+O$ by driving it to the left. Greater amounts of O_2 had a deleterious effect on laser operation, possibly due to the large electron attachment cross section of O_2 or to the formation of CO_2, in their opinion. Hartwick and Walder[37] found that total laser output increased and that the laser became more stable with the addition of O_2 to a CO-He discharge. The optimum mixture was found to be 28 torr He, 2 torr CO, and 0.1 torr O_2. In addition, they measured the gas temperature in the plasma using a thermocouple and correlated it to laser output finding that the minimum in temperature, approximately 295 $^{\circ}$K, corresponded to the maximum in power output as the O_2 flow rate was varied for a liquid nitrogen cooled laser. At slow oxygen flow rates the measured kinetic temperature was approximately 320 $^{\circ}$K.

Extensive work involving the effects of O_2 upon CO lasers has been done by Keren, Avivi, and Dothan[38,39]. They found that the addition of O_2 increased the power output and decreased the operating E/N of a water cooled CO flow laser.

39

At a constant current of 17 mA   the laser output power
reached a maximum of 4 watts with the addition of 50 m-torr
of O_2 to a mixture of 1.4 torr CO in 18 torr He and the axial
field strength in the discharge dropped from 136 V/cm to
88 V/cm. Power output then decreased with the addition of
larger concentrations of O_2 and lasing was completely
quenched at an O_2 partial pressure of 100 m-torr. They also
pointed out that the discharge was very unstable and that
laser action could not be obtained in the absence of the
O_2 additive. On the basis of the measured decrease in E/N
and a calculation of the fraction of electron energy flowing
into CO vibrational and electronic states as a function of
E/N (similar to that presented in Figure III-3 here) they
concluded that the enhanced power output was due to more
efficient vibrational pumping because of the lower E/N.

Keren, et al.[39] also analyzed the composition of the
ions leaving the discharge using a mass spectrograph and
found that with the addition of 20 m-torr O_2 to the laser
plasma (1.4% of the CO partial pressure), O_2^+ became the dom-
inant positive ion in the discharge. With no oxygen present
the dominant ion is the $C_2O_2^+$ cluster as has been observed
in the past[40]. They suggest that the dominance of O_2^+ is due
to ionization via a three step process:

$$e^- + CO \rightarrow CO^*(a^3\Pi) + e^-$$
$$CO^* + O_2 \rightarrow CO + O_2^*(\text{metastable})$$
$$O_2^* + e^- \rightarrow O_2^+ + 2e^-$$
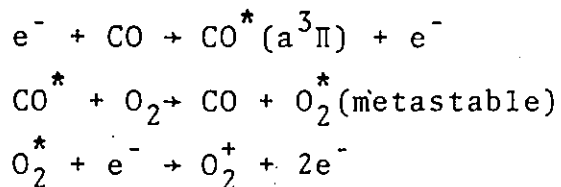
claiming that the probability of producing O_2^+ by direct

ionization is at least a factor of twenty lower than the probability of this process. They discount the charge transfer reaction,

$$CO^+ + O_2 \rightarrow O_2^+ + CO$$
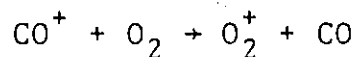
as a means of forming the O_2^+ because, in their opinion, it cannot explain the decrease in E/N that occurs with the addition of molecular oxygen. Using this three step model they compute that about 0.5% of the O_2 molecules are excited to O_2^* for a total O_2 partial pressure of 25 m-torr.

Because very small amounts of molecular oxygen added to a CO laser have significant effects upon laser performance, it appears clear that the plasma properties of the discharge are affected but, at present, it is not known how. The calculations that follow are directed toward providing some systematic explanation of the observed properties of additive O_2 in a CO discharge. This is accomplished by studying the electron impact excitation processes in the discharge using the electron energy distribution calculation described above and by studying the chemical kinetics of the system by numerically integrating the rate differential equations for the formation and removal of each chemical species.

Electron Impact Processes

The cross sections for electron impact excitation of the vibrational modes of CO have been discussed in section IV above. For the electronic excitation of CO by electron impact

there is little data available. What most workers have used
in the past has been a single composite cross section, due
to Hake and Phelps[27], with a threshold of 6 eV and a peak
value of 5×10^{-16} cm^2 at 10 eV. This corresponds to the
$CO(a^3\Pi)$ state. This cross section, however, is not a meas-
ured or computed cross section but, rather, just a value that
was included in their calculations to "prevent electrons
which penetrate the vibrational barrier from reaching unreal-
istically large energies."[27] They point out that "the magni-
tude chosen for this cross section is probably much larger
than the true excitation cross section for this state."[27]
This became apparent when, in the course of this work, com-
puted ionization rate coefficients were several orders of
magnitude smaller than their values realistically should
have been. For example, in a 7% CO and 93% He mixture with
$E/N=3 \times 10^{-16}$ $V-cm^2$ the Hake and Phelps electronic cross sect-
ion gives an ionization rate coefficient of 1.3×10^{-13} cm^3/sec
while the cross sections discussed below give a coefficient
of 2.3×10^{-10} cm^3/sec. This comes about because the ioniza-
tion rate coefficient, which is the integral over energy of
the ionization cross section times the distribution function
(equation 1 of section I), is very sensitive to the magnitude
and shape of the high energy tail of the distribution function.
As the electronic cross section is increased, the tail of the
distribution function drops and thus the ionization rate
coefficient decreases.

The information available on CO electronic cross sections

is summarized as follows. Lassettre and Silverman[41] and Trajmar, Williams, and Cartwright[42] have published experimental differential cross sections for the excitation of a number of CO electronic states. Their data is of little use in this work because it is taken at energies substantially higher than the energy range of importance in gas discharges--400 to 600 eV in reference (41) and 20 eV in reference (42). We need total cross sections from threshhold to about 25 eV. For this we have the work of Mumma, Stone, and Zipf[43] on the excitation of $CO(a^3\Pi)$ and $CO(A^1\Pi)$, and the theoretical work of Chung and Lin[45] on the excitation of eleven CO electronic states.

In these calculations we have included the two CO electronic states with the largest cross sections: the $a^3\Pi$ state at 6.04 eV and the $A^1\Pi$ state at 8.07 eV. The cross sections used are composites of those given in references 43-54. They are in substantial agreement with a similar set of cross sections due to Sawada, et al.[46]. It should be pointed out that revisions such as this in the electronic excitation cross sections used in solving the Boltzmann equation have a negligible effect on the results of the calculations presented thus far. They will affect energy flow calculations such as those shown in Figure III-3 but that particular figure is meant just to be an illustration of how vibrational pumping efficiency can vary with E/N.

The references to all of the cross section data used

in these calculations are given in Table V-1. Some comments are in order for several of the excitation processes shown. With reference to excitation of the $A^3\Sigma$ and $B^3\Sigma$ states of O_2, it is known that these excited states predissociate. The $O_2(A^3\Sigma_u^+)$ state[49] predissociates into $O(^3P) + O(^3P)$[48] and $O_2(B^3\Sigma_u^-)$ predissociates into $O(^3P) + O(^1D)$[48,49]. Although there are several ways for the $O_2(B)$ state to predissociate into $O(^3P) + O(^3P)$ via curve crossings[49] the probabilities of this occurring are unknown. It has been assumed in this work that all of the excitation follows the $^3P + {}^1D$ predissociative path. The cross section for ionization of the O_2^* metastable is unknown and has been taken to be the same as that for ionization of $O_2(X)$. This is about the least arbitrary method of obtaining an estimate of the cross section for this process in the absence of experimental or theoretical data. There is some support for this assumption from the work of Burrow[50] on dissociative attachment from O_2^*. He measured the ratio of the ionization cross section of the $a^1\Delta_g$ state to that of the $x^3\Sigma_g^-$ state at approximately 0.5 eV above each respective threshold and found it to be 0.8 ± 0.3.

Chemistry of the $CO-O_2$-He system

In order to assess the importance of some of the processes that can occur in the discharge, the computer code for calculating the electron energy distribution function

Electron Impact Processes	Energy Loss (eV)	Reference
$e^- + CO$:		
1. CO^+ (8 levels)	0.266-2.034	26
2. $CO(a^3\Pi)$	6.04	see text
3. $CO(A^1\Pi)$	8.07	see text
4. $C + O^-$	9.00	75
5. $C^+ + O^-$	12.55	75
6. CO^+	14.013	7
$e^- + O_2$:		
7. O_2^+ (8 levels)	0.193-1.46	7
8. $O_2(a^1\Delta_g)$	0.98	76
9. $O_2(b^1\Sigma_g^+)$	1.64	76
10. $O_2(A^3\Sigma_u^+)$	4.5	27,77
11. $O_2(B^3\Sigma_u^-)$	8.4	27,77
12. 9.7 eV allowed[51]	9.7	77
13. $O + O^-$	3.62	75
14. O_2^+	12.063	7
15. $O^+ + O$	19.54	75
$e^- + O$:		
16. $O(^1D)$	1.96	78
17. $O(^1S)$	4.17	78
18. O^+	13.6	7
$e^- + O_2^*$:		
19. O_2^+	11.0	see text

Table V-1: Electron impact processes in the CO-O_2 system.

was combined with a chemical kinetics code. This allows
the concentrations of chemical species to be computed as
a function of time. Since we are studying a CW laser,
this computation is carried out in time until the species
concentrations are approximately in steady state. We
integrate the differential rate equations rather than di-
rectly solving the steady state equations because the coupled
non-linear algebraic equations that arise out of a steady
state analysis are exceedingly difficult to solve in a
systematic way. In addition, there are some species in a
fast flow laser (such as CO_2 in a CO laser) that do not
reach steady state. The chemistry code that was used in
this work is based on the Runge-Kutta-Merson algorithm for
the integration of stiff differential equations used by
Keneshea[52] in his studies of ionospheric chemistry. In
this scheme initial CO, O_2, and He densities and an initial
electron density close to their expected steady
state values are specified. A value for E/N and an ini-
tial vibrational temperature are also specified as inputs
to the calculation of the electron energy distribution. As
time progresses and the CO vibrational temperature changes
the electron distribution function is recomputed and new
rate coefficients calculated to reflect these changes.

A list of the seventy nine chemical reactions included
in this calculation is presented in Table V-2. Only a
relative few, however, are really important and will be dis-
cussed here. The rate coefficients for the reactions and

Reactions					Rate Coeff.	Ref.
1. CO + E–	= CO' + E–				9.4E–09	
2. CO' + E–	= CO + E–				2.2E–08	
3. CO + E–	= CO* + E–				6.8E–11	
4. CO* + E–	= CO + E–				1.6E–08	
5. CO + E–	= CO+ + E–	+ E–			2.4E–14	
6. CO + E–	= C + O–				2.8E–14	
7. CO + E–	= C+ + O–	+ E–			9.3E–17	
8. CO' + E–	= CO+ + E–	+ E–			2.4E–14	
9. O2 + E–	= O2' + E–				2.3E–10	
10. O2' + E–	= O2 + E–				4.2E–10	
11. O2 + E–	= O2* + E–				1.9E–10	
12. O2* + E–	= O2 + E–				5.4E–10	
13. O2 + E–	= O2+ + E–	+ E–			6.6E–14	
14. O2 + E–	= O + O	+ E–			5.1E–11	
15. O2 + E–	= O + O–				5.5E–12	
16. O2 + E–	= O+ + O–	+ E–			6.1E–18	
17. O2 + E–	= O + O*	+ E–			2.6E–11	
18. O + E–	= O* + E–				6.1E–10	
19. O + E–	= O+ + E–	+ E–			4.9E–14	
20. O2* + E–	= O2+ + E–	+ E–			1.6E–13	
21. O– + CO	= CO2 + E–				7.3E–10	53
22. CO* + CO	= CO' + CO'				9.9E–11	54
23. CO* + CO	= C + CO2				1.1E–11	54
24. CO+ + CO + CO	= C2O2+ + CO				1.4E–28	55–58
25. C2O2+ + CO	= CO+ + CO	+ CO			2.1E–12	55–58
26. C2O2+ + E–	= CO + CO				7.4E–08	40
27. O2+ + E–	= O + O				1.0E–08	59
28. O2+ + E–	= O + O*				1.0E–08	59
29. O* + O2	= O + O2				7.5E–11	60
30. O2 + O + M	= O3 + M				6.4E–34	61
31. O* + O3	= O2 + O2				3.8E–12	60
32. O + O3	= O2 + O2				2.0E–14	61
33. O2 + O3	= O2 + O2	+ O			1.5E–13	61
34. O+ + O2	= O2+ + O				4.0E–11	62
35. O2+ + E– + M	= O2 + M				8.0E–29	52
36. O– + O2+	= O + O2				1.0E–07	63
37. O– + O	= O2 + E–				2.0E–10	63
38. O– + O2	= O3 + E–				5.0E–15	63
39. O3 + E–	= O– + O2				1.0E–11	63
40. O– + O2*	= O3 + E–				3.0E–10	63
41. O– + O2+ + M	= O3 + M				1.9E–27	EST.
42. O2 + E– + M	= O2– + M				1.0E–33	64
43. O + E– + M	= O– + M				1.0E–31	52
44. C + O2	= CO' + O*				3.3E–11	65
45. C + CO2	= CO + CO				7.0E–19	65
46. C + O2+	= CO+ + O				2.3E–10	65
47. C+ + CO2	= CO+ + CO				1.8E–09	62
48. C+ + O2	= CO+ + O				1.1E–09	62
49. CO+ + E–	= C + O				9.2E–08	65
50. CO+ + E– + M	= CO + M				8.5E–27	63

Table V-2: Reactions used in the plasma chemistry calculation.

Reactions

Reactions					Rate Coeff.	Ref.
51. C + O + M	= CO + M				1.0E-32	65
52. CO+ + O2	= CO + O2+				2.0E-10	62
53. CO+ + O	= CO + O+				1.4E-10	63
54. C2O2+ + O2	= CO + CO + O2+				2.0E-10	†
55. O+ + CO2	= O2+ + CO				1.1E-09	63
56. CO* + O2	= CO + O2*				2.0E-10	54
57. O* + CO	= O + CO'				1.7E-11	66
58. O* + CO	= O + CO				5.6E-11	66
59. O + CO'	= O + CO				5.9E-15	67
60. O2- + O	= O3 + E-				5.0E-10	62
61. O2- + O	= O2 + O-				3.3E-10	63
62. O2- + O2+	= O2 + O2				4.2E-07	63
63. O2- + O2	= O2 + O2 + E-				2.0E-18	63
64. O2- + O3	= O2 + O3-				4.0E-10	63
65. O2- + O2*	= O2 + O2 + E-				2.0E-10	63
66. O- + O3	= O + O3-				1.0E-09	63
67. O2+ + O3-	= O3 + O + O				1.0E-07	68
68. O2+ + O3-	= O3 + O2				2.0E-07	68
69. O3- + O	= O2- + O2				1.0E-10	68
70. O3- + O	= O2 + O2 + E-				1.0E-13	68
71. O2+ + O2 + O2	= O4+ + O2				2.8E-30	63
72. O2+ + O2 + M	= O4+ + M				1.0E-31	63
73. O4+ + O2	= O2+ + O2 + O2				2.0E-13	63
74. O4+ + O	= O2+ + O3				3.0E-10	63
75. CO' + HE	= CO + HE				1.7E-17	69
76. CO' +	= CO +				3.4E+01	1
77. O2' + HE	= O2 + HE				1.6E-15	70
78. O4+ + E-	= O2 + O2				1.1E-07	59
79. O+ + E- + M	= O + M				2.0E-27	63

†This rate coefficient has been taken to be equal to that of reaction (52).

Table V-2 cont.

references to them are also given in Table V-2. The rate coefficients for the first twenty reactions, except number (8), are computed using the electron energy distribution code and the cross sections discussed above. The rate coefficient used for ionization of vibrationally excited CO (reaction 8) is taken to be the same as that for ionization of ground state CO (reaction 5). The rate coefficients shown in Table V-2 for reactions (1) through (20) were computed using an $E/N = 1 \times 10^{-16} V\text{-}cm^2$, and a CO vibrational temperature of 3000° K for a gas mixture corresponding to 1.4 torr CO, 50m-torr O_2, and 18 torr He. These values are shown for illustrative purposes as they are typical for the conditions being discussed in this work. The electron temperature under these conditions is 1.0 eV. The gas temperature has been taken to be $300^\circ K$. The rate coefficients in reactions (21) through (79), where they are dependent upon electron or gas temperature, have been computed using these values.

To illustrate how the parameters critical to the calculations being presented here vary with E/N and vibrational temperature we have in Figures V-1 through V-3 plots of the ionization rate coefficient of CO, mean electron energy, and CO^+, $C_2O_2^+$, and O_2^+ recombination rate coefficients. These were computed for mixtures of 1.4 torr CO, 50 m-torr O_2, and 18 torr He corresponding to the experimental conditions of Keren, et al.[39,39]. The sensitivity
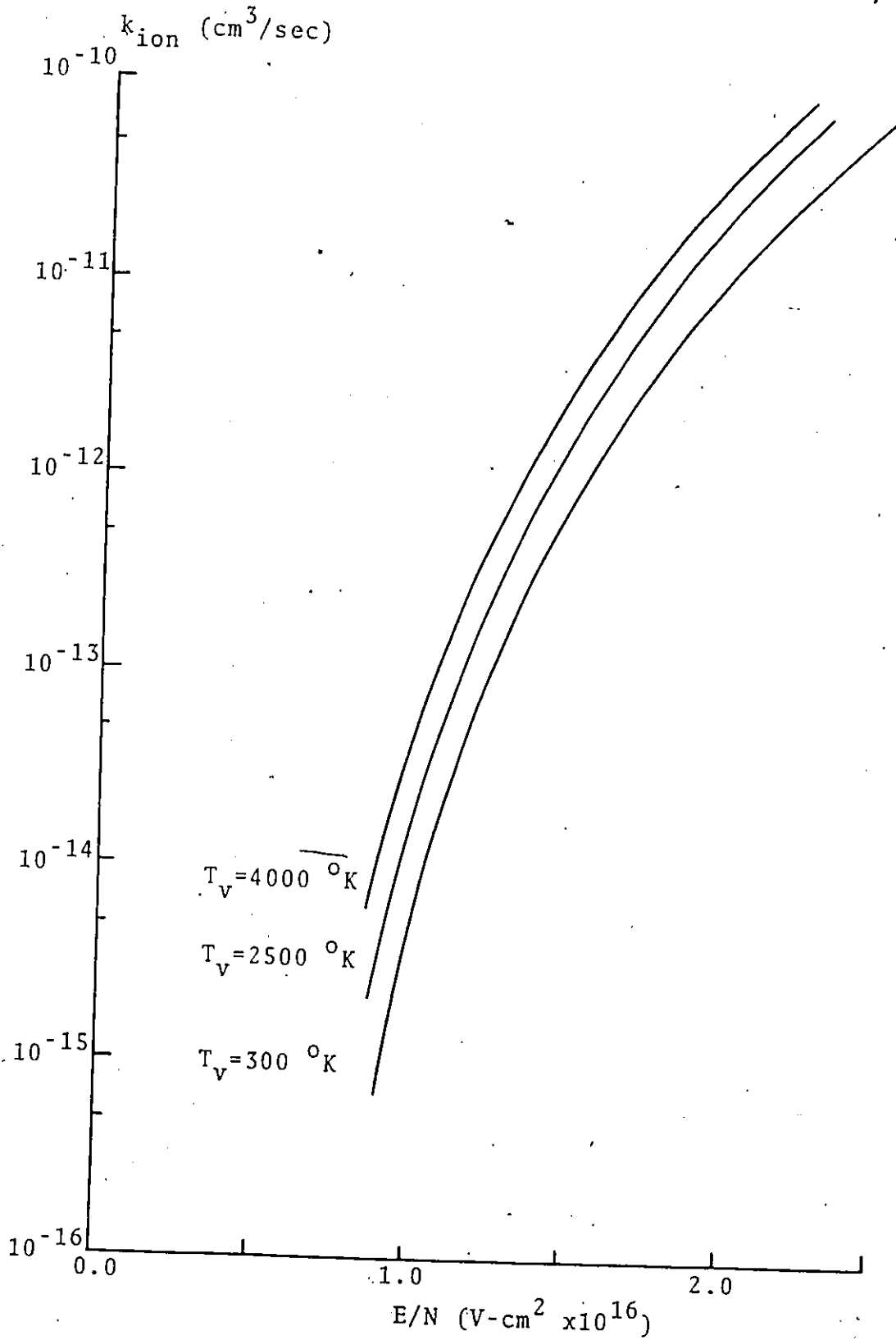
Figure V-1: CO ionization rate coefficients for a 7% CO-93% He mixture.
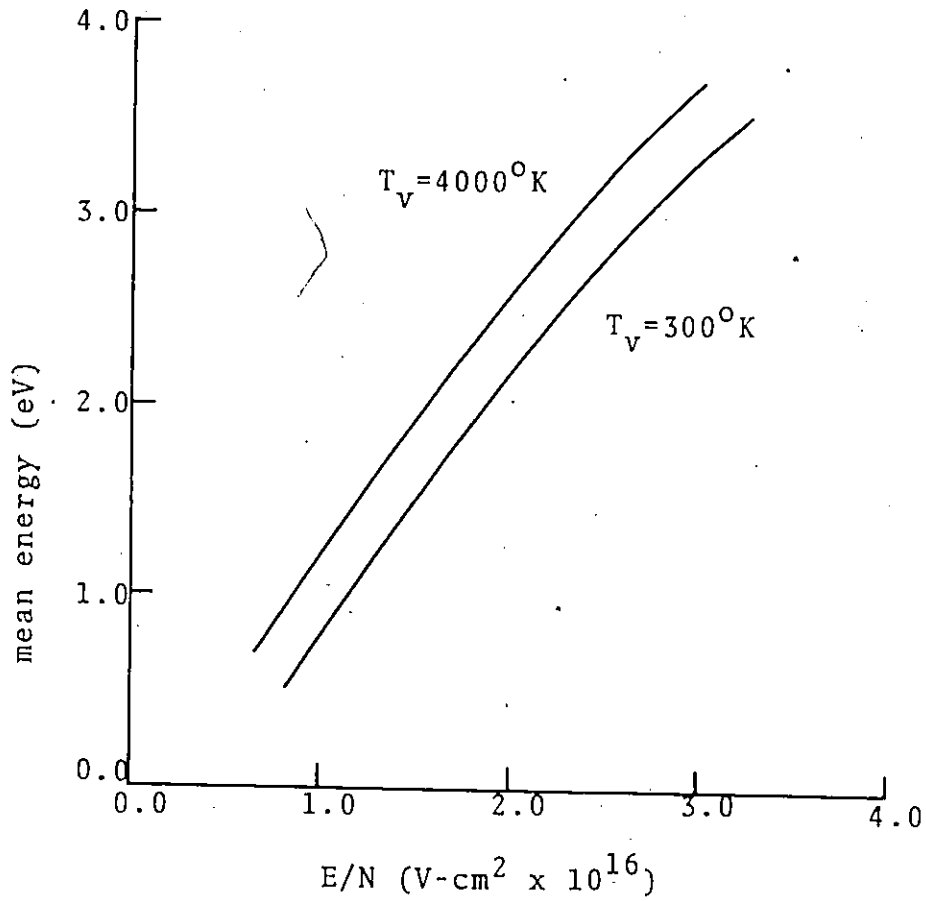
Figure V-2: Electron Mean Energy as a Function of E/N and CO Vibrational Temperature for a Mixture of 7% CO and 93% He.

$$k_{co}^+ = 1.33 \times 10^{-5} \, T_e^{-.53}$$

$$k_{c_2o_2}^+ = .243 \, T_e^{-1.6}$$

$$k_{o_2}^+ = 3.88 \times 10^{-6} \, T_e^{-5.6}$$
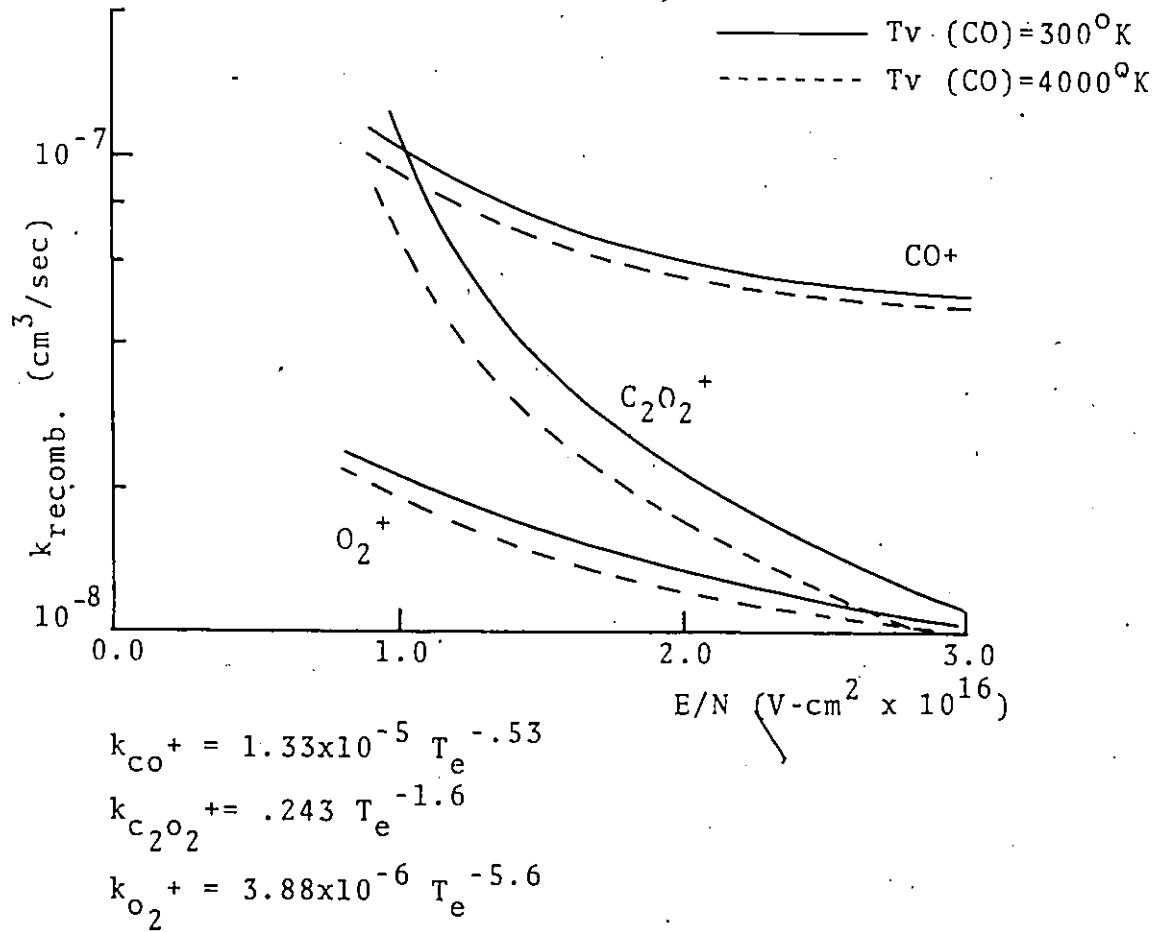
Figure V-3:   Recombination Rate Coefficients as Functions of E/N and Vibrational Temperature.

of the ionization rate coefficient to E/N (Fig. V-1) is striking and graphically explains why, for the sake of stability, these discharges are operated in a current regulated mode[36].

The results of the calculation of the time evolution of chemical species in a $CO-O_2$-He discharge are displayed in Figures V-4 through V-7. In these calculations, the electron density was taken to be 5×10^{-9} cm^{-3} initially with a gas mixture of 1.4 torr CO, 50μ O_2, and 18 torr He and E/N equal to 1.05^{-16} V-cm^2. The initial CO vibrational temperature was chosen to be 1000°K and as it increased the electron impact rate coefficients were recomputed at T_{vib} = 1500°, 2000°, 2200°, 2400°, etc. The species CO, O_2, O , O_2^*, and He were included in the calculation of the electron energy distribution function, but, as can be seen in Figure V-8 for a $CO-O_2$-He mixture, the presence of oxygen in small concentrations has little effect upon the shape of the distribution function.

These calculations show that O_2^+ becomes the dominant ion in CO lasers containing O_2 due to charge transfer reactions and that, as a consequence of recombination kinetics, it is responsible for the lowering of the E/N in a current regulated discharge. This is in direct opposition to the explanation advanced by Keren, et al.[38,39]. This lowering of E/N allows for more efficient pumping of the CO vibrational levels leading to increased power output. The calculations also demonstrate that O atoms, formed by
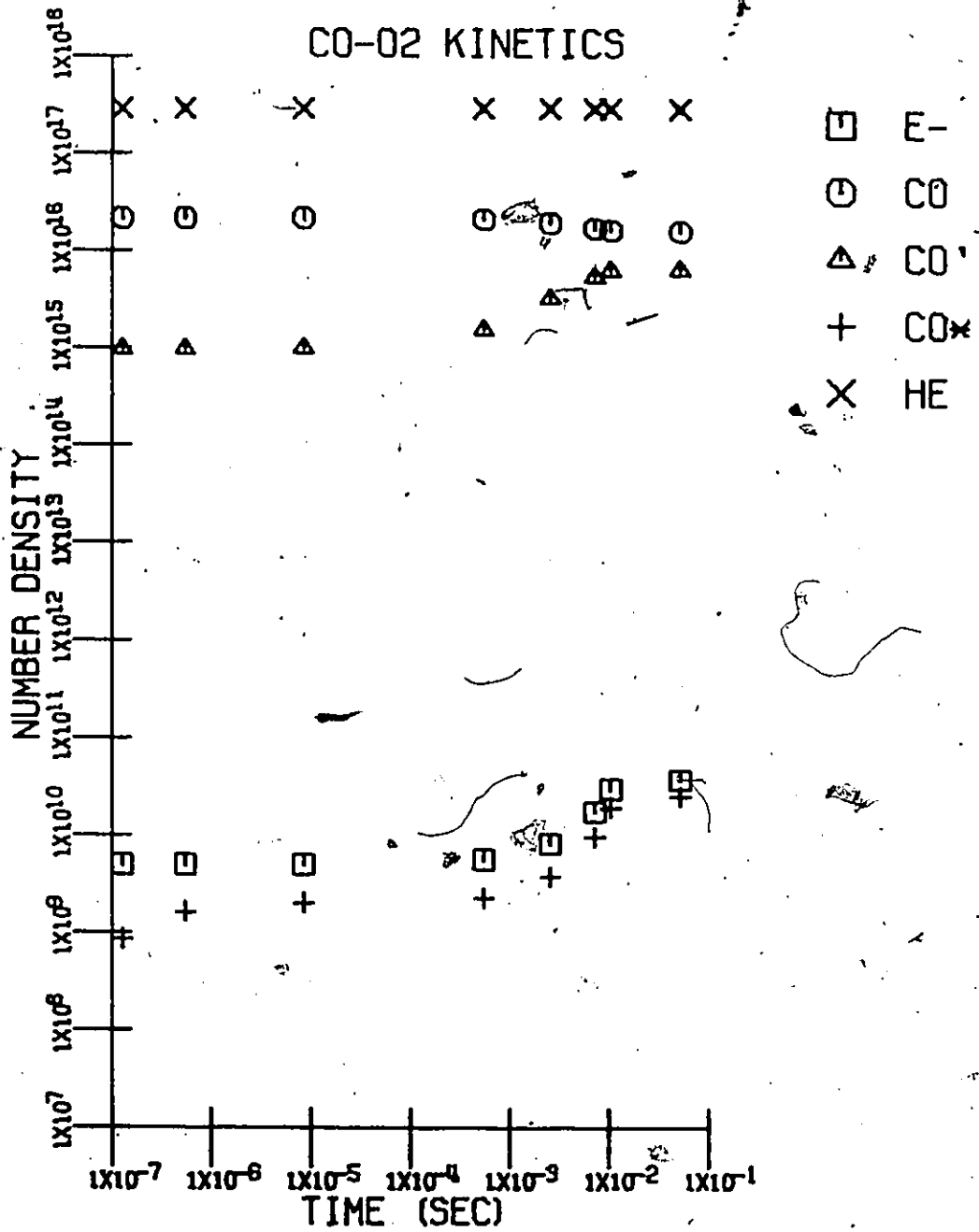
Figure V-4: CO-O_2 Kine[tics]

Figure V-5: CO-O$_2$ Kinetics

CO-O2 KINETICS

Legend:
- ⊟ CO+
- ⊕ C2O2+
- △ O2+
- + O+

NUMBER DENSITY (vertical axis): 1×10^7, 1×10^8, 1×10^9, 1×10^{10}, 1×10^{11}, 1×10^{12}, 1×10^{13}, 1×10^{14}, 1×10^{15}, 1×10^{16}, 1×10^{17}, 1×10^{18}

TIME (SEC) (horizontal axis): 1×10^{-7}, 1×10^{-6}, 1×10^{-5}, 1×10^{-4}, 1×10^{-3}, 1×10^{-2}, 1×10^{-1}
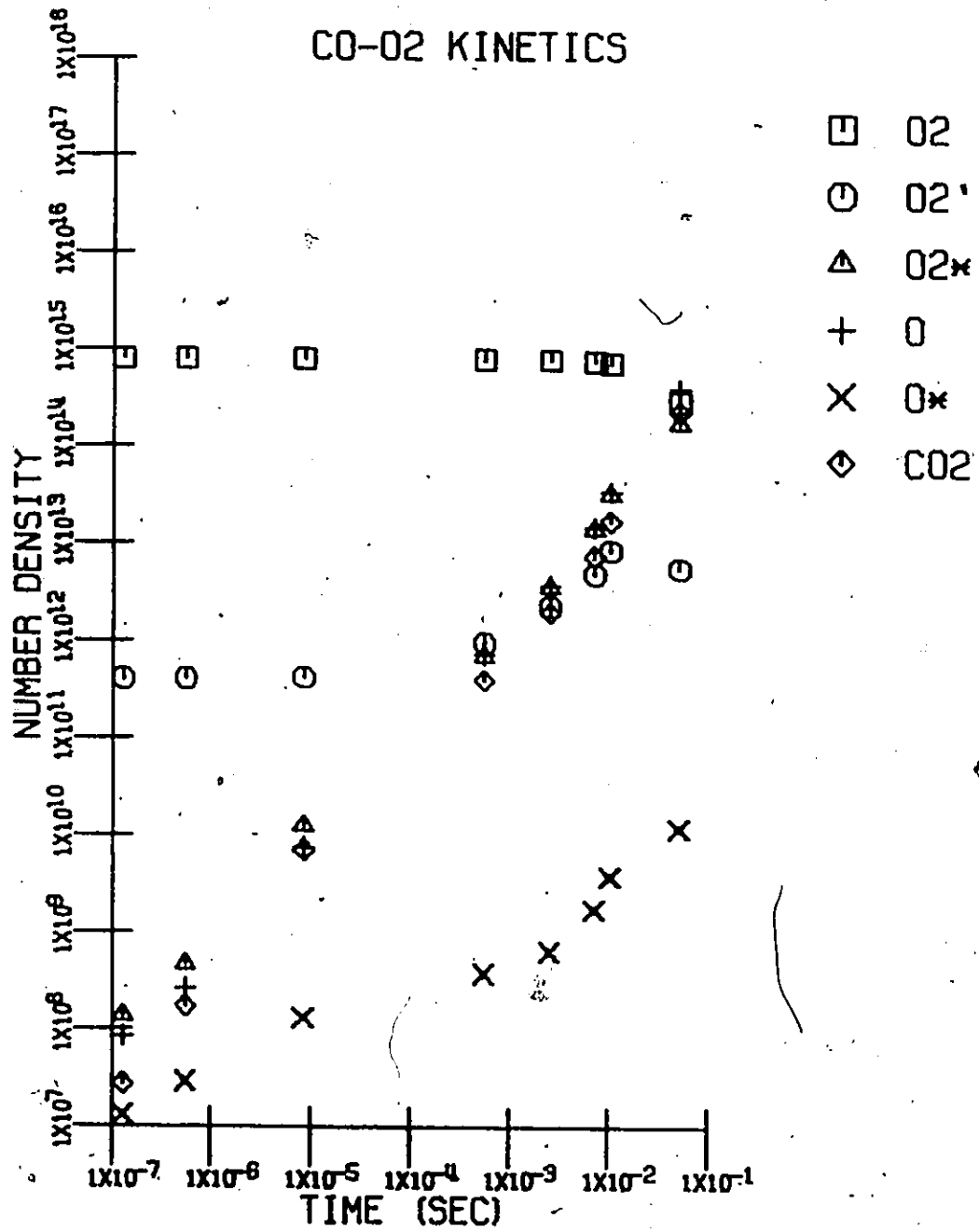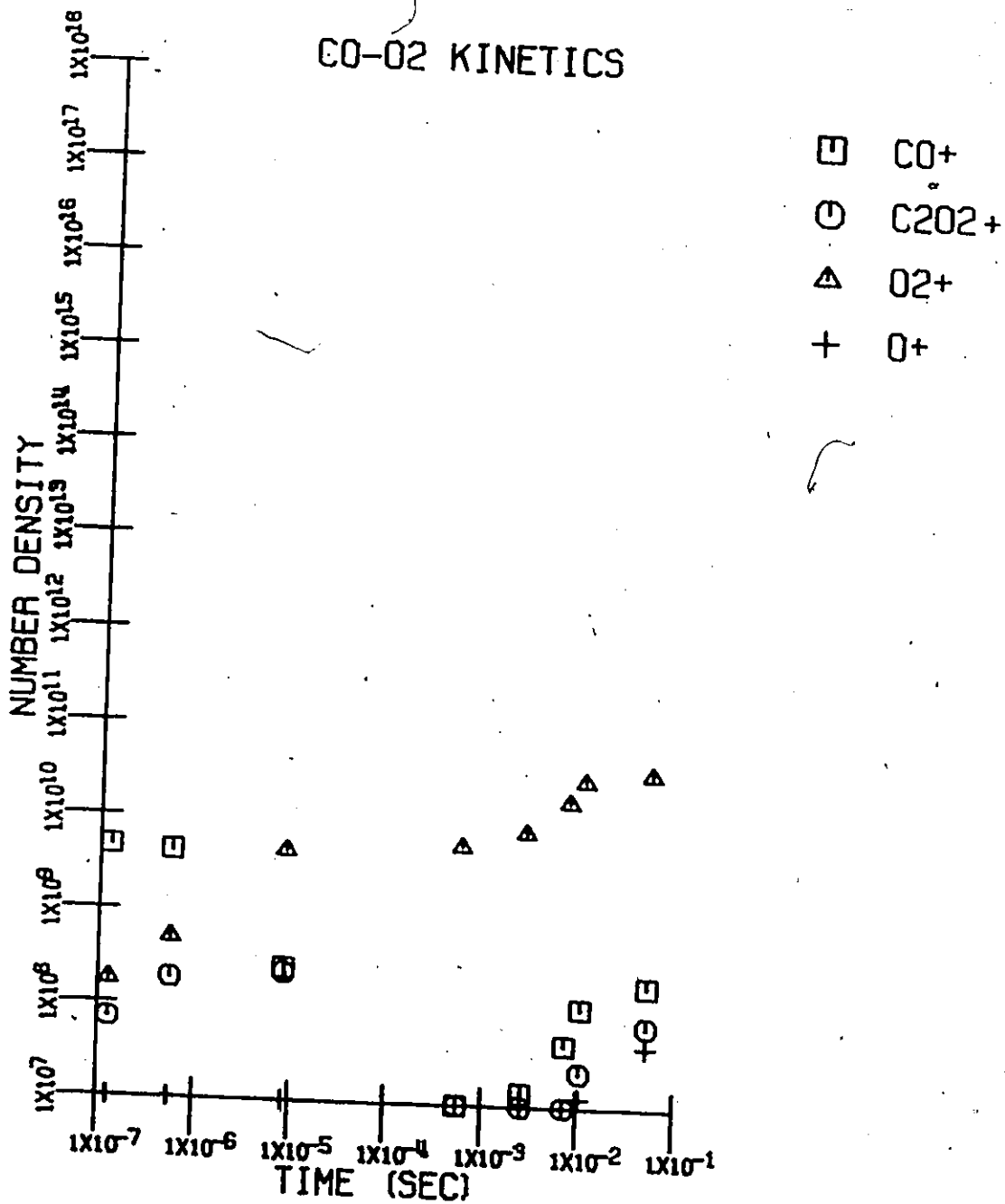
Figure V- 6   CO-O$_2$ Kinetics

CO-O2 KINETICS

Figure V-7: CO-O$_2$ Kinetics

58

1.4 torr CO
18 torr He
$E/N = 1.0 \times 10^{-16}$ V$_{-cm^2}$
Tv (CO) = 3000°K

1 - 0.0μ O_2
2 - 50 μ O_2
3 - 100μ O_2
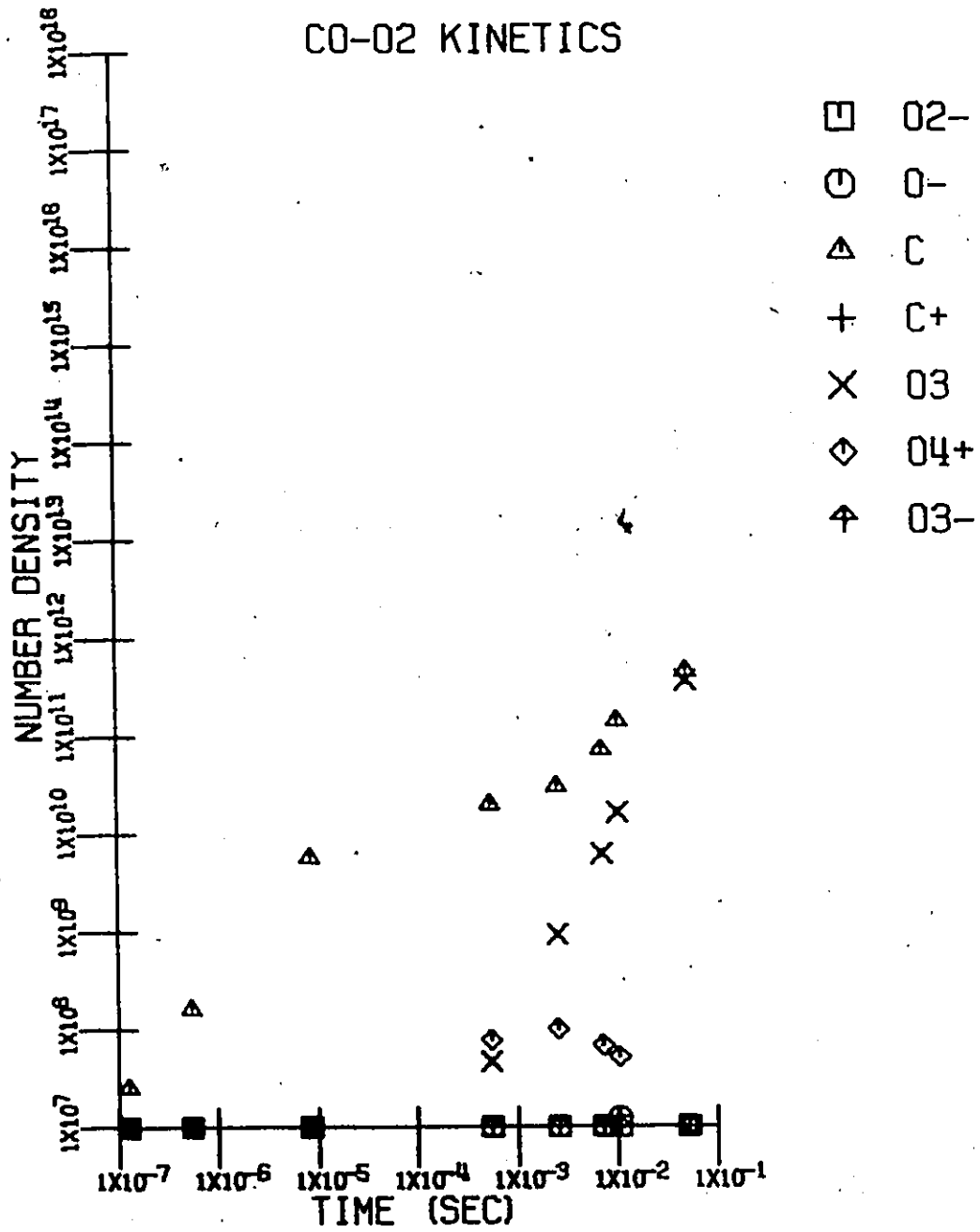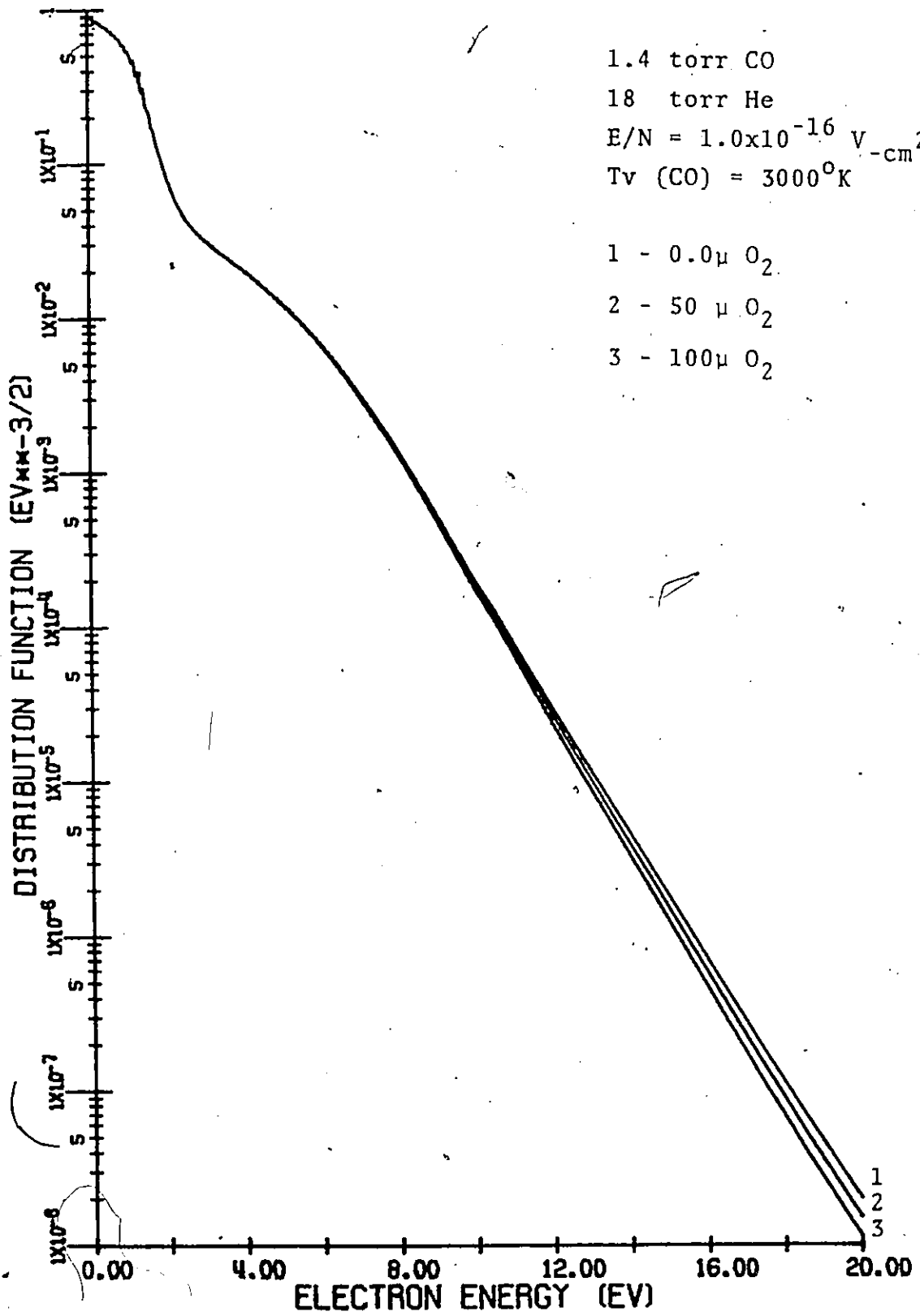
Figure V-8: Electron Energy Distribution Function for CO-O_2-He Mixture.

electron impact dissociation of O_2, have an adverse effect upon laser performance when O_2 is added in large enough concentrations. This is due to relaxation of the CO laser levels by vibrational translational energy exchange in CO-O collisions. The details of these findings, and others, are presented in the following sections.

Ion kinetics of the $CO-O_2$-He discharge

It was pointed out above that O_2^+ is found[39] to be the dominant positive ion in CO discharges containing oxygen, even when the O_2 is present in partial fractions less than 1%. The results of the calculation (Figure V-6) are in agreement with this observation. The dominance of O_2^+ is due to O_2 having the lowest ionization potential of the major species in the discharge and is formed almost entirely through charge transfer reactions. $C_2O_2^+$, which is the dominant ion in CO discharges without oxygen, and CO^+ both readily charge transfer with O_2 (reactions 52 and 54). Even though there is a large amount of atomic oxygen formed in the discharge, as will be discussed later, the O^+ ion does not appear in large concentrations because it too has a large rate coefficient for charge transfer with O_2 (reaction 34). The same is true of CO_2^+ although it has not been included in these calculations.

Ionization from the O_2 metastable, which appears in large concentrations due to reactions (11) and (56), $O_2 + e^- \rightarrow O_2^* + e^-$ (11); $CO^* + O_2 \rightarrow CO + O_2^*$ (56), has been included in

these calculations but is unimportant as a source of O_2^+ in comparison to the charge transfer processes. This observation is in disagreement with Keren et al.[38,39] who postulated that ionization via metastable O_2 is the dominant process for O_2^+ production.

This replacement of CO^+ and $C_2O_2^+$ by O_2^+ as the major ionic species has an important effect upon the voltage-current characteristics of the discharge. As can be seen in Figure V-3 the rate coefficient for recombination of O_2^+ is substantially smaller than that of either CO^+ or $C_2O_2^+$. This results in an increased electron density so that, under constant current operation, the electric field must be reduced. As has been repeatedly pointed out in this work, a lower electric field increases the efficiency of electron impact excitation of the CO vibrational states eventually resulting in increased power output.

As a test of this hypothesis a simple calculation was performed in which, given a recombination rate coefficient (as a function of electron temperature), E/N and CO vibrational temperatures were varied and ionization rate coefficients calculated in order to achieve a chosen current density. Current density, j (amp/cm^2) is related to electron drift velocity v_d (cm/sec) and number density Ne (cm^{-3}) by

$$j = ev_dN_e \text{ where } e = 1.6 \times 10^{-19} \text{ Coul.}$$

The usual assumption[71] is that the radial distribution of electron density in a cylinder of radius R is proportional

to the zeroth Bessel function of r/R:

$$\frac{N_e(r)}{N_e(o)} = J_o \left(2.4 \frac{r}{R}\right)$$

so that $N_e(r = R) = 0$. The total current, i, is then the integral of the current density over the discharge area,

$$i = 4\pi e v_d N_e(0) \int_0^R J_o\left(2.4 \frac{r}{R}\right) r dr$$

$$= 2.72 R^2 j \text{ (A)}$$

Hence, the experiments of Keren, et al.[38] on a 0.5 cm radius discharge at a current of 17 mA involve a current density of about 25 mA/cm^2. The drift velocity v_d can be computed from the electron energy distribution function. If one assumes that the only formation and removal processes for electrons are ionization and recombination, respectively, a steady state electron density can be computed from

$$\frac{d[e^-]}{dt} = k_{ion}[e^-][CO] - k_{recomb}[e^-][+ \text{ ion}]$$

If the ion and electron densities are assumed to be equal (i.e., one ion dominates), at steady state:

$$\frac{d[e^-]}{dt} = 0 \rightarrow [e^-]_{ss} = \frac{k_{ion}}{k_{recomb}}[CO]$$

Now if the same procedure is carried out for excitation of CO (v =1) by electrons and dexcitation by superelastic collisions with electrons, which is predicted (see below) to be the major loss process for low vibrational levels, we find at steady state

$$\frac{[CO\ (v=1)]}{[CO\ (v=0)]} = \frac{k_{0\to1}}{k_{1\to0}}$$

Using these two expressions and the equation for current density we can choose an E/N and CO vibrational temperature, solve the Boltzmann equation obtaining rate coefficients, temperature, and drift velocity, and calculate a current density and new vibrational temperature. This process can be repeated until the assumed and computed vibrational temperatures are equal and the desired current density has been obtained. This approach is, admittedly, crude, but contains the essence of the processes involved in establishing the electron density in the plasma. The greatest inaccuracy lies in the assumption concerning vibrational excitation and deexcitation of CO(v=1) since there are other important processes, such as excitation and de-excitation to and from CO(v=2, 3, ...), that affect the population of the V=1 level.

Despite its defects, this calculation gives results reasonable enough to illustrate the point concerning the relationship between recombination rate, E/N, and efficiency of vibrational excitation. The results are presented in Table V-3. To achieve similar current densities and vibrational temperatures using the O_2^+ recombination coefficient required a 10% decrease in E/N from the value needed using k_{recomb} (CO^+). The lowering of E/N resulted in a 34% decrease in the fraction of energy flowing into CO electronic states and a 9% increase in the fraction being

	Using k_{CO^+}	Using $k_{O_2^+}$
E/N (V-cm^2)	1.12×10^{-16}	1.01×10^{-16}
$[e^-]$ (cm^{-3})	$4.93 \times 10^{+10}$	$4.99 \times 10^{+10}$
j (amp/cm^2)	23.4×10^{-3}	22.2×10^{-3}
$\bar{\epsilon}$ (eV)	1.27	1.09
v_{drift} (cm/sec)	$2.97 \times 10^{+6}$	$2.78 \times 10^{+6}$
f(CO*)	21.3 %	14.0 %
f(CO$_{v=1}$)	18.1 %	19.8 %

Table V-3: Results of the simplified calculation of
ionization-recombination processes.

channeled into v=1 alone. Thus, in contrast to Keren et al., we have shown that O_2^+ directly effects both the E/N of the plasma and the excitation of CO vibrational energy, in agreement with the experimental observations.

Negative ions in a CO discharge

The time development of the negative ion densities is shown in Figure V-7. Although O^- is rapidly formed by dissociative attachment of CO and O_2, $CO + e^- \rightarrow C + O^-$ (6), $O_2 + e^- \rightarrow O + O^-$ (15), it is rapidly removed by detachment collisions with CO: $CO + O^- \rightarrow CO_2 + e^-$ (21). This is in contrast to the chemistry of CO_2 lasers as discussed by Nighan and Wiegand[5] and by Garscadden and his collaborators[72,73], where negative ions appear to control the stability of the discharge at low E/N. The results obtained here are consistent with the observation[5] that additions of CO to CO_2 lasers stabilize the discharge through electron detachment reactions with the negative ionic species.

The role of atomic oxygen in the discharge

As mentioned earlier in this section, at higher O_2 partial pressures the laser output power is found to decrease and the neutral temperature increase. Our calculations indicate that both of these effects are due to the formation of O atoms in the plasma. The cross sections for electron impact excitation of predissociative O_2 electronic states are large. This leads to large production

rates of oxygen atoms (reactions 14 and 17) and, conse-
quently, large O concentrations in the discharge. The
calculated time development of neutral oxygen species is
shown in Figure V-5.

For small concentrations of O_2 as an additive to
CO lasers the dissociation into O atoms has little effect
upon laser performance. Above some threshold O_2 concentra-
tions, however, vibrational-translational energy transfer
collisions between CO and O (reaction 59) is expected to
become the dominant deexcitation mechanism for high CO
vibrational levels. Since it is the higher vibrational
levels that dominate the laser output spectrum, the pre-
sence of O atoms will degrade the laser output. Examples
of vibrational deexcitation rate coefficients for CO (v=1)
and CO (v=12) are shown in Table V-4. For low vibrational
states (v=1 to v≈8) superelastic collision with electrons
is the primary deexcitation process. In the absence of
oxygen, radiation (reaction 76) and VT collision with He
(reaction 75) are primarily responsible for CO vibrational
deexcitation. The radiative rate per CO (v=12) molecule is
given by the Einstein A coefficient in Table V-4. The
deactivation rate per CO (v=12) by collision with He is
$k_{VT}[He]$ = 262 sec^{-1} for 18 torr of He. This is approxima-
tely the same as the radiation rate. Using the superelastic
rate coefficient for v = 1→0, which is probably too large
for the v = 12→11 transition, and an electron density of
10^{-10} gives a deexcitation rate of 10 - 100 sec^{-1}. Hence

Process	$v=1\to0$	$v=12\to11$
Radiation[1], A=	33.6 sec^{-1}	239.9 sec^{-1}
V-T with He[69], k= ($T_{gas}=300^{\circ}$K)	1.7×10^{-17} cm^3/sec	9.0×10^{-16} cm^3/sec
V-T with O[67], "	5.9×10^{-15} "	$\gtrsim2.9\times10^{-13}$[†] "
V-T with O_2[74], "		2.1×10^{-14} "
V-T with CO_2[74],"		8.6×10^{-14} "
Superelastic " with e$^-$,	10^{-9}-10^{-8}[††] "	

[†]The value shown is computed assuming the same scaling with v as the CO-He V-T process.

[††]The rate coefficient is typically in this range with its exact value depending upon the electron energy distribution function.

Table V-4: Deexcitation of CO vibrational levels.

radiation and He V-T exchange are likely to be the dominant deexcitation mechanisms.

When O atoms are present, even in small concentrations, they may strongly affect vibrational relaxation since the CO-O V-T rate coefficient is more than one hundred times larger than that for CO-He. If the same scaling with v is assumed for V-T relaxation by O atoms as exists for the He V-T process, an O partial pressure of 52 m-torr would be needed for CO-O V-T to be equal to the radiation or the CO-He V-T processes. Laser performance will be degraded when the contribution of the CO-O V-T rates is non-negligible in comparison to the fixed radiation and CO-He V-T rates. The scaling of vibrational relaxation rate coefficients with increasing vibrational level is, in general, uncertain. However, the collision system of $O(^3P) + CO(^1\Sigma, v')$, which correlates with the triplet state of CO_2, offers the possibility of a strong "chemical" interaction through curve crossing to the $CO_2(^1\Sigma)$ state and the enhanced energy transfer possibilities associated with a short lived triatomic complex.

Although these arguments are qualitative in nature, it is entirely plausible that the partial pressure of O_2 at which the laser output is seriously degraded (i.e., 100 m-torr) yields a 20% dissociation to O (i.e., 40 m-torr since each O_2 yields 2 O atoms) and the CO-O V-T process begins to relax the vibrationally excited CO leading to reduced laser output.

It can be seen from the rate coefficients in Table V-4 that vibrational relaxation by O_2 will be unimportant for the concentrations being discussed here. The same will be true for small concentrations of CO_2, which is formed primarily by reactions (21) and (23),

$$O^- + CO \rightarrow CO_2 + e^- \quad (21); \quad CO^* + CO \rightarrow C + CO_2 \quad (23).$$

The density of CO_2 is still increasing, however (Figure V-6), at the end of the calculation indicating that there may be a large buildup of this species in closed CO systems. In flowing discharges with a residence time of .1 - .5 sec this may not be a problem but in a sealed system CO_2 may be present in large enough concentrations to be a major source of vibrational deexcitation.

Additional discussion of CO laser chemistry

Carbon in the CO laser is formed primarily by reaction (23). Reactions (22) and (23)

$$CO^* + CO \rightarrow CO^+ + CO^+ \quad (22)$$

$$CO^* + CO \rightarrow C + CO_2 \quad (23)$$
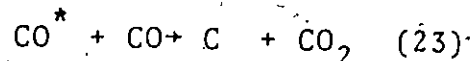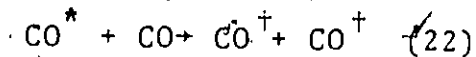
correspond to two channels for deexcitation of CO^* by CO. The total rate coefficient is known[54], but the branching ratio is not. It has been assumed in these calculations that 10% of the CO^* + CO reactions follow the C + CO_2 branch. The C production rate is critically dependent upon this branching ratio and there is, unfortunately, no information on the branching ratio or even on the carbon concentrations found in CO discharges. The carbon is

readily removed by reaction (44)

$$C + O_2 \rightarrow CO^\dagger + O^* \qquad (44)$$

with O_2. This is a satisfactory explanation of the observation that the addition of O_2 to a CO discharge reduces the quantity of carbon deposited in the system. The products of this reaction have been assumed to be $CO^\dagger$ and $O(^1D)$ as these are spin allowed and energetically accessible.

Finally, mention should be made of the possible role of $O(^1D)$ in the discharge. It is rapidly formed by reactions (17) and (28):

$$O_2 + e^- \rightarrow O + O^* + e^- \qquad (17)$$

$$O_2^+ + e^- \rightarrow O + O^* \qquad (28)$$
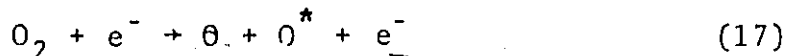
and, perhaps, (44) as discussed above. The O^* is then rapidly removed in reactions (57) and (58).

$$O^* + CO \rightarrow O + CO^\dagger \qquad (57)$$

$$O^* + CO \rightarrow O + CO \qquad (58)$$
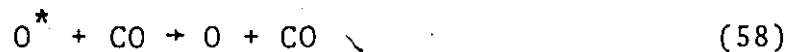
Although O^* has little effect upon the chemistry of the system it may, in this way, be an important source for heating the gas.

Using the reaction rates for both $O(^1D)$ quenching into translational energy (reaction 58) and relaxation of $CO^\dagger$ into translational energy (reaction 59) as given in Table V-5, the total energy flux from these reactions is

1. 9.22^{-9}, 5.36^{18}

2. 2.24^{-8}, 5.19^{18}

3. 7.67^{-11}, 4.46^{16}

4. 1.57^{-8}, 1.47^{13}

5. 2.98^{-14}, 1.73^{13}

6. 3.29^{-14}, 1.91^{13}

7. 1.12^{-16}, 6.50^{10}

8. 2.98^{-14}, 6.90^{12}

9. 2.35^{-10}, 1.16^{15}

10. 4.16^{-10}, 3.94^{13}

11. 1.88^{-10}, 9.35^{14}

12. 5.44^{-10}, 2.93^{15}

13. 8.02^{-14}, 3.98^{11}

14. 5.51^{-11}, 2.73^{14}

15. 5.97^{-12}, 2.93^{13}

16. 7.46^{-18}, 3.70^{7}

17. 2.99^{-11}, 1.48^{14}

18. 6.16^{-10}, 1.44^{16}

19. 5.97^{-14}, 1.39^{12}

20. 1.90^{-13}, 1.03^{12}

21. 7.30^{-10}, 4.87^{13}

22. 9.90^{-8}, 3.95^{16}

23. 1.10^{-11}, 4.39^{15}

24. 1.43^{-28}, 8.42^{12}

25. 2.10^{-12}, 4.44^{12}

26. 7.32^{-08}, 3.62^{11}

27. 1.01^{-08}, 1.30^{13}

28. 1.01^{-08}, 1.30^{13}

29. 7.50^{-11}, 1.64^{14}

30. 6.43^{-34}, 1.67^{13}

31. 3.80^{-12}, 3.01^{10}

32. 2.00^{-14}, 6.14^{12}

33. 1.50^{-13}, 9.79^{12}

34. 4.00^{-11}, 2.64^{11}

35. 8.00^{-29}, 3.13^{10}

36. 1.00^{-07}, 1.47^{10}

37. 2.00^{-10}, 5.35^{11}

38. 5.00^{-15}, 2.84^{06}

39. 1.00^{-11}, 1.79^{11}

40. 3.00^{-10}, 1.86^{11}

41. 1.90^{-27}, 8.53^{07}

42. 1.00^{-33}, 1.52^{09}

43. 1.00^{-31}, 7.15^{11}

44. 3.30^{-11}, 4.38^{15}

45. 6.98^{-19}, 2.23^{08}

46. 2.30^{-10}, 7.87^{12}

47. 1.80^{09}, 5.42^{10}

48. 1.10^{-09}, 1.08^{10}

49. 9.20^{-08}, 8.05^{11}

50. 8.40^{-27}, 2.25^{10}

Table V-5: Rate Constants and Rates of Individual Reactions[†]
at t = 0.1 sec

Table V-5, continued

51. 1.00^{-32}, 1.91^{12}

52. 2.00^{-10}, 1.08^{10}

53. 1.40^{-10}, 2.10^{13}

54. 2.00^{-10}, 3.61^{12}

55. 1.10^{-09}, 2.21^{13}

56. 2.00^{-10}, 6.82^{14}

57. 1.72^{-11}, 4.42^{15}

58. 5.58^{-11}, 1.43^{16}

59. 5.90^{-15}, 2.34^{16}

60. 5.00^{-10}, 1.83^{09}

61. 3.28^{-10}, 1.20^{09}

62. 4.20^{-07}, 8.42^{07}

63. 2.00^{-18}, 1.56^{00}

64. 4.00^{-10}, 1.12^{06}

65. 2.00^{-10}, 1.69^{08}

66. 1.00^{-09}, 2.05^{09}

67. 1.00^{-07}, 9.67^{07}

68. 2.00^{-07}, 1.93^{08}

69. 1.00^{-10}, 1.76^{09}

70. 1.00^{-13}, 1.76^{06}

71. 2.80^{-30}, 1.75^{09}

72. 1.00^{-31}, 1.43^{11}

73. 2.00^{-13}, 2.00^{07}

74. 3.00^{-10}, 1.41^{11}

75. 1.70^{-17}, 3.09^{16}

76. 3.36^{+01}, 2.11^{17}

77. 1.60^{-15}, 1.19^{15}

78. 1.11^{-07}, 3.05^{09}

79. 2.00^{-27}, 1.11^{09}

[†]See Table V-2 for a listing of the reactions

sufficient to explain the observed[37] gas temperature increase with increasing O_2 pressure beyond the optimum pressure for laser output..

VI. Conclusion

This report has outlined the theory and methodology behind modeling the steady state plasma of a molecular laser system incorporating both the inelastic and superelastic processes appropriate to a given laser mix. Sample calculations on the CO/N_2 laser system have confirmed the non-Boltzmann character of the electron energy distribution function in substantial agreement with the earlier work of Nighan[4] and Rockwood[3]. The effect of added N_2 is shown to increase the density of electrons in the energy range for maximum coupling to CO vibrational energy but detailed calculations on excitation rates indicate that this shift is essentially compensated for by the decrease in CO partial pressure required to maintain a constant total molecular density (constant E/N). If superelastic processes are included in the CO/N_2 mixture case, further support is given to pure CO being the optimum mixture for coupling the electron energy into CO.

The laser plasma code discussed in this report is very efficient and is easily extended to any number of molecular or atomic constituents for which cross section information is available. The results of the plasma calculations presented here are in substantial agreement with the results of other workers as well as measured drift velocities for N_2 and CO. There are, however, clear indications from the results of the calculations presented in

this report that reliable cross section information is critical to the understanding and optimization of laser plasma performance.

We have presented results of calculations on the chemical kinetics of the CO laser with O_2 as an additive. We have shown that vibrational temperature is an important parameter in the evaluation of ionization and recombination rate coefficients, and, in these calculations, have used rate coefficients for excitation and ionization computed from an electron energy distribution that includes the effects of gas composition and vibrational temperature. These calculations have demonstrated that O_2^+ is the dominant ion in $CO-O_2$ systems as a consequence of charge transfer reactions with CO^+ and $C_2O_2^+$. In a current regulated discharge this results in a lowering of the E/N leading to more efficient pumping of the CO vibrational levels. We have also found, from these calculations, that O atoms, formed by electron impact dissociation of O_2, have a deleterious effect upon CO laser performance for large concentrations of O_2 as an additive. This is due to relaxation of the CO laser levels by vibrational translational energy exchange in $CO^\dagger$-O collisions.

These results suggest that Xe and Hg, which are known to enhance laser output even if present in very small concentrations[36] may affect the plasma chemistry of the CO laser in a similar manner to O_2 as the Xe^+ and Hg^+ ions can be expected to recombine much more slowly than O_2^+. In

addition, due to their low ionization potentials, they may
enhance ionization rates. With knowledge of the funda-
mental processes occurring in laser discharges and the
ability to perform plasma and kinetics calculations such
as those presented in this work, one should be able to
search systematically for additives that affect the plasma
chemistry in such a way as to produce desired laser per-
formance characteristics.

References

1. G. Abraham and E. R. Fisher, J. Appl. Phys., 43, 4621 (1972).

2. E. R. Fisher, J. Appl. Phys., 44, 5031 (1973).

3. S. D. Rockwood, J. E. Brau, W. A. Proctor, and G. H. Canavan, J.Q.E., 9, 120 (1973).

4. W. L. Nighan and W. J. Wiegand, Phys. Rev., A10, 922 (1974).

5. W. L. Nighan, Phys. Rev., A2, 1989 (1970).

6. J. J. Lowke, A. V. Phelps and B. W. Irwin, Westing-house Research Labs Scientific Paper 73-1V8-ARCPL-P1, January (1973); J. Appl. Phys., 44, 4664 (1973).

7. L. J. Kieffer, JILA Report No. 13, September (1973).

8. K. Huang, Statistical Mechanics, Wiley (New York), 1963; I. P. Shkarofsky, et al., The Particle Kinetics of Plasmas, Addison-Wesley (Reading, Mass.); Kinetic Processes in Gases and Plasmas, A. R. Hochstim, ed., Academic Press (New York),1969.

9. R. A. Haas, Phys. Rev., A8, 1017 (1973).

10. T. Holstein, Phys. Rev., 70, 367 (1946); I. Abdelnabi and H. S. W. Massey, Proc. Phys. Soc. of London A66, 288 (1953); V. L. Ginzburg and A. V. Gure-vich, Usp. Fiz. Nauk., 70, 201 (1960), (Sov. Phys. Usp., 3, 115).

11. W. L. Nighan, Op. Cit.; I. P. Shkarofsky, Op. Cit.; A. R. Hochstim, Op. Cit.

12. K. Huang, Op. Cit.

13. T. Holstein, Op. Cit.; I. P. Shkarofsky, Op. Cit.; A. R. Hochstim, Op. Cit.

14. T. Y. Wu and T. Ohmura, Quantum Theory of Scattering, Prentice-Hall (Englewood Cliffs, New Jersey), 1962; L. S. Frost and A. V. Phelps, Phys. Rev., 127, 1621 (1962).

15. L. S. Frost and A. V. Phelps, Op. Cit.

16. N. P. Carleton and L. R. Megill, Phys. Rev., 126, 2089 (1962).

17. K. K. Gibson, Aust. J. Phys., 23, 283 (1970).

18. C. J. Elliot, O. P. Judd, A. M. Lockett, and S. D. Rockwood, Los Alamos Scientific Laboratory Report, LA-5562-MS (1974).

19. S. D. Rockwood, Phys. Rev., A8, 2348 (1974).

20. I. P. Shkarofsky, Op. Cit.

21. B. Sherman, J. of Math. Anal. and Applications, I, 342 (1960).

22. B. Carnahan, et al., Applied Numerical Methods, Wiley (New York), 1969.

23. J. C. Y. Chen, J. Chem. Phys., 40, 3507 (1964).

24. G. Abraham and E. R. Fisher, Research Institute for Engineering Sciences, Wayne State University, Report No. RIES 71-31, March 1971).

25. M. J. W. Boness and G. J. Schulz, Phys. Rev., A8, 2883 (1973).

26. H. Ehrhardt, L. Langhans, E. Liner and H. S. Taylor, Phys. Rev., 173, 222 (1968).

27. R. D. Hake and A. V. Phelps, Phys. Rev., 158, 70 (1967).

28. A. G. Engelhardt, A. V. Phelps and C. G. Rick, Phys. Rev., 135, A1566 (1964).

29. S. D. Rockwood, Los Alamos Scientific Labs Preprint, December (1972).

30. H. S. W. Massey and E. H. S. Burhop, Electronic and Ionic Impact Phenomena, Vol. II, Oxford Press, (1969).

31. C. E. Treanor, J. W. Rich, R. G. Rehm, J.C.P., 48, 1798 (1968).

32. E. R. Fisher and R. H. Kummler, J.C.P., 49, 1075, 1085 (1968).

33. G. E. Caledonia and R. E. Center, J.C.P., 55, 552 (1971).

34. J. W. Rich, J.A.P., $\underline{42}$, 2719 (1971).

35. S. Yarema, MS Thesis, Dept. of Electrical Engineering, Wayne State University, June (1974).

36. M. L. Bhaumik, W. B. Lacina and M. M. Mann, IEEE.J.Q.E., $\underline{8}$, 150 (1972).

37. T. S. Hartwick and J. Walder, IEEE J. Q. E., $\underline{8}$, 455 (1972).

38. H. Keren, P. Avivi, F. Dothan, IEEE J. Q. E., $\underline{11}$, 590 (1975).

39. H. Keren, P. Avivi, F. Dothan, IEEE J. Q. E., $\underline{12}$, 58 (1976).

40. R. E. Center, J. Appl. Phys., $\underline{44}$, 3538 (1973).

41. E. N. Lassetre and S. M. Silverman, J. C. P., $\underline{40}$, 1256 (1964).

42. S. Trajmar, W. Williams, and D. C. Cartwright, Proc. Seventh Int. Conf. on Physics of Electronic and Atomic Collisions, ed. L. M. Branscomb, et al. (North-Holland, Amsterdam), 1971.

43. M. J. Mumma, E. J. Stone, E. C. Zipf, J. Chem. Phys., $\underline{54}$, 2627 (1971).

44. J. M. Ajello, J. Chem. Phys., $\underline{55}$, 3158 (1971).

45. S. Chung, C. C. Lin, Phys. Rev., $\underline{A8}$. 2463 (1973).

46. T. Sawada, D. L. Sellin, A. E. S. Green, J. G. R., $\underline{77}$, 4819 (1972).

47. This transition is thought to go to the $c^1\Sigma_u^-$ state rather than the $A^3\Sigma_u^+$ state by S. Trajmar, W. Williams, and A. Kupperman, J. Chem. Phys., $\underline{56}$, 3759 (1972).

48. P. H. Krupenie, J. Phys. Chem. Ref. Data, $\underline{1}$, 423 (1972).

49. H. F. Schaefer III, and W. H. Miller, J.C.P., $\underline{55}$, 1107 (1971).

50. P. D. Burrow, J. C. P., $\underline{59}$, 4922 (1973).

51. The 9.9 eV energy loss process has been recently identified as a $^3\pi_u$ Rydberg state by D. C. Cartwright W. J. Hunt, W. Williams, S. Trajmar, and W. A. Goddard III, Phys. Rev., A8, 2436 (1973).

52. T. Keneshea, Air Force Cambridge Research Laboratory, Report No. AFCRL-67-0221, Environmental Paper No. 263, 1967.

53. D. A. Parkes, Trans. Faraday Soc., 68, 627 (1972).

54. G. W. Taylor and D. W. Setser, J. Chem. Phys., 58, 4040 (1973).

55. J. J. Leventhal and L. Friedman, J. Chem. Phys., 46, 997 (1967).

56. M. Saporoschenko, J. Chem. Phys., 49, 768 (1968).

57. S. L. Chang and J. L. Franklin, J. Chem. Phys, 54, 1487 (1971).

58. R. L. Horton, J. L. Franklin, B. Masseo, J. Chem. Phys., 62, 1739 (1975).

59. J. M. Bardsley and M. A. Biondi, "Dissociative Recombination," in Advances in Atomic and Molecular Physics, ed. D. R. Bates, Vol. 6 (Academic Press, New York, 1970).

60. R. J. Donovan and D. Hussain, Chemical Reviews, 70, 489 (1970).

61. K. Schofield, Planet. Space Sci., 15, 643 (1967).

62. E. W. McDaniel, et al., Ion-Molecule Reactions (Wiley-Interscience, New York, 1970).

63. M. H. Bortner, R. H. Kummler, T. Baurer, "Summary of Suggested Rate Constants," Defense Nuclear Agency Reaction Rate Handbook, Ch. 24, DNA 1948H (Revision No. 3, September 1973).

64. E. W. McDaniel, Collision Phenomena in Ionized Gases (Wiley, New York, 1964).

65. M. B. McElroy and J. C. McConnell, J. Geophys. Res., 76, 6674 (1971).

66. R. G. Shortridge and M. C. Lin, to be published in J. Chem. Phys.

67. R. E. Center, Proc. Ninth Int. Shock Tube Symposium, ed. D. Bershader and W. Griffith (Stanford Univ. Press, Stanford, Calif., 1973).

68. F. E. Niles, J. Chem. Phys., 52, 408 (1970).

69. M. R. Verter and H. Rabitz, J. Chem. Phys., 64, 2939 (1976).

70. R. C. Millikan and D. R. White, J. Chem. Phys., 39, 3209 (1963).

71. J. D. Cobine, Gaseous Conductors (Dover, New York, 1958).

72. J. F. Prince and A. Garscadder, Appl. Phys. Lett., 27, 13 (1975).

73. P. Bletzinger, et al., IEEE J. Q. E., 11, 317 (1975).

74. G. Hancock and I. W. M. Smith, Appl. Optics, 10, 1827 (1971).

75. D. Rapp and D. D. Briglia, J. Chem. Phys., 43, 1480 (1965).

76. S. Trajmar, D. C. Cartwright, W. Williams, Phys. Rev., A4, 1482 (1971).

77. C. E. Watson, et al., J. Geophys. Res., 72, 3961 (1967).

78. L. D. Thomas and R. K. Nesbet, Phys. Rev., A11, 170 (1975).

PART II

CALCULATION OF THE RELATIVISTIC FORM FACTOR

FOR ELECTRON IMPACT IONIZATION OF ARGON

I. Introduction

This work arose out of an effort to model the physical processes involved in pumping high pressure gas lasers using a relativistic electron beam.[1] In these systems, the energetic electrons in the incident beam produce many low energy secondary electrons as a result of ionizing collisions with the target laser gas. The secondary electrons are then responsible for most of the subsequent excitation processes in the gas.

As a specific example, energy loss calculations for a relativistic electron beam in argon depend upon a knowledge of the ionization cross-section differential in energy loss $d\sigma/dW$. Large discrepancies were found at relativistic energies between the total cross-section computed from the semi-empirical analytic form for $d\sigma/dW$ based on the Bethe-Born approximation, as given by Peterson and Allen[2], and the experimental cross sections[3]. The Peterson and Allen total cross sections have the correct non-relativistic $A \ln E/E + B/E$ energy dependence, where E is the incident electron energy, but it incorrectly retains this energy dependence for larger relativistic impact energies (i.e., above about 10^5 eV). Since the experimental $\sigma(E)$ starts to level off at about 10^5 eV and even rises at higher energy, due to relativistic effects that will be discussed later,

81

the Peterson and Allen total ionization cross section is too small at relativistic impact energies. It is, for example, approximately a factor of five too small at 10^6 eV and is even worse at higher energy.

Although the reason for this was the use of the non-relativistic Bethe-Born approximation by Peterson and Allen the problem stimulated interest in doing a completely relativistic calculation of the so-called Bethe surface for the ionization of argon within the framework of the Bethe-Born approximation.[4] This is what is attempted in the presentation that follows.

Although this problem is now far removed from the laser studies mentioned above, and, in fact, is much more detailed and involved than is necessary for the laser modelling work, it does have merit in its own right. It serves as a test of the relativistic Bethe-Born approximation and is, to my knowledge, the first time that a proper calculation of the relativistic Bethe surface using relativistic self-consistent atomic wave functions has been attempted.

In the discussion that follows, cgs units have been used except for energy, which is given in electron volts. In analyses taken from other authors, their units, whatever they may be, have been converted to the cgs-eV system for the sake of consistency.

II. The Bethe-Born Theory for Ionization of Atoms by Relativistic Electrons

As shown by Bethe[5,4], the relativistic form of the differential cross section for ionization by electron impact is given, in first order perturbation theory, by

$$\frac{d^2\sigma}{dWd\Omega} = \frac{1}{4\pi^2} \frac{E_i}{\hbar^4} \frac{E_f}{c^4} \frac{k_f}{k_i} |U|^2 \quad cm^2/eV/sr \qquad (1)$$

where E_i and E_f are, respectively, the initial and final total energy of the incident electron,

$$E_i = (m^2c^4 + c^2\hbar^2k_i^2)^{1/2}$$

$$E_f = (m^2c^4 + c^2\hbar^2k_f^2)^{1/2} = E_i - W$$

W is the energy loss, k_i and k_f are the initial and final propagation vectors ($\vec{k} \equiv \vec{p}/\hbar$), and $d\Omega$ is the element of solid angle for the scattered electron.

The matrix element U is proportional to the interaction energy between the incident electron and the atom and is given by

$$U = \int \Psi_f^*(\vec{r}) \, V(\vec{r}) \, \Psi_i(\vec{r}) \, d\vec{r} \qquad (2)$$

where $V(\vec{r})$ = the potential energy of the incident electron and the atom;

$\Psi_i(\vec{r})$ = the initial wavefunction of the system of incident electron + atom;

$\Psi_f(\vec{r})$ = the final wavefunction of the system.

In the first Born approximation[6] the wavefunctions of the incident electron and of the atom are assumed to be

independent and thus the wavefunction of the system is describable as a product of the electron wavefunction, $\phi(\vec{r})$, and the atom wavefunction, $\psi(\vec{r}_i)$ for the ith atomic electron. If the atom has z electrons, the matrix element (2) becomes

$$U = \int \phi_f^*(\vec{r})\, \psi_f^*(\vec{r}_1,\ldots,\vec{r}_z)\, V(\vec{r};\vec{r}_1,\ldots,\vec{r}_z) \quad (3)$$
$$\phi_i(\vec{r})\, \psi_i(\vec{r}_1,\ldots,\vec{r}_z)\, d\vec{r}_1\ldots d\vec{r}_z d\vec{r}$$

In the Born approximation, the electron wavefunctions $\phi(r)$ are taken to be plane wavefunctions, $e^{i\vec{k}\cdot\vec{r}}$ in non-relativistic theory, and $u(\vec{p})e^{i\vec{k}\cdot\vec{r}}$ in the relativistic case. The Dirac plane wavefunctions will be discussed in a later section.

In the Bethe-Born approximation we assume that the collision can be described as a binary collision between the incident electron and the atomic electron that is ejected as a result of the collision. Using this assumption and the Møller[7],[8] formula for the interaction between two relativistic electrons, the matrix element (3) becomes

$$U = e^2 \int\limits_{\vec{r}_1}\int\limits_{\vec{r}_2} \phi_f^*(\vec{r}_1)\psi_f^*(\vec{r}_2)\, \frac{1-\vec{\alpha}_1\cdot\vec{\alpha}_2}{|\vec{r}_1-\vec{r}_2|}\, e^{i\frac{W}{\hbar c}|\vec{r}_1-\vec{r}_2|}$$

$$\phi_i(\vec{r}_1)\, \Psi_i(\vec{r}_2)\, d\vec{r}_1\, d\vec{r}_2 \quad (4)$$

where $|\vec{r}_1-\vec{r}_2|$ is the distance between the two electrons and $\vec{\alpha}_1$ and $\vec{\alpha}_2$ are the Dirac operators. Here the $\vec{\alpha}_1$ and

the $\vec{\alpha}_2$ operate on the $\phi_i(\vec{r}_1)$ and $\psi_i(\vec{r}_2)$ respectively. The exponential is the retardation factor, which is due to the finiteness of the speed of light. The terms involving the $\vec{\alpha}$'s arise from the magnetic interaction of the spins of the two electrons, electron spin being an intrinisic part of relativistic quantum theory. The Bethe-Born approximation is used not only because it is a good approximation for high energy encounters[4], but also because it is about the only way of doing relativistic calculations since, in relativistic theory, there is no known general form for the many body interaction energy in closed form.

The exchange matrix element is the same as (4) except with the final wavefunction given by $\phi_i(\vec{r}_2)$ $\psi_f(\vec{r}_1)$. As shown by Mott and Massey[40], by Rudge[41], and, for relativistic interactions, by Perlman[10], the exchange matrix element is negligible for high (relative to the ionization energy) impact energies such as are being dealt with in this work. Hence it will be neglected here.

For the ionization calculation ψ_i is a bound state wavefunction and ψ_f is a continuum wavefunction. If the wavefunctions ϕ_i and ϕ_f are taken to be plane waves we have the Born approximation.

Let

$$\phi_i(\vec{r}_1) = u_i(\vec{p}_i)e^{i\vec{k}_i \cdot \vec{r}_1}$$

$$\phi_f(\vec{r}_1) = u_f(\vec{p}_f)e^{i\vec{k}_f \cdot \vec{r}_1}$$

then

$$U = e^2 \int_{r_2} \int_{r_1} \left\{ e^{i(\vec{k}_i - \vec{k}_f) \cdot \vec{r}_1} \quad \frac{e^{i\frac{W}{\hbar c}|\vec{r}_1 - \vec{r}_2|}}{|\vec{r}_1 - \vec{r}_2|} d\vec{r}_1 \right\} \tag{5}$$

$$u_f^* \psi_f^*(\vec{r}_2)(1 - \vec{\alpha}_i \cdot \vec{\alpha}_2) u_i \psi_i(\vec{r}_2) d\vec{r}_2$$

The integral over $\vec{r}_1$ is[8,10]

$$\frac{4\pi}{K^2 - \frac{W^2}{(\hbar c)^2}} \quad e^{i\vec{K} \cdot \vec{r}_2}$$

where $\vec{K} = \vec{k}_i - \vec{k}_f$.

This gives for the cross section,

$$\frac{d^2\sigma}{dWd\sigma} = \frac{4e^4}{\hbar^4 c^4} E_i E_f \left(\frac{k_f}{k_i}\right) \frac{1}{\left[K^2 - \frac{W^2}{\hbar^2 c^2}\right]^2} \tag{6}$$

$$\Sigma \left| \int_{\vec{r}_2} e^{i\vec{K} \cdot \vec{r}_2} u_f^* \psi_f^*(\vec{r}_2)(1 - \vec{\alpha}_1 \cdot \vec{\alpha}_2) u_i \psi_i(\vec{r}_2) d\vec{r}_2 \right|^2$$

The integral over $\vec{r}_2$ is defined as the relativistic form factor[5], $\eta(W,K)$. The calculation of this quantity is the main object of this work and will be discussed later. The Σ represents a sum over all degenerate final states (angular momenta, electron spins, etc.) and an average over all degenerate initial states.

If the variable Q is defined as[4,5,11]

$$Q \equiv \frac{1}{2m}(\hbar^2 K^2 - W^2/c^2)$$

which is approximately the recoil kinetic energy of the ejected electron, then the element of solid angle, $d\Omega$

can be replaced by

$$d\Omega = \frac{2\pi K dK}{k_i k_f} = \frac{2\pi m}{\hbar^2} \frac{dQ}{k_i k_f}$$

and the cross section becomes

$$\frac{d^2\sigma}{dWdQ} = \frac{2\pi e^4}{\beta^2 mc^2} \left(\frac{E_f}{E_i}\right) \frac{|\eta(W,Q)|^2}{Q^2}$$

where $\beta^2 = (E_i^2 - m^2c^4)/E_i^2 \equiv (v_i/c)^2$. The total cross section is then

$$\sigma = \frac{2\pi e^4}{\beta^2 mc^2} \int_I^{(E_i+I)/2} dW \int_{Q_{min.}}^{Q_{max}} |\eta(W,Q)|^2 \frac{dQ}{Q^2}$$

where Q_{min} and Q_{max} are defined by $K_{min} = k_i - k_f$ and $K_{max} = k_i + k_f$. The factor of E_f/E_i has been neglected here as it is very close to unity.

As can be seen here, the important quantity in the theory of ionization is the form factor, $\eta(W,Q)$. In non-relativistic theory this reduces to the familiar matrix element $E(W,K) = <W|e^{i\vec{K}\cdot\vec{r}}|0>$. In atomic physics, the generalized oscillator strength,

$$\frac{df(K,W)}{dW} = \frac{W}{R_y(a_oK)^2} |\eta(W,K)|^2$$

where R_y is the Rydberg energy (13.6eV) and a_o is the Bohr radius, is generally used instead of the form factor.

$\frac{df}{dW}$ as a function of W and K defines a surface, called the

Bethe surface, which is characteristic of the atom. As pointed out by Inokuti[4], this is a useful generalization of the familiar optical dipole oscillator strength. In the limit of $K \rightarrow 0$, for high primary electron energy, this goes into the optical oscillator strength, df_o/dW[12]. For photoionization the energy loss, W, is equivalent to the photon energy, $\hbar\omega$, and the cross section is given by[13]:

$$\sigma(\omega) = \frac{2\pi^2 e^2 \hbar}{mc} \frac{df_0}{dW} = 1.098 \times 10^{-16} (cm^2 eV) \frac{df_0}{dW}$$

The existence of this limit allows some comparison[4] to be made between electron impact data and photoionization data as will be shown later.

III. Calculation of the Relativistic Form Factor

As defined previously the relativistic form factor
is given by $\eta(W,K) = \int\limits_{r_2} e^{i\vec{K}\cdot\vec{r}_2} u_f^* \psi_f^*(\vec{r}_2)(1-\vec{\alpha}_1\cdot\vec{\alpha}_2) u_i\psi_i(\vec{r}_2)d\vec{r}_2$

$$(1)$$

This is independent of the direction of $\vec{K}$ because the co-ordinate system is chosen so that $\vec{K}$ points along the z-axis which is also taken to be the quantization axis for the wavefunctions.

Here the initial four-vector Dirac wavefunctions, u_i and ψ_i, of the incident and bound electron, respectively, are operated on by the Dirac matrices $\vec{\alpha}_1$ and $\vec{\alpha}_2$. The $\vec{\alpha}$'s have three components which are[6]

$$\alpha_x = \begin{pmatrix} 0 & 0 & 0 & 1 \\ 0 & 0 & 1 & 0 \\ 0 & 1 & 0 & 0 \\ 1 & 0 & 0 & 0 \end{pmatrix} \quad \alpha_y = \begin{pmatrix} 0 & 0 & 0 & -i \\ 0 & 0 & i & 0 \\ 0 & -i & 0 & 0 \\ i & 0 & 0 & 0 \end{pmatrix} \quad \alpha_z = \begin{pmatrix} 0 & 0 & 1 & 0 \\ 0 & 0 & 0 & -1 \\ 1 & 0 & 0 & 0 \\ 0 & -1 & 0 & 0 \end{pmatrix}$$

The components of $\vec{\alpha}$ operating on a four-vector $\vec{\phi} = \begin{pmatrix} \phi_1 \\ \phi_2 \\ \phi_3 \\ \phi_4 \end{pmatrix}$

give the following:

$$\alpha_x\vec{\phi} = \begin{pmatrix} \phi_4 \\ \phi_3 \\ \phi_2 \\ \phi_1 \end{pmatrix} \qquad \alpha_y\vec{\phi} = i\begin{pmatrix} -\phi_4 \\ \phi_3 \\ -\phi_2 \\ \phi_1 \end{pmatrix} \qquad \alpha_z\vec{\phi} = \begin{pmatrix} \phi_3 \\ -\phi_4 \\ \phi_1 \\ -\phi_2 \end{pmatrix}$$

The form factor, written in terms of components, is:

$$\eta(W,K) = \int\limits_{\vec{r}_2} e^{i\vec{K}\cdot\vec{r}_2}\Bigg[u_f^*\psi_f^*(\vec{r}_2)u_i\psi_i(\vec{r}_2) \qquad\qquad (2)$$

$$-u_f^*\psi_f^*(\vec{r}_2)\big[\alpha_x u_i\alpha_x\psi_i(r_2) + \alpha_y u_i\alpha_y\psi_i(\vec{r}_2)$$

$$+\alpha_z u_i\alpha_z\psi_i(\vec{r}_2)\big] \times d\vec{r}_2\Bigg]$$

When all of the four-vector products are carried out this becomes a sum of sixty-four integrals, each of the form,

$$u_f^{*(\alpha)} u_i^{(\beta)} \int_{\vec{r}_2} d\vec{r}_2 e^{i\vec{K}\cdot\vec{r}_2} \psi_f^{*(\gamma)}(\vec{r}_2) \psi_i^{(\delta)}(\vec{r}_2) \qquad (3)$$

where the $u_f^{(\alpha)}$, $u_i^{(\beta)}$, $\psi_f^{(\gamma)}$, $\psi_i^{(\delta)}$ are each a component of the corresponding four-vector wavefunction. With cancellations the number of terms reduces to forty.

In computing the integrals (3) the well known expansion[14],

$$e^{i\vec{K}\cdot\vec{r}_2} = \sum_{n=0}^{\infty} i^n (2n+1) j_n(Kr_2) P_n(\cos\theta)$$

is used. Here j_n is the nth spherical Bessel function, P_n is the Legendre polynomial of order n, and θ is the angle between $\vec{K}$ and $\vec{r}_2$.

The wavefunction components $\psi^{(i)}$ have the form,

$$\psi^{(i)} = a^{(i)}(r_2) C_{\ell i, m i} Y_{\ell i, m i}(\vec{n})$$

as discussed in the section on wavefunctions. Hence the integrals (3) are of the form,

$$u_f^{*(\alpha)} u_i^{(\beta)} \int_{\vec{r}_2} C_{\ell_f \gamma m_f \gamma} C_{\ell_i \delta m_i \delta} a_f^{(\gamma)}(r_2) a_i^{(\delta)}(r_2)$$

$$Y_{\ell_f \gamma m_f \gamma}^{*} Y_{\ell_i \delta m_i \delta} \sum_{n=0}^{\infty} i^n (2n+1) j_n(Kr_2).$$

$$P_n(\cos\theta)\, r_2^2\, dr_2 d\vec{n}_2$$

Rearranging this gives,

$$u_f^*{}^{(\alpha)} u_i{}^{(\beta)} C_{\ell_f \gamma m_f}^{\gamma} C_{\ell_i \delta m_i}^{\delta} \qquad \sum_{n=0}^{\infty} i^n (2n+1) \qquad (4)$$

$$\left[\int_0^{\infty} a_f^{(\gamma)}(r_2) \, a_i^{(\delta)}(r_2) \, j_n(Kr_2) \, r_2^2 dr_2 \right]$$

$$\left[\int_{\vec{\Omega}} P_n(\cos\theta) \, Y_{\ell_f m_f}^{*}{}^{\gamma} \, Y_{\ell_i m_i}^{\delta} \, d\vec{\Omega} \right].$$

Using the following relations[14,15]:

$$\int_{\vec{\Omega}} Y_{n0} Y_{\ell m}^{*} Y_{\ell' m'} \, d\vec{\Omega} = \frac{1}{2\pi^{1/2}} (2n+1)^{1/2} (2\ell+1)^{1/2} (2\ell'+1)^{1/2}$$

$$\cdot \begin{pmatrix} n & \ell & \ell' \\ 0 & m & m' \end{pmatrix} \begin{pmatrix} n & \ell & \ell' \\ 0 & 0 & 0 \end{pmatrix} \qquad (5a)$$

$$Y_{n0}(\theta,\phi) = \left(\frac{2n+1}{4\pi}\right)^{1/2} P_n(\cos\theta) \qquad (5b)$$

$$Y_{\ell m}^{*} = (-1)^m Y_{\ell,-m} \qquad (5c)$$

the angular integral in equations (4) becomes

$$(-1)^{m_f^{\gamma}} (2\ell_f^{\gamma}+1)^{1/2} (2\ell_i^{\delta}+1)^{1/2} \begin{pmatrix} n & \ell_f^{\gamma} & \ell_i^{\delta} \\ 0 & -m_f^{\gamma} & m_i^{\delta} \end{pmatrix} \begin{pmatrix} n & \ell_f^{\gamma} & \ell_i^{\delta} \\ 0 & 0 & 0 \end{pmatrix}$$

where the $\begin{pmatrix} a & b & c \\ \alpha & \beta & \gamma \end{pmatrix}$ are Wigner 3-j symbols[15].

Since the 3-j symbol vanishes unless $\alpha+\beta+\gamma=0$, we have the selection rule that $m_f^{\gamma} = m_i^{\delta} = m$. In addition, the 3-j symbol with $\alpha=\beta=\gamma=0$ vanishes unless $a+b+c$ is even. This means that in the sum, n takes on only even values such that $|\ell_f^{\gamma} - \ell_i^{\delta}| \leq n \leq \ell_f^{\gamma} + \ell_i^{\delta}$. The series then is finite.

With these simplifying features, the integral (4) becomes,

$$u_f^*(\alpha)\, u_i(\beta)\left(\frac{1}{4\pi}\right)(2\ell_f^\gamma+1)^{1/2}\,(2\ell_i^\delta+1)^{1/2} \tag{6}$$

$$C_{\ell_f^\gamma m}^*\, C_{\ell_i^\delta m} \sum_{n=|\ell_f^\gamma-\ell_i^\delta|}^{\ell_f^\gamma+\ell_i^\delta} i^n (2n+1)$$

$$\begin{pmatrix} n & \ell_f^\gamma & \ell_i^\delta \\ 0 & -m & m \end{pmatrix} \begin{pmatrix} n & \ell_f^\gamma & \ell_i^\delta \\ 0 & 0 & 0 \end{pmatrix}$$

$$\left[\int_0^\infty a_f^{(\gamma)}(r_2)\, a_i^{(\delta)}(r_2)\, j_n(Kr_2)\, r_2^2 dr_2\right]$$

This is now complete, except for the need to average over initial electron spin polarizations and initial m values and sum over final electron spin polarizations, final m values, and final angular momentum quantum numbers of the ejected electron. These sums and averages are taken on the matrix element squared. The sum and average over m gives a factor of $1/(2j_i+1)$. In summing over the final angular momentum quantum numbers of the ejected electron the number of j values required to achieve convergence to five per cent or better varied from a minimum of four for small momentum transfer to as many as ten for large momentum transfer and large energy loss. The sum and average over electron spin polarizations is discussed in the section on wavefunctions. The sum of the forty terms, each of the form (6) is then the relativistic form factor $\eta(W,K)$.

IV. The Calculation of Wavefunctions

The calculation of the wavefunctions used in the scattering integral involves the solution of the time independent Dirac equation[6,7],

$$(-i\hbar c\vec{\alpha}\cdot\vec{\nabla}+\beta mc^2 +V)\psi =E\psi \tag{1}$$

where $\vec{\alpha} =\begin{pmatrix} 0 & \vec{\sigma} \\ \vec{\sigma} & 0 \end{pmatrix}$, the $\vec{\sigma}$ representing the Pauli spin matrices, and $\beta =\begin{pmatrix} \vec{I} & 0 \\ 0 & -\vec{I} \end{pmatrix}$ with $\vec{I}$ being the 2x2 identity matrix. Since the Dirac equation applies only to a spin 1/2 particle in an external field (there exists no general formulation for a system of mutually interacting particles in relativistic quantum theory) the independent particle model must be used in its application to atomic systems. That is, each atomic electron is considered to be orbiting in an external field due to all of the other atomic electrons.

The wavefunction ψ is a four component spinor that can be written in the following form[7, 16],

for $j = \ell + 1/2$,

$$\psi_{jm}(\vec{r}) = \begin{bmatrix} ig_{j\ell}(r) \left[\dfrac{\ell+m+1/2}{2\ell+1}\right]^{1/2} Y_{j-1/2}^{m-1/2} \\ ig_{j\ell}(r) \left[\dfrac{\ell-m+1/2}{2\ell+1}\right]^{1/2} Y_{j-1/2}^{m+1/2} \\ -f_{j\ell}(r) \left[\dfrac{\ell'-m+1/2}{2\ell'+1}\right]^{1/2} Y_{j+1/2}^{m-1/2} \\ f_{j\ell}(r) \left[\dfrac{\ell'+m+1/2}{2\ell'+1}\right]^{1/2} Y_{j+1/2}^{m+1/2} \end{bmatrix} \tag{2a}$$

where $\ell' = \ell + 1$.

For $j = \ell - 1/2$,

$$\psi_{jm}(\vec{r}) = \begin{pmatrix} -ig_{j\ell}(r)\left(\dfrac{\ell-m+1/2}{2\ell+1}\right)^{1/2} Y^{m-1/2}_{j+1/2} \\[2mm] ig_{j\ell}(r)\left(\dfrac{\ell+m+1/2}{2\ell+1}\right)^{1/2} Y^{m+1/2}_{j+j/2} \\[2mm] -f_{je}(r)\left[\dfrac{\ell'+m+1/2}{2\ell'+1}\right]^{1/2} Y^{m-1/2}_{j-1/2} \\[2mm] f_{j\ell}(r)\left[\dfrac{\ell'-m+1/2}{2\ell'+1}\right]^{1/2} Y^{m+1/2}_{j-1/2} \end{pmatrix} \qquad (2b)$$

where $\ell' = \ell - 1$.

If we let $\kappa = \pm(j+1/2)$ for $j = \ell\pm1/2$ and let $G(r)=rg(r)$, $F(r)=rf(r)$ the equations for the radial wavefunctions are,

$$\frac{dG(r)}{dr} = -\frac{\kappa}{r} G(r) - \left[\frac{E+mc^2}{\hbar c} + \frac{\alpha Z(r)}{r}\right] F(r) \qquad (3)$$

$$\frac{dF(r)}{dr} = \left[\frac{E-mc^2}{\hbar c} + \frac{\alpha Z(r)}{r}\right] G(r) + \frac{\kappa}{r} F(r)$$

Here E is the total relativistic energy of the electron, $E = (c^2p^2+m^2c^4)^{1/2}$, and α is the fine structure constant, $\alpha = e^2/hc = 1/137.036$. $Z(r)$ is the screened atomic charge of the atom, varying from Z inside the innermost atomic shell to Z-N+1 at infinity, where N is the total number of atomic electrons[8]. $G(r)$ is known as the large component of the wavefunction and reduces to the solution of the Schrodinger equation in the non-relativistic limit. These wavefunctions are normalized such that $\int_{r=0}^{\infty}\left(|G|^2+|F|^2\right)dr = 1$.

We need to solve these radial equations under the independent particle and central field assumptions for the wavefunction $G(r)$ and $F(r)$ and for the quantity $Z(r)$. The approach taken is to solve the radial equations for the neutral atom using the Hartree-Fock-Slater Self-Consistent Field method to obtain the bound state wavefunctions and the screened charge, $Z(r)$. The radial equations are then again solved using $Z(r)$ for the continuum wavefunctions which, when $Z(r)$ is given, are functions only of the angular momentum (via kappa) and the energy of the ejected electron. The calculation of continuum wavefunctions will be discussed later.

Self-Consistent-Field Calculations

The computer code for the calculation of SCF solutions to the radial Dirac equation was obtained from Dr. Chien-ping Lin[17]. Detailed discussion of the SCF method can be found in references 18, 19, and 20. Discussion of the method applied to the Dirac equation is given in references 21 through 24.

In these calculations the wavefunction for the system is represented as a product of one-electron wavefunctions. Each electron is assumed to move independently of all the other electrons in a time-averaged, central, electrostatic field produced by the nucleus and all the other electrons. Minimization of the average energy of the system in this representation gives variational equations for the wave-

functions'. These equations, the Hartree-Fock equations, contain exchange terms that account for statistical correlation in the motion of pairs of electrons of like spin. In the Hartree-Fock-Slater method used here the exchange terms in the Hartree-Fock equations are simplifed by use of the approximate Slater free electron exchange potential ,

$$V^{exch}(\rho) = -6 \ [\frac{3}{8\pi} \ |\rho|]^{1/3} \ \text{Rydberg}$$

where ρ is the total electron density. This is simply a means, based on the relationship between the potential and charge density in a free electron gas, of replacing the individual exchange potentials for different orbitals by a single average exchange potential depending only upon the local electronic charge density. The equations are then solved by iteration until the desired degree of consistency is achieved.

The Dirac-Hartree-Fock-Slater bound state wavefunctions for the argon M_{III} shell are shown in Figure IV-1. The screened charge $Z(r)$ is shown in Figure IV-2. In Table IV-1 are displayed the shell energies for argon computed using this DHFS program, those computed by Herman and Skillman[20], and some obtained from x-ray data[25]. A diagram of the shell structure of argon is shown in Figure IV-3.

Continuum Wavefunctions

The radial continuum wavefunctions are obtained by integrating the radial equations (3) from r=0 to large r
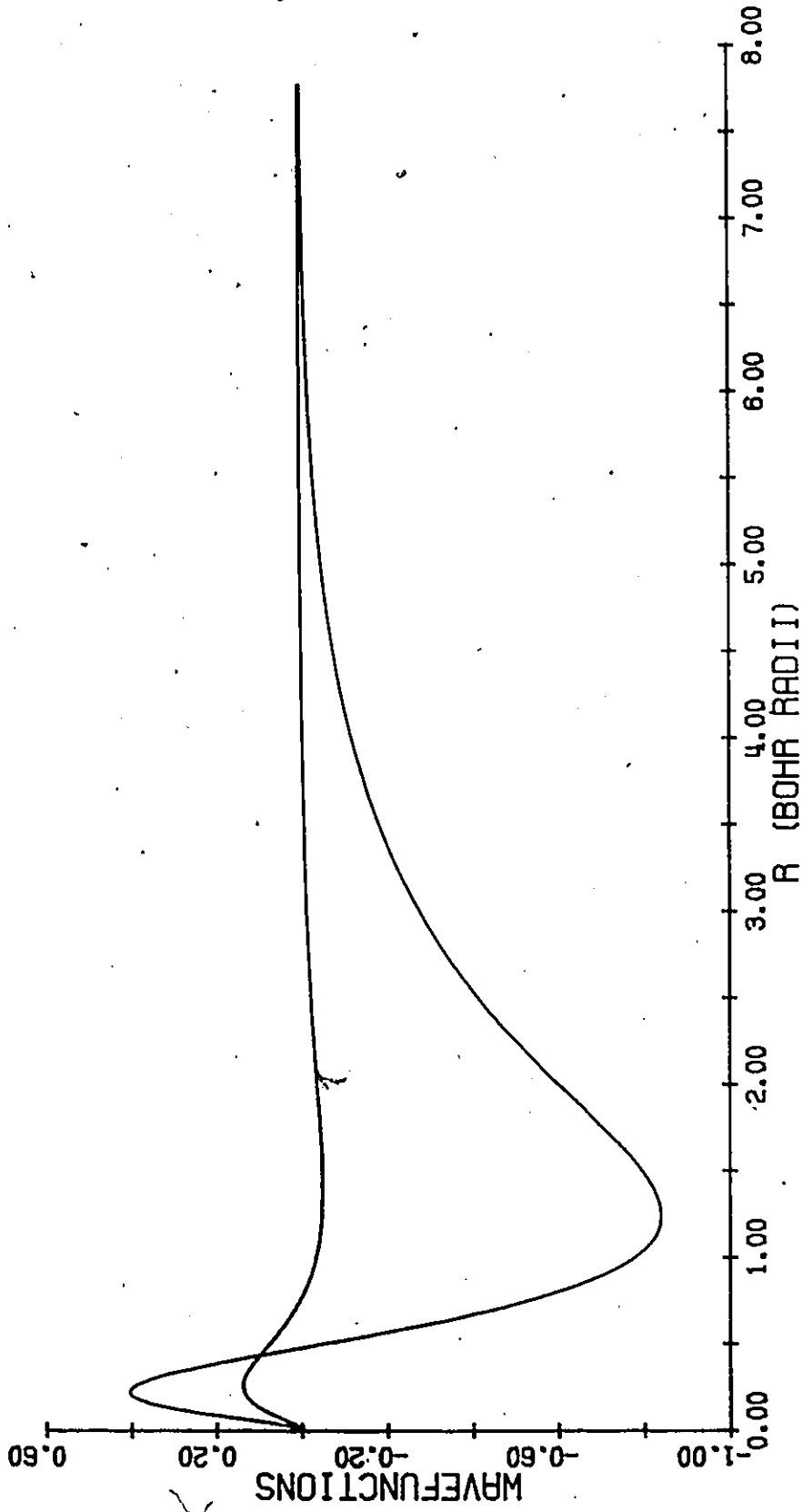
Figure IV-1: DHFS Wavefunctions for M_{III} Shell of Argon.

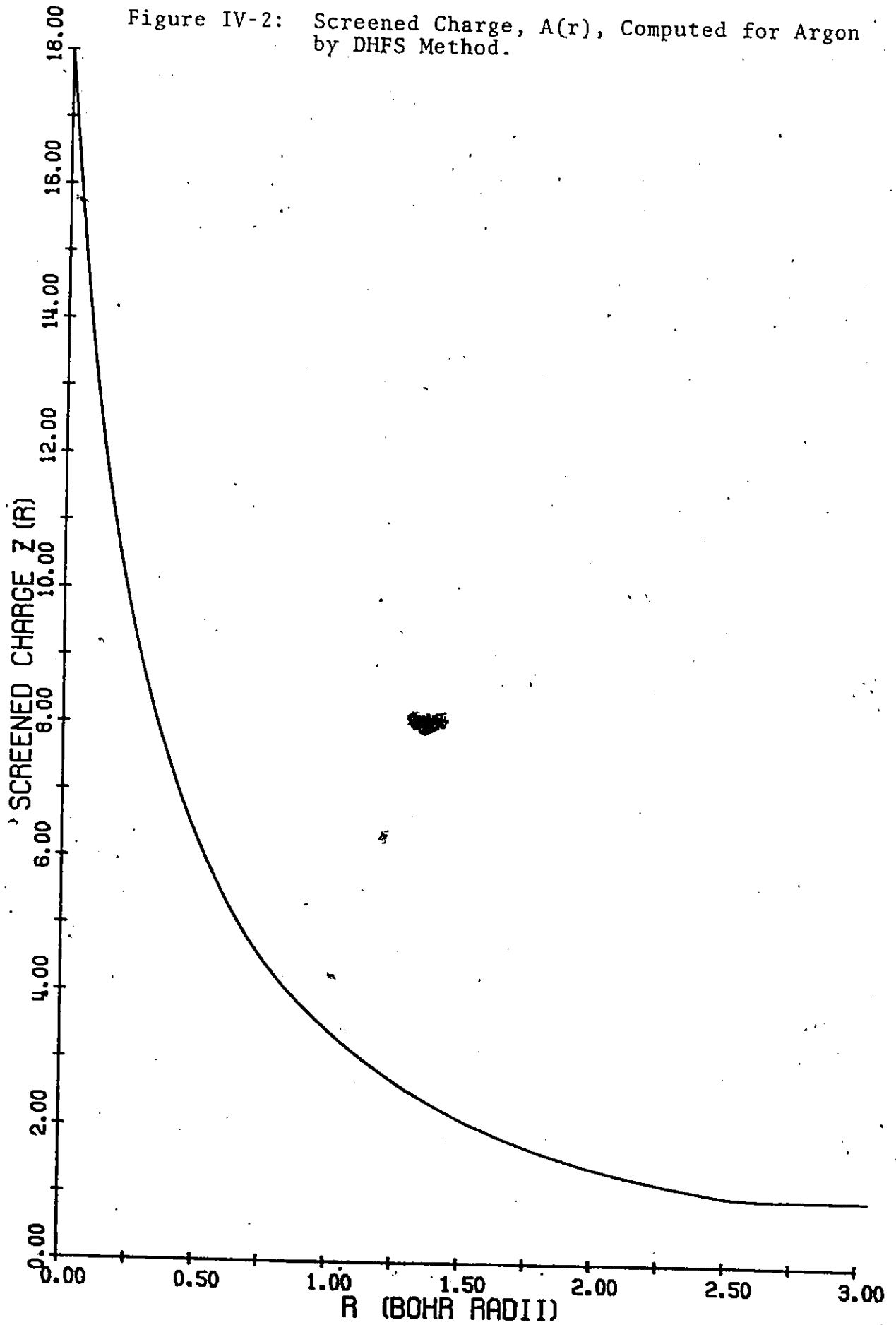Figure IV-2: Screened Charge, A(r), Computed for Argon by DHFS Method.

Table IV-1: Energies (eV) for Argon

Shell	This Calculation	Herman and Skillman	Herman and Skillman with Relativistic Corrections	X-ray Emission
$K_I(1'S_{1/2})$	3177.45	3163.68	3181.53	3202.86
$L_I(2^2S_{1/2})$	313.43	311.08	314.43	319.99
$L_{II}(2^2P_{1/2})$	249.43	247.70	248.23	247.37
$L_{III}(2^2P_{3/2})$	247.06			245.16
$M_I(3^2S_{1/2})$	28.92	28.66	29.08	
$M_{II}(3^2P_{1/2})$	14.62	14.49	14.56	
$M_{III}(3^2P_{3/2})$	14.42			

$l=0$

K_I, $j=1/2$ $(1\,^2S_{1/2})$

K $n=1$

$l=0$

L_I, $j=1/2$ $(2\,^2S_{1/2})$

$l=1$

L_{II}, $j=1/2$ $(2\,^2P_{1/2})$

L_{III}, $j=3/2$ $(2\,^2P_{3/2})$

L $n=2$

$l=0$

M_I, $j=1/2$ $(3\,^2S_{1/2})$

$l=1$

M_{II}, $j=1/2$ $(3\,^2P_{1/2})$
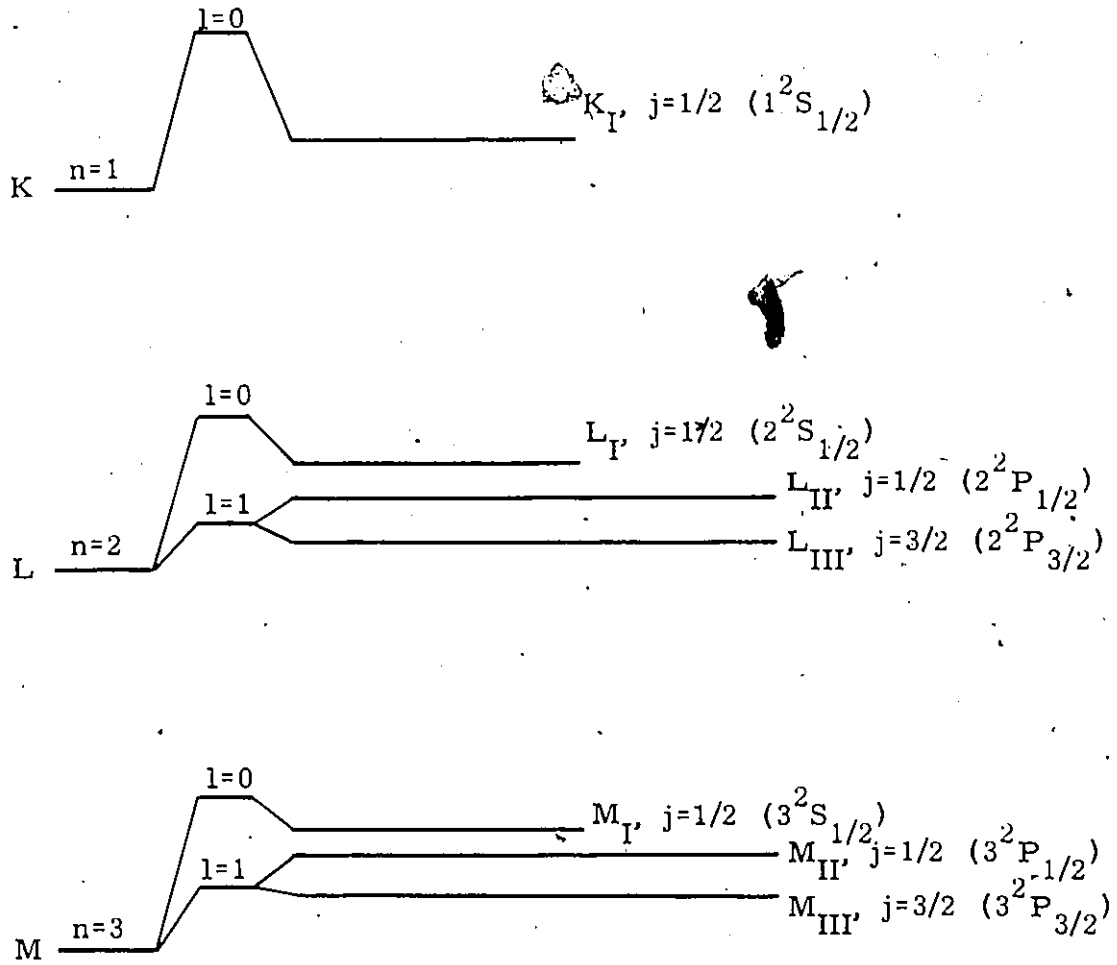
M_{III}, $j=3/2$ $(3\,^2P_{3/2})$

M $n=3$

Figure IV-3: Grotrian Diagram of the Energy Level Structure
of Argon.

using the screened charge, Z(r), obtained from the DHFS calculation. In these calculations a fourth order Runge-Kutta scheme[26] with variable step size is used for the integration. The computed radial wavefunctions are normalized per unit energy by matching them to the analytic asymptotic continuum solutions for an electron in the field of a nuclear charge $Z_a = Z-N+1$. These solutions are shown by Akheiser and Berestetkii[7] to be:

$$iG(r) = \left[\frac{m}{\pi\hbar p}\right]^{1/2}\left[1+\frac{E}{mc^2}\right]^{1/2} \sin\left[\frac{pr}{\hbar} - \ell\frac{\pi}{2} + \delta + \nu\ell n\frac{2pr}{\hbar}\right]$$

$$F(r) = (-1)^{\ell'-\ell}\left[\frac{m}{\pi\hbar p}\right]^{1/2}\left[\frac{E}{mc^2} -1\right]^{1/2}$$

$$\sin\left[\frac{pr}{\hbar} - \ell'\frac{\pi}{2} + \delta + \nu\ell n\frac{2pr}{\hbar}\right]$$

(4)

where

$$\nu = Z_a\alpha/\beta \quad (\beta=v/c)$$

$$\gamma = (K^2-Z_a^2\alpha^2)^{1/2}$$

$$\delta = \xi - \arg\Gamma(\gamma+i\nu) - \frac{\pi}{2}(\gamma-\ell-1)$$

and ξ is defined by,

$$e^{2i\xi} = \frac{K-iZ_a\alpha\left(\frac{mc}{p}\right)}{-\gamma+iZ_a\alpha\left(\frac{E}{cp}\right)}$$

The units of G and F are (energy - length)$^{-1/2}$. The exact solutions to the radial Dirac equations for the bound Coulomb problem are confluent hypergeometric functions of complex argument which reduce to these trigonometric functions in the asymptotic limit. Some examples of the wavefunctions computed for various values of kappa and electron

kinetic energy using the $Z(r)$ of Figure IV-2 are shown in Figures IV-4 through IV-6.

The quantity $-e^2 Z(r)/r$ represents the screened central potential seen by any one of the N independent electrons of the atom as it moves in the combined fields of the other N-1 electrons plus the nucleus. The use of the screened charge in the calculation of the continuum wavefunctions is commonly called the "frozen core" approximation in that during the collision process the wavefunctions of the other N-1 non-participating electrons remain unchanged. Hence the potential represents that of the unrelaxed atomic ion. This is, of course, strictly correct only for large r. Further discussion on the use of screened charges and the calculation of continuum wavefunctions can be found in the articles by Cooper[27] and by Pratt, Ron, and Tseng[28].

Dirac Plane Wavefunctions

In the Born approximation being used for this scattering calculation the primary electron is treated as a plane wave before and after the collision. The relativistic plane wavefunctions for electrons of right (R) and left (L) handed helicity are given by[6]:

$$\phi^{(R)}(\vec{p}) = \frac{e^{i\vec{K}\cdot\vec{r}}}{\left[1+\frac{c^2p^2}{(E+mc^2)^2}\right]^{1/2}} \begin{pmatrix} 1 \\ 0 \\ \frac{cp_z}{E+mc^2} \\ \frac{c(p_x+ip_y)}{E+mc^2} \end{pmatrix} e^{-i\omega t} \qquad (5a)$$
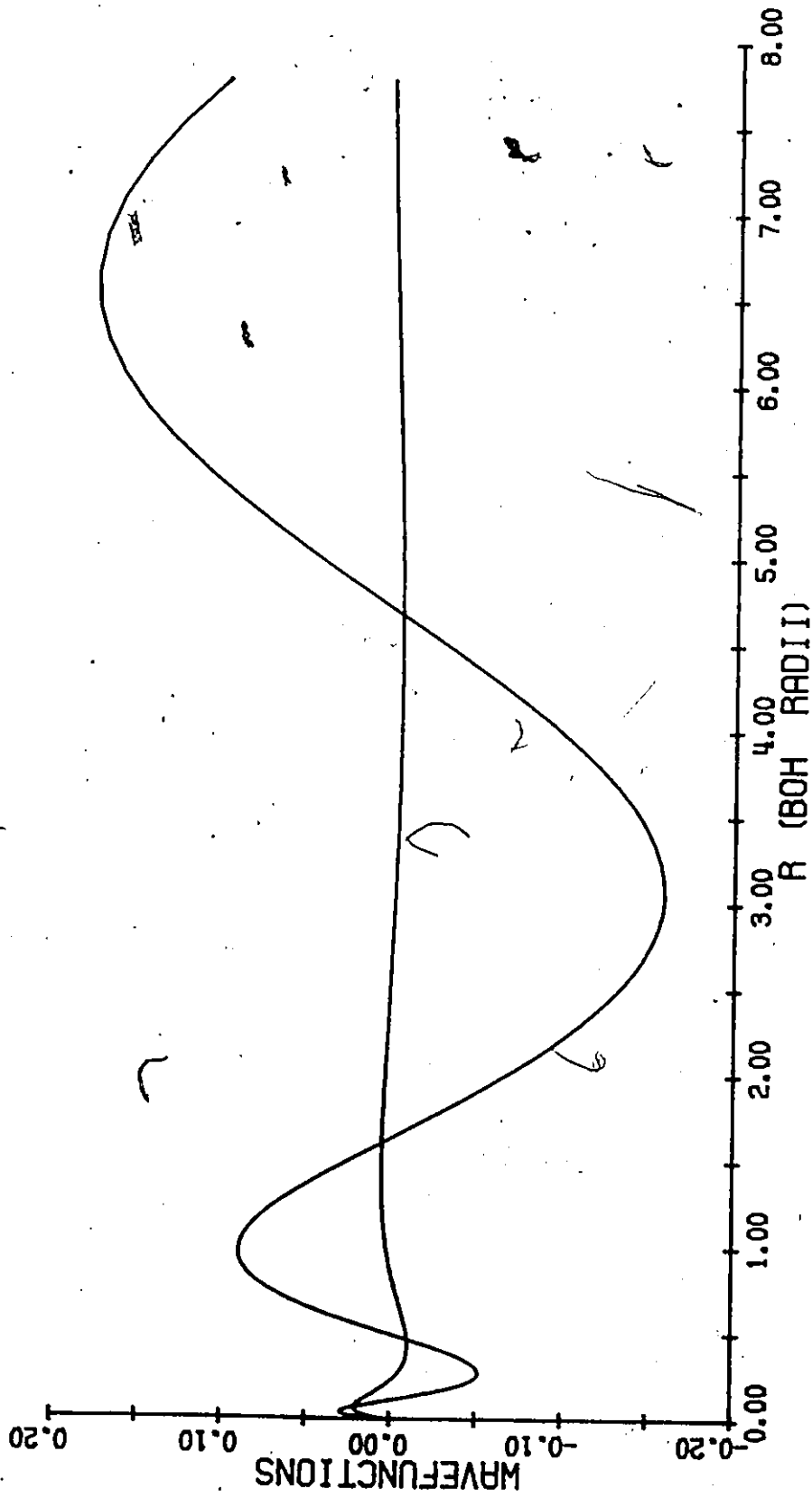
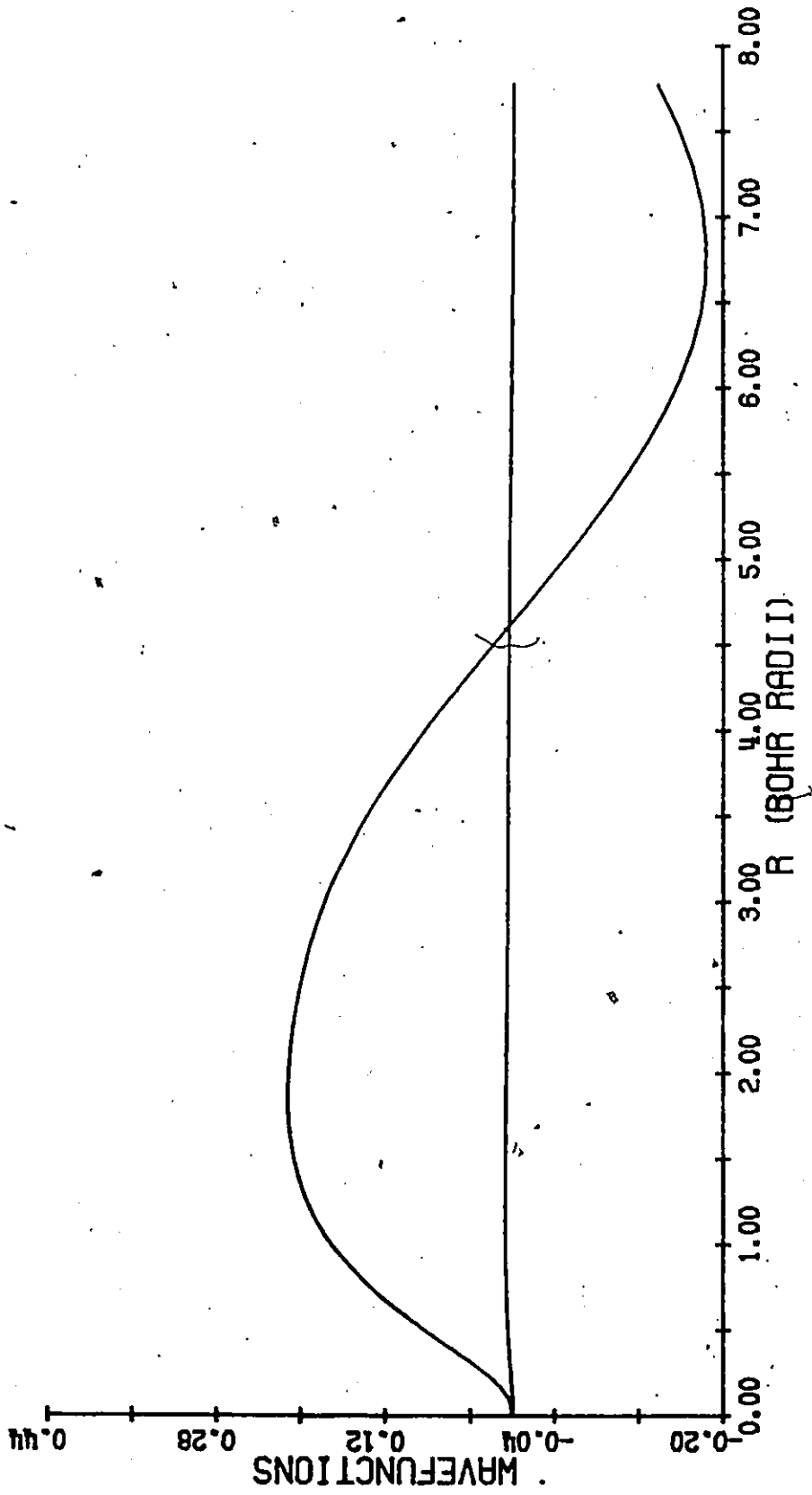Figure IV-4: Argon Continuum Wavefunctions: Electron Energy = 5 eV; Kappa = -1.

Figure IV-5: Argon Continuum Wavefunctions: Electron Energy = 5eV; Kappa - -3.
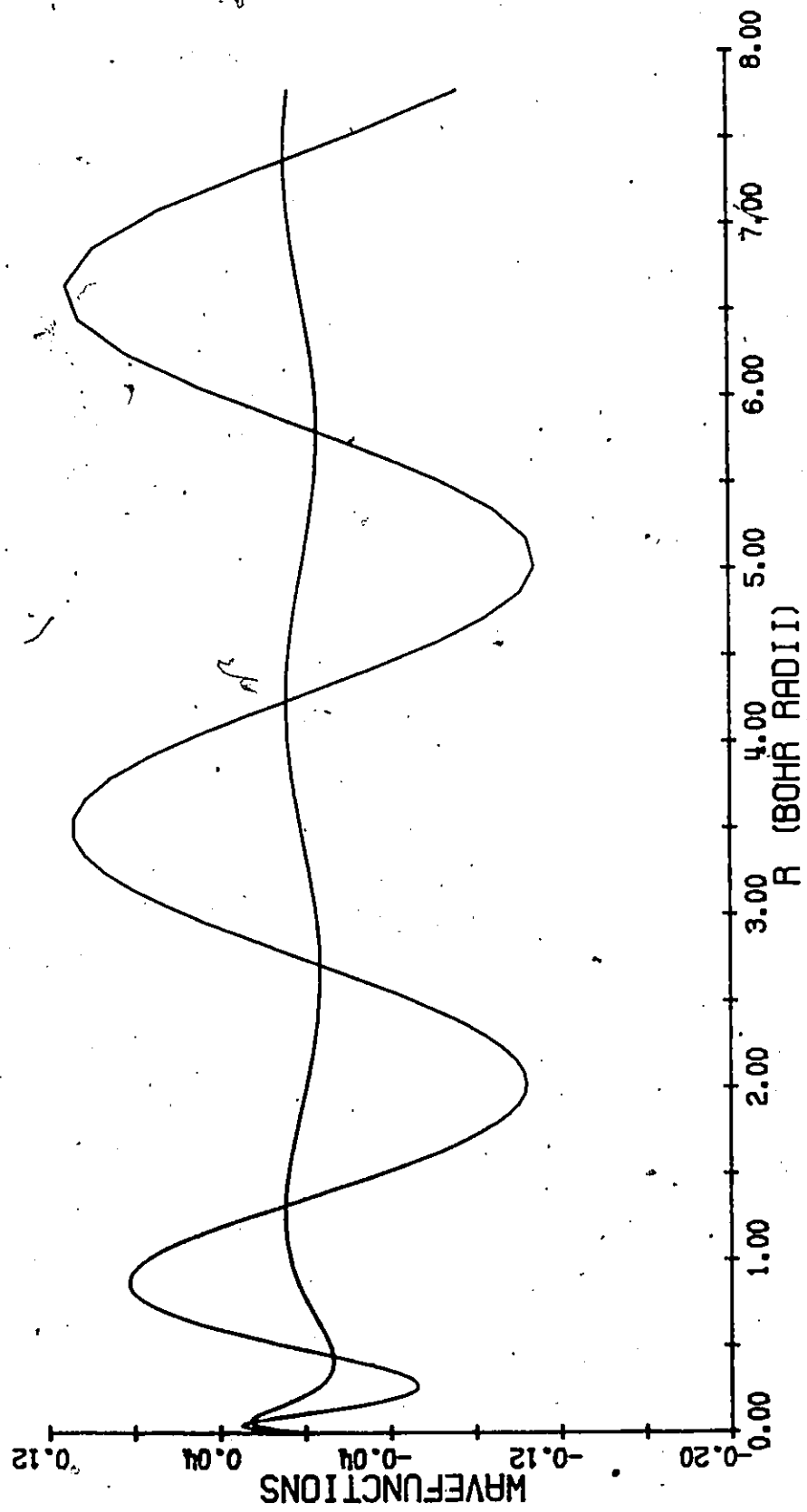
Figure IV-6: Argon Continuum Wavefunctions: Electron Energy = 50 eV; Kappa = -1.

$$\phi^{(L)}(\vec{p}) = \frac{e^{i\vec{k}\cdot\vec{r}}}{\left[1 + \frac{c^2 p^2}{(E+mc^2)^2}\right]^{1/2}} \begin{bmatrix} 0 \\ 1 \\ \frac{c(p_x - ip_y)}{E+mc^2} \\ \frac{-cp_z}{E+mc^2} \end{bmatrix} e^{-i\omega t} \qquad (5b)$$

where right and left handed helicities correspond to elec-
tron spin components +1/2 and -1/2 in the direction of
travel $\vec{p}$[29].

The calculation of the relativistic form factor in-
volves an average over initial helicities and a sum over
final helicities. If the primary electron is taken to be
moving in the z-direction initially, as shown in Figure IV-7,
the momentum transfer P is related to the initial and final
primary electron momenta, p_i and p_f, by the kinematical
relation,

$$P^2 = p_i^2 + p_p^2 - 2p_i p_f \cos\theta \qquad (6)$$

In relativistic theory momentum, p, is related to kinetic
energy, T, by the relation,

$$c^2 p^2 = (T + mc^2)^2 - m^2 c^4 \qquad (7)$$

Given the momentum transfer and the energy loss, for electron
impact ionization the scattering angle, θ, can be computed
using relations (6) and (7).

Since the x and y components of the final momentum are
not unique, but are needed in the post collision electron
wavefunction, they are summed over the x-y plane in the
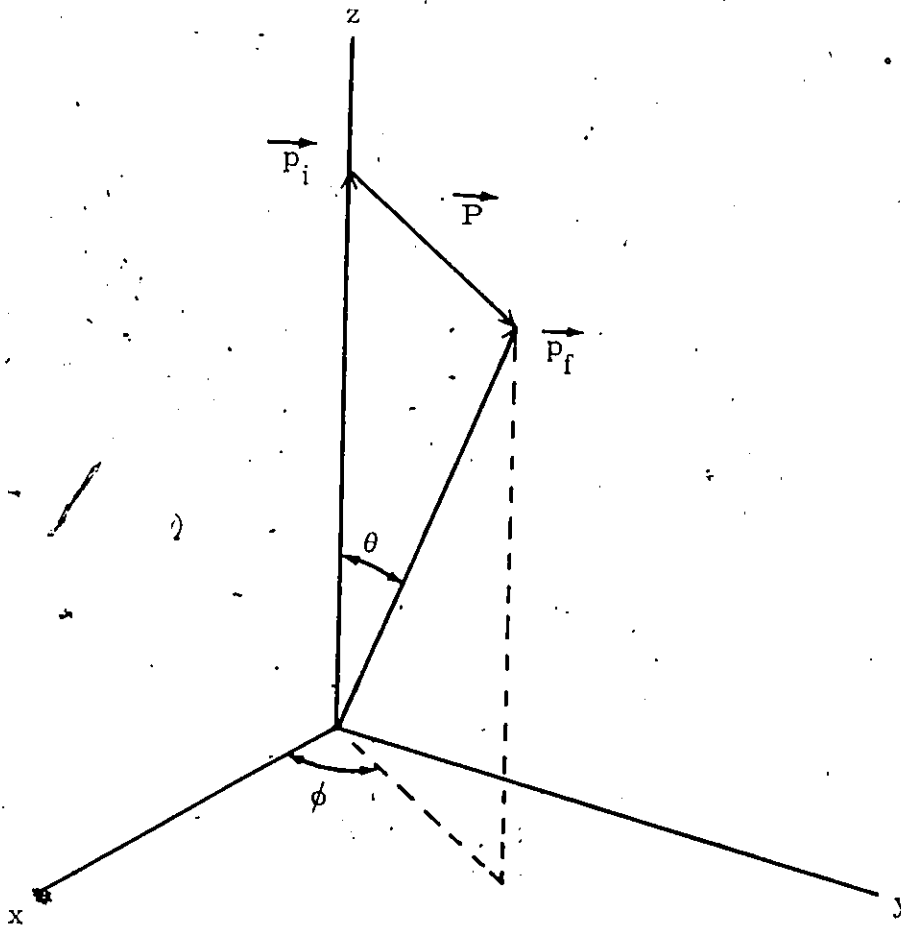calculation of $|\eta|^2$.

Figure IV-7:   Coordinates and Angles for Electron Scattering
Calculation.

In non-relativistic theory, the components of momentum do not appear explicitly in the spinor multiplying exp $(i\vec{k}\cdot\vec{r} - i\omega t)$ in the plane wavefunction. This allows the square of the matrix element to be greatly simplified as shown by Manson[17].

V. Photoionization Calculations

As pointed out in Section II, the electron impact ionization cross section calculated in the limit of small momentum transfer, that is, $K \to 0$, corresponds to the photoionization cross section. As a test of the computational technique and the computer program this calculation was performed for the M_{III} subshell of argon. The results are shown in Figure V-1 along with the experimental photoionization cross section data from Samson[31].

In the limit $K \to 0$, the $e^{i\vec{K} \cdot \vec{r}}$ factor in the matrix element is, approximately,

$$e^{i\vec{K} \cdot \vec{r}} \to 1 + i\vec{K} \cdot \vec{r} + \dots$$

In principle, the first term will vanish due to the orthogonality of the initial and final electron wavefunctions leaving the $\vec{K} \cdot \vec{r}$ "dipole" term. Since numerical wavefunctions are used in these calculations, however, the overlap integral $\int \psi_f^* \psi_i d\vec{r}$ is, in general, not identically zero. This can lead to large errors in the calculation of the matrix element and hence, when $|\vec{K}|$ is very small, in the computed photoionization cross section. Thus, the photoionization cross sections presented in Figure V-1 are computed from the matrix element of the quantity $(e^{i\vec{K} \cdot \vec{r}} - 1)$.

These calculated photoionization cross sections are in good agreement with those computed by Cooper[28,32] and by McGuire[33] for argon using the non-relativistic dipole theory.
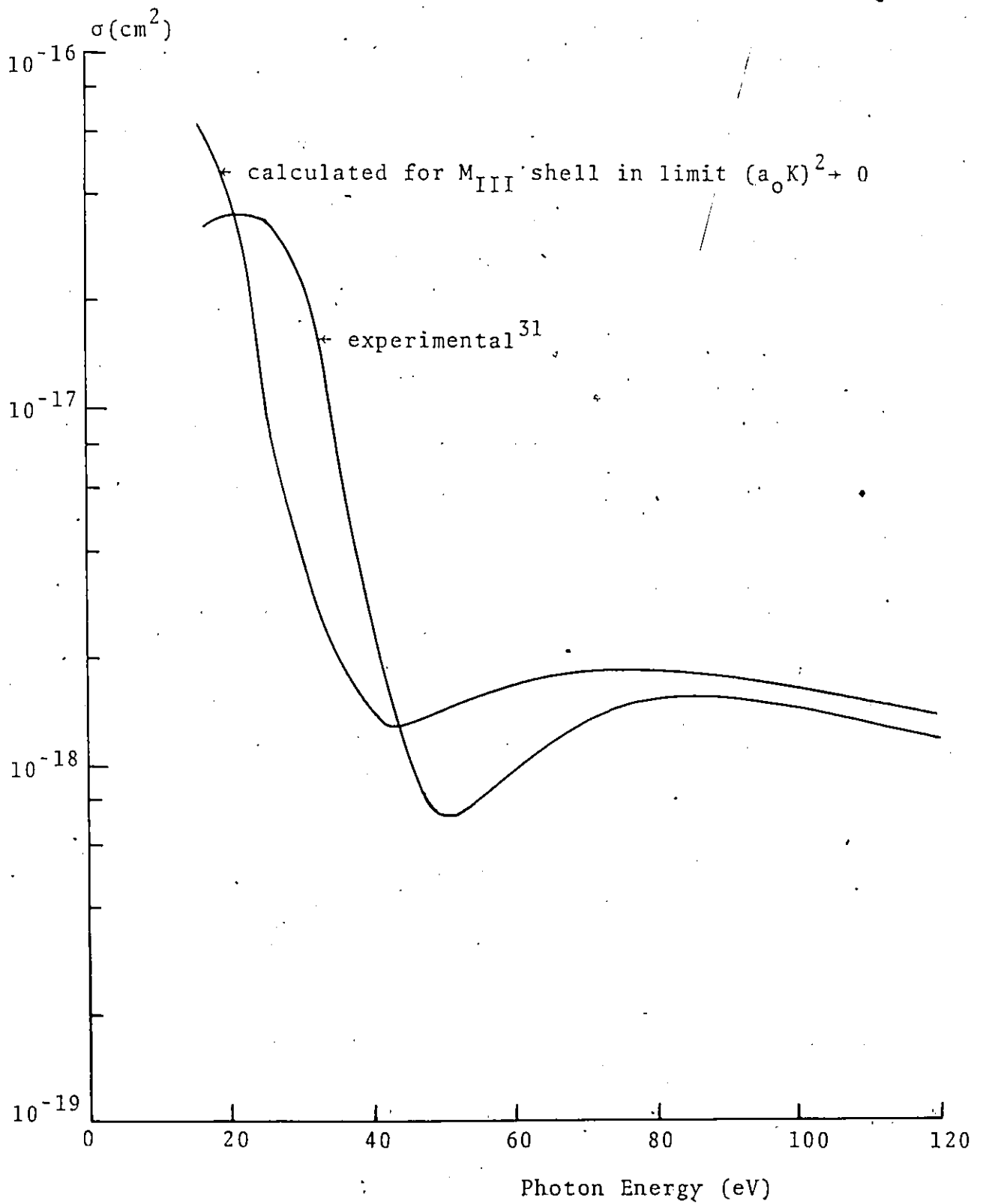
Figure V-1: Argon Photoionization Cross Section.

They are, however, very different from the measured cross sections, particularly at low energy. This is a well known characteristic of single electron models and has been discussed by a number of authors[34, 35, 36, 37]. It is due to a neglect of many-body correlation effects that are most important at low energies. This is a problem that cannot be easily treated in relativistic theory, however, since, as has been mentioned previously, there is no relativistic quantum theory of many body interactions in closed form.

Relativistic Electric Dipole Photoeffect Calculations

Further photoionization calculations were performed using the formalism described by Grant[38]. He computed the matrix element, $M_{\alpha\beta}$, for a radiative transition from β to α,

$$M_{\alpha\beta} = \left(\frac{\omega}{\pi c}\right)^{1/2} \int \psi_\alpha^*(\vec{r})\, [\Phi(\vec{r}) + c\vec{\alpha}\cdot A(\vec{r})]\, \psi_\beta(\vec{r})\, d\vec{r}$$

using a multipole expansion of the vector potential. The reduction of this to radial matrix elements gives

$$\overline{M}_{\alpha\beta}^e(G_L) = \overline{M}_{\alpha\beta}^e(0) + G_L \overline{M}_{\alpha\beta}^\ell$$

with

$$\overline{M}_{\alpha\beta}^e(0) = i^L \left\{ \left(\frac{L}{L+1}\right)^{1/2} [(\kappa_\alpha - \kappa_\beta)\, I_{L+1}^+ + (L+1) I_{L+1}^-] \right.$$
$$\left. -\left(\frac{L+1}{L}\right)^{1/2} [(\kappa_\alpha - \kappa_\beta) I_{L-1}^+ - L I_{L-1}^-] \right\}$$

and

$$\overline{M}_{\alpha\beta}^\ell = i^L \left\{ (2L+1)\, J^{(L)} + (\kappa_\alpha - \kappa_\beta)(I_{L+1}^+ + I_{L-1}^+) \right.$$
$$\left. - L I_{L-1}^- + (L+1)\, I_{L+1}^- \right\}$$

The radial integrals are

$$I_L^+(\omega) = -\int_0^\infty (G_\alpha F_\beta + F_\alpha G_\beta) \, j_L \left(\frac{\omega r}{c}\right) dr$$

$$I_L^-(\omega) = -\int_0^\infty (G_\alpha F_\beta - F_\alpha G_\beta) \, j_L \left(\frac{\omega r}{c}\right) dr$$

$$J^{(L)}_{(\omega)} = \int_0^\infty (G_\alpha G_\beta + F_\alpha F_\beta) \, j_L \left(\frac{\omega r}{c}\right) dr$$

where ω is the photon frequency.

The Einstein coefficient in units of $\tau_0 = \dfrac{\hbar^3}{me^4} = 2.4188 \times 10^{-17}$ sec is given by

$$A_{\beta \to \alpha} = 2\alpha \, \frac{W}{2R_y} \cdot \frac{2j_\alpha + 1}{2L + 1} \begin{pmatrix} j_\beta & L & j_\alpha \\ 1/2 & 0 & -1/2 \end{pmatrix}^2 |\bar{M}_{\alpha\beta}|^2$$

and the oscillator strength is

$$f_{\beta \to \alpha} = \frac{A_{\beta \to \alpha}}{2\alpha^3 \left(\frac{W}{2R_y}\right)^2}$$

where R_y is the Rydberg of energy.

For photoionization calculations we want[21]

$$f_{\alpha \to \beta} = \frac{(2j_\beta + 1)}{(2j_\alpha + 1)} \, f_{\beta \to \alpha}$$

For photoionization, this becomes the differential oscillator strength $\dfrac{df_0}{dW}$ of section I as the continuum wavefunctions are normalized per unit energy.

In the above equations $\bar{M}^e_{\alpha\beta}$ represents the matrix element of the electric (transverse) vector potential and $\bar{M}^\ell_{\alpha\beta}$ is the matrix element of the longitudinal vector

potential. G_L is the gauge parameter (L = multipole quantum number) defined such that the Coulomb gauge, for which the longitudinal component vanishes, corresponds to $G_L = 0$. Grant shows that $\overline{M}^\ell_{\alpha\beta}$ should vanish for all pairs of states α and β that are eigensolutions of the same Dirac hamiltonian since transition probabilities should be independent of gauge. He also shows that the matrix element in the Coulomb gauge reduces, in the non-relativistic limit, to the dipole-velocity form. He shows further that $\overline{M}^\ell_{\alpha\beta}(G_L)$ reduces, for $G_L = (\frac{L+1}{L})^{1/2}$, to the non-relativistic dipole-length form.

Using this formalism the dipole (L = 1) photoionization cross section for argon M_{III} has been calculated in both gauges and the results are shown in Figure V-2. This calculation is in good agreement with the previous calculation. Although the longitudinal matrix element cannot be expected to vanish identically for the DHFS approximate wave functions, it should, at least, be substantially smaller than the transverse matrix element. This then serves as a test of the accuracy of the wave functions. For energies of about 60 eV both gauges give the same result with $\overline{M}^\ell_{\alpha\beta}$ being, typically, less than one per cent of $\overline{M}^e_{\alpha\beta}$. This is not the case, however, at lower energies.

The problem here may be due to the use of the frozen core approximation in the calculation of continuum wave
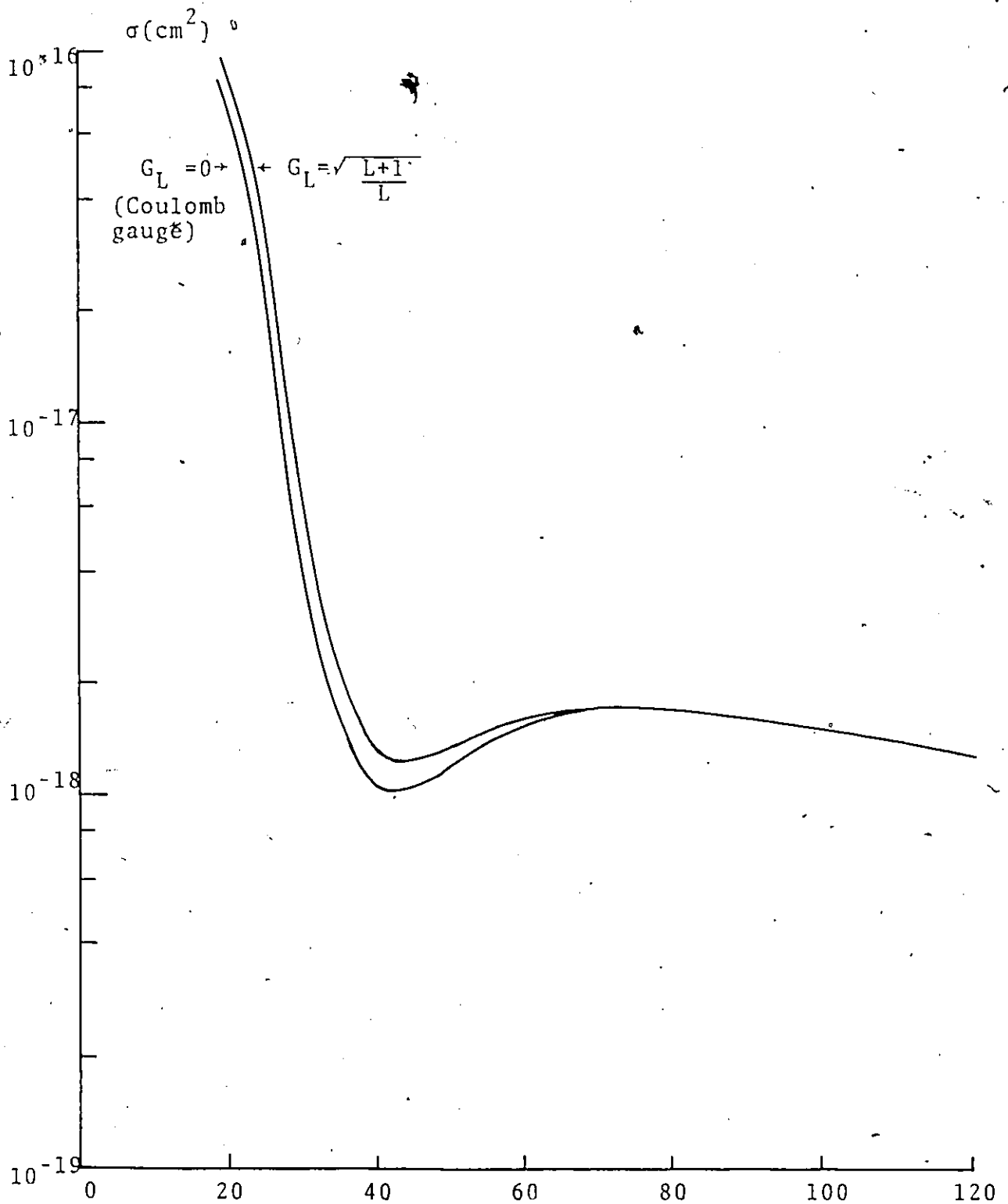
Figure V-2: Argon M_{III} Photoionization Cross Section Calculated from the Theory Given by Grant[38].

functions. These wave functions should be more sensitive to the central atomic potential at low energy and at small radii so that the use of the potential of the unrelaxed ion should lead to inaccurate wave functions. Also, in these photoeffect calculations, the dominant contribution comes from the integrals $I^{\pm}_{L-1}(\omega)$ and $J^{(L)}$ containing spherical Bessel functions which weight the integrands toward small radii for small ω and $L = 1$.

VI. Bethe Surface and Total Cross-Section Calculations

Low Energy Calculations

As a test of the computational technique and the computer code itself, calculations were made for electron impact ionization of argon in the non-relativistic limit. Cross sections differential in energy and angle were calculated for 4 keV electrons incident upon the M_{III} subshell of argon. These results and the experimental 4 keV data of Afrosimov, et al.[39] are plotted in Figure VI-1. There is good agreement between the Bethe-Born calculation and the experiment for small energy loss and small scattering angle. This is a well known characteristic of Born approximations[40, 41]. For larger values of energy loss (there are, unfortunately, no data for energy loss between 20 eV and 100 eV), the calculated cross sections have approximately the correct shape but are low by factors between two and three. This might be expected, however, because the computed cross section does not include contributions from the M_{II} shell, which has nearly the same ionization potential and wave function as the M_{III} shell. In addition, at energy loss greater than about 29 eV, there will be contributions from the M_{I} shell which, of course, have also been neglected.

It should also be noted that these calculations give approximately the same results as those obtained by Amus'ya, et al.[42] in their calculations using the first Born approximation and the Herman-Skillman[20] wave functions and
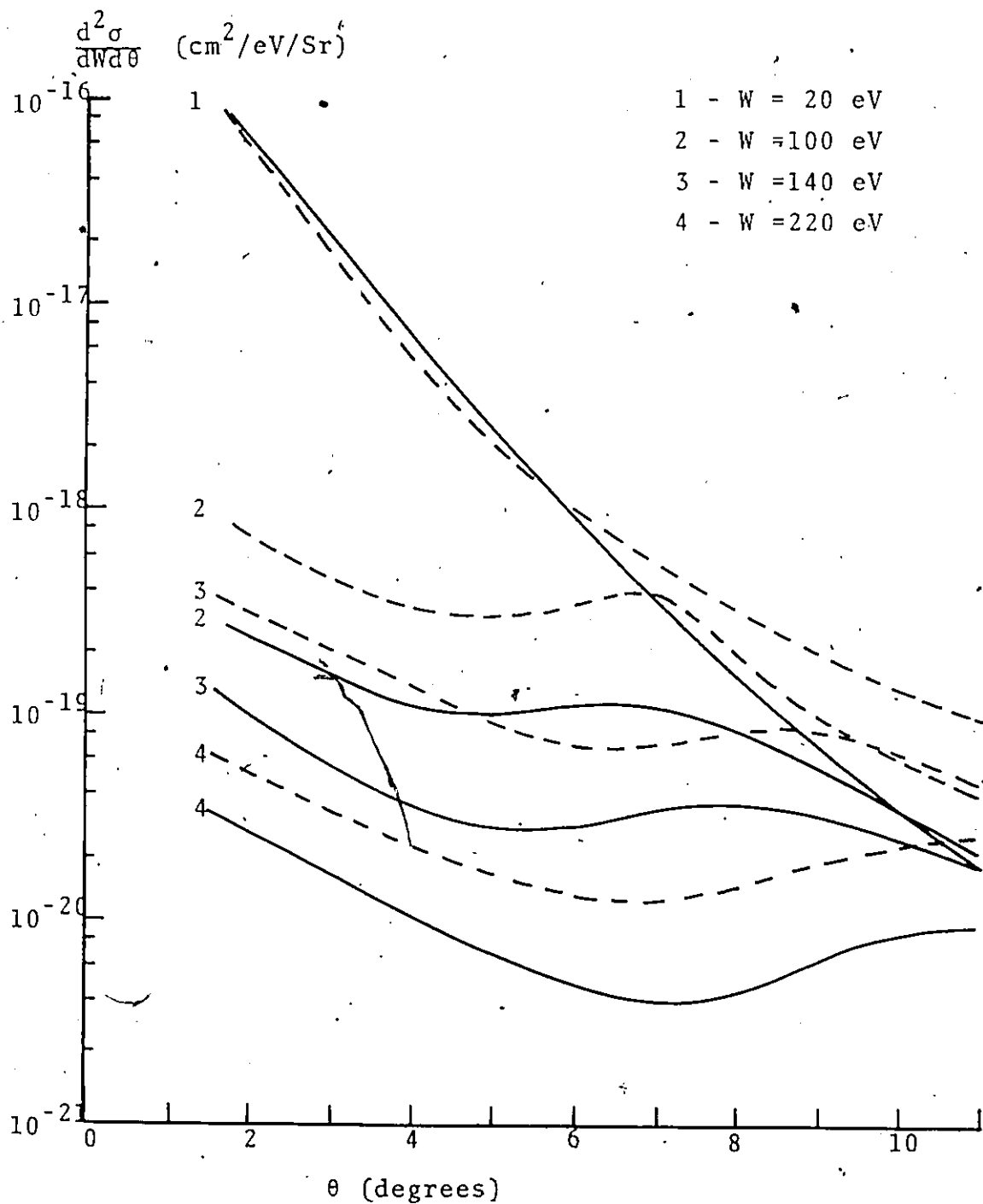
Figure VI-1:   Differential Cross Sections for Ionization of
               Argon by 4 keV electrons; ---- measured by
               Afrosimov, et al., —— calculated for M_{III}
               Shell of Argon.

potential.

High Energy Calculations

The Bethe surface computed using the theory presented previously is displayed in Figures VI-2 through VI-6 for primary electron energies of 4 keV, 10 keV, 100 keV, 1 MeV, and 10 MeV. Several characteristics common to all Bethe surfaces are apparent in Figure VI-2.

First, for large energy loss, each curve of df/dW vs. $\ln(a_oK)^2$ possesses a definite peak that moves to larger values of K as W increases. This peak, as a function of energy loss, is called the Bethe ridge. It corresponds to the scattering angle where, classically, momentum is conserved in the collision between the incident and atomic electron. At the Bethe ridge energy loss and momentum transfer are related by

$$(a_oK)^2 = W/Ry \quad \text{(non-relativistic[4])} \tag{1}$$

$$(a_oK)^2 = [(W + mc^2)^2 - m^2c^4]2Ry \cdot me^2 \text{ (relativistic)}$$

The finite width of the Bethe ridge is a quantum mechanical effect due to the binding of the struck electron. Because the momentum of the atomic electron is not well defined, collisions with momentum transfer different from that given by (1) do occur and thus give the oscillator strength as a function of momentum transfer a finite width around the Bethe ridge. The width of the peak is related to the binding energy, B, of the atomic electron by[4]

Figure VII-2: Computed Argon M_{III} Bethe Surface for 4keV Electrons; each curve represents a constant energy loss in eV.
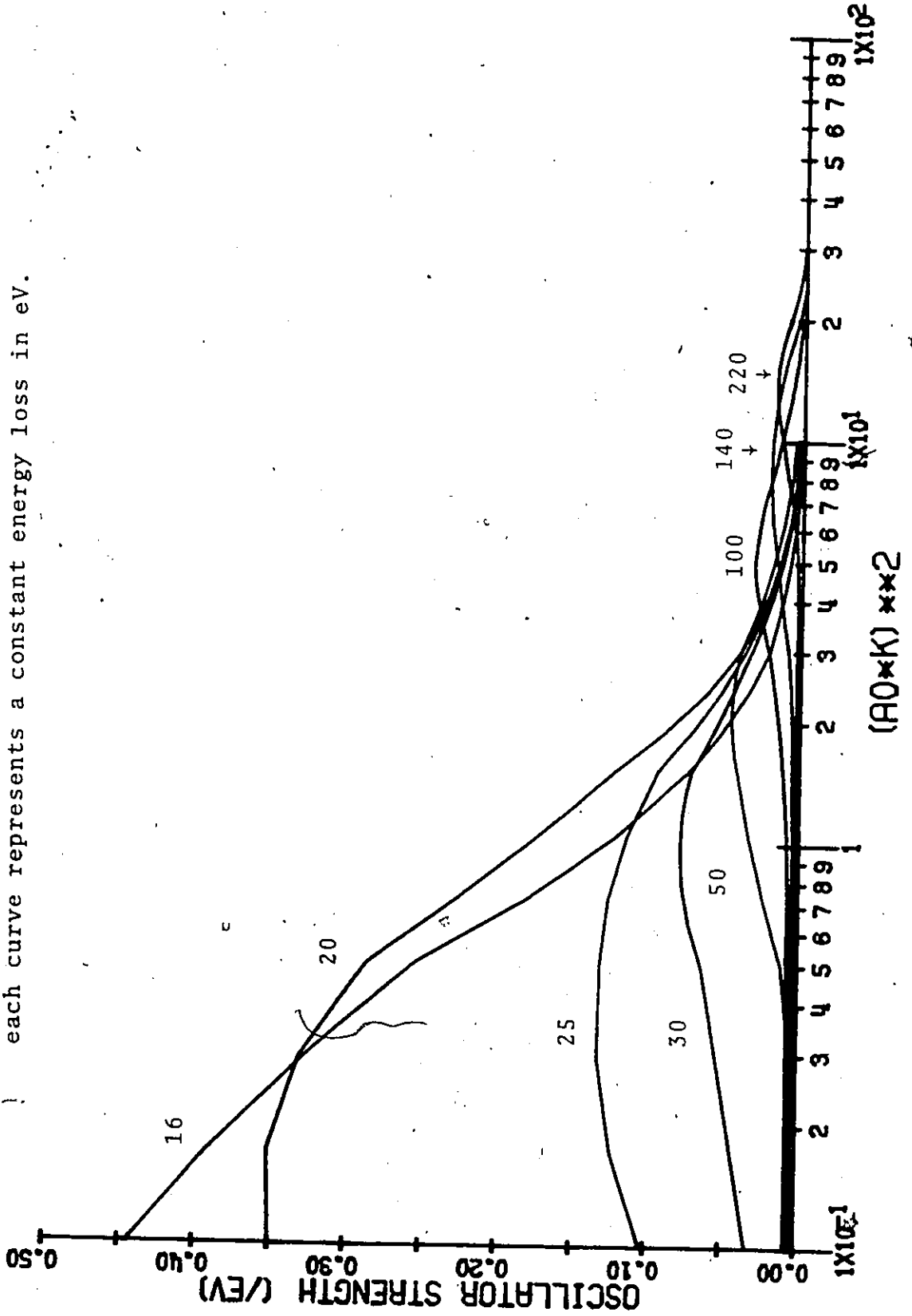
OSCILLATOR STRENGTH (/EV)

$(AO*K) **2$

0.50 0.40 0.30 0.20 0.10 0.00

$1X10^1$

$1X10^1$ $1X10^2$

16 20 25 30 50 100 140 220
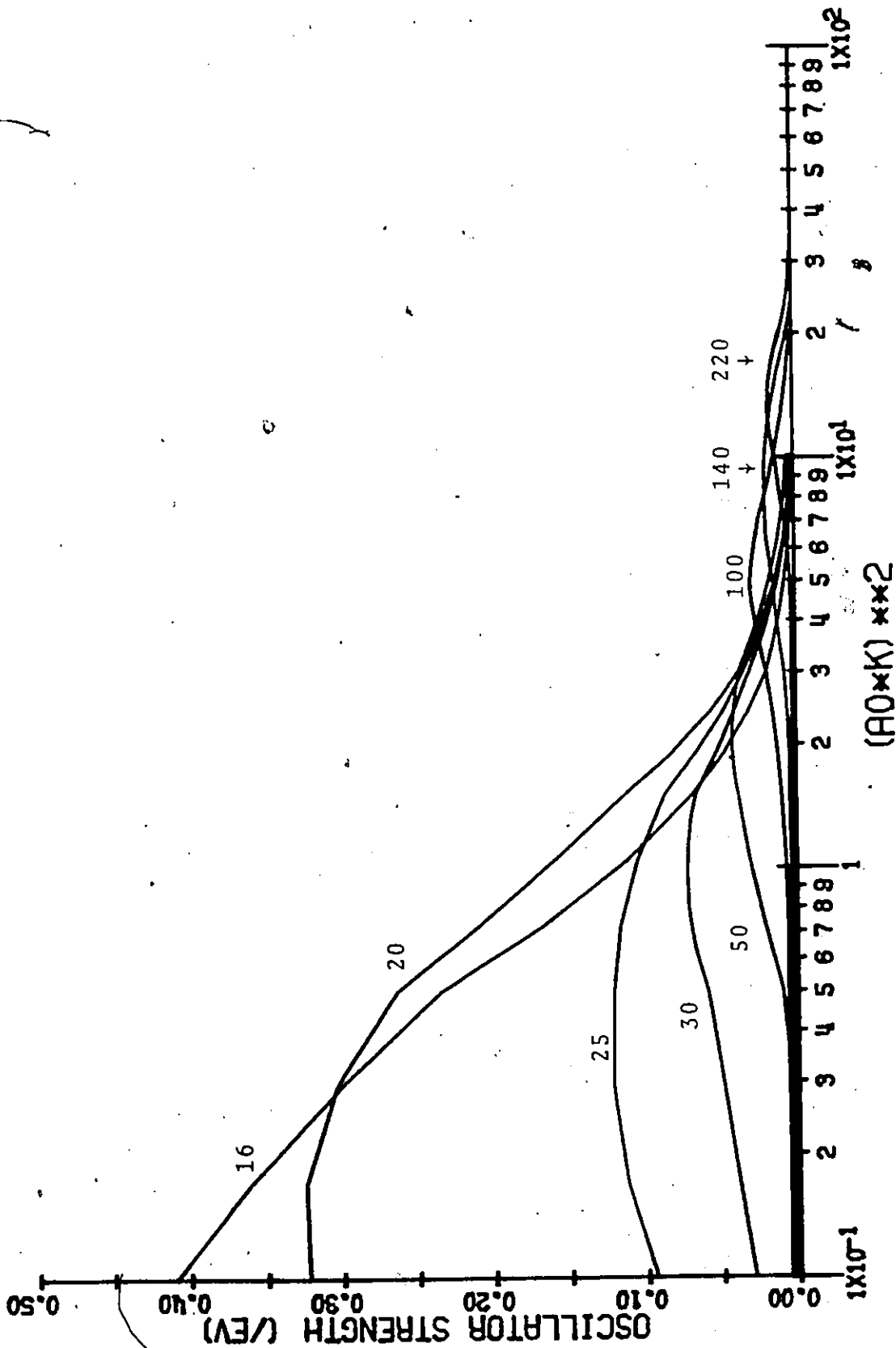
Figure VI-3: Electron Energy = 10 keV.
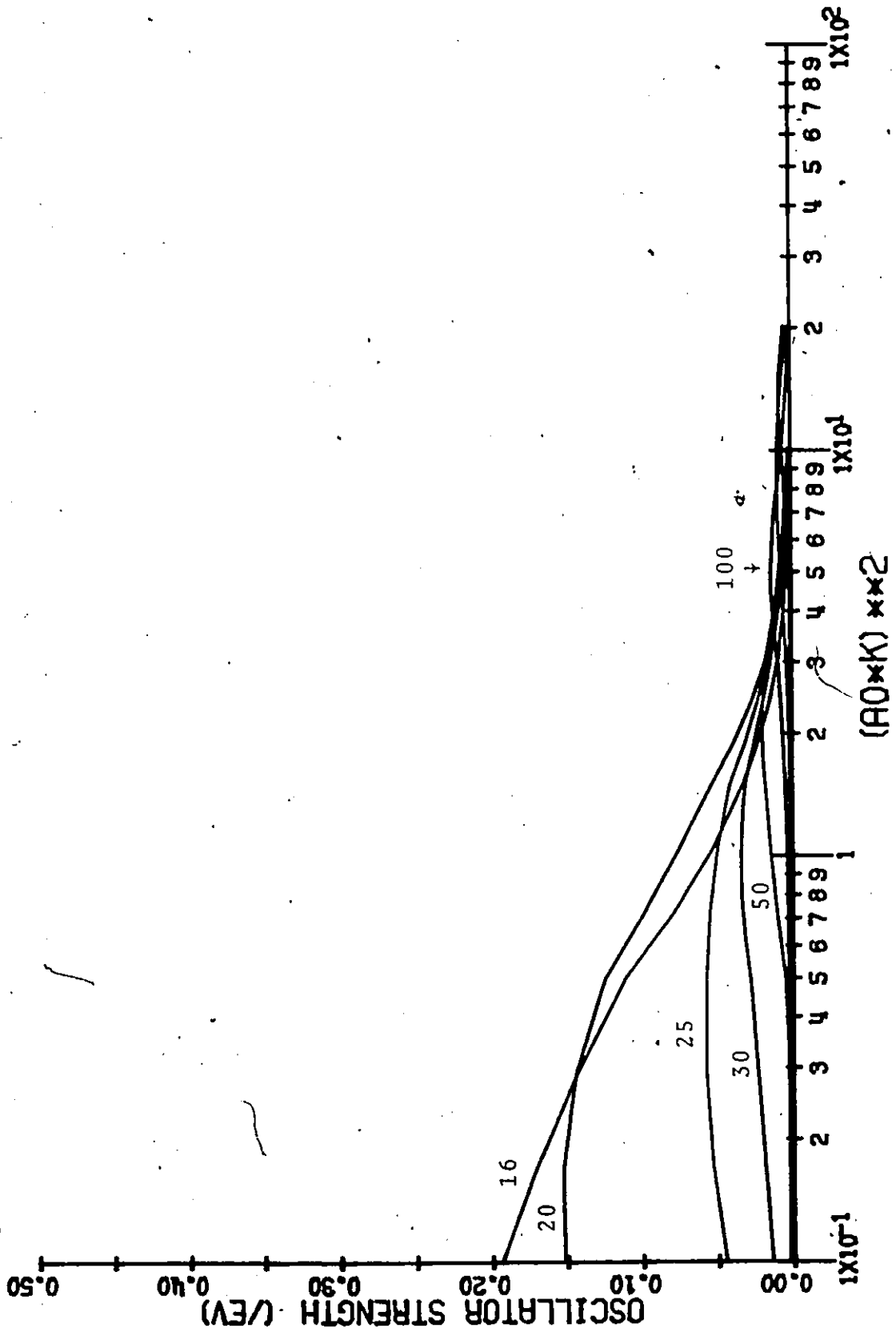
121

Figure VI-4: Electron Energy = 100 keV.

Figure VI-5: Electron Energy - 1 meV.
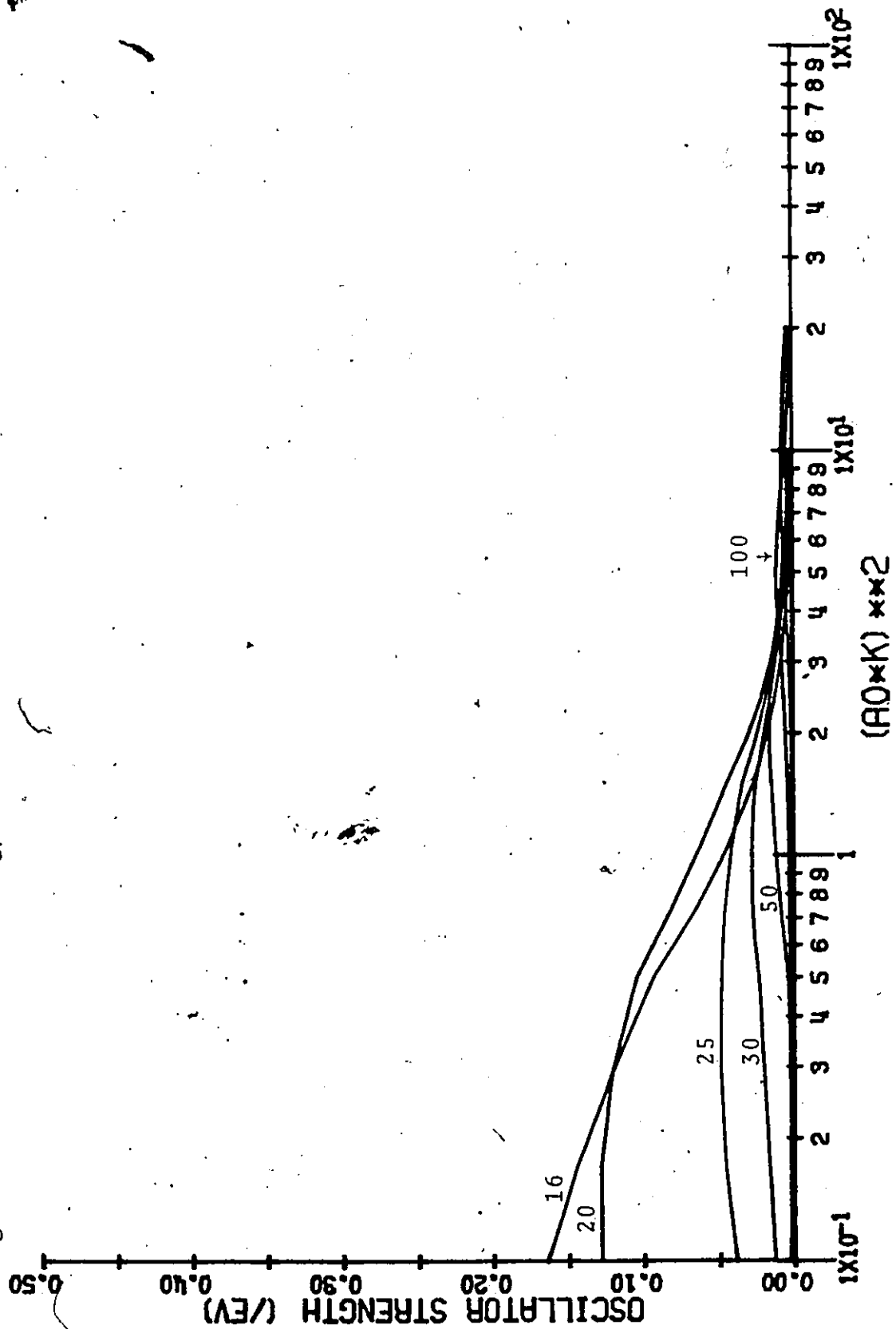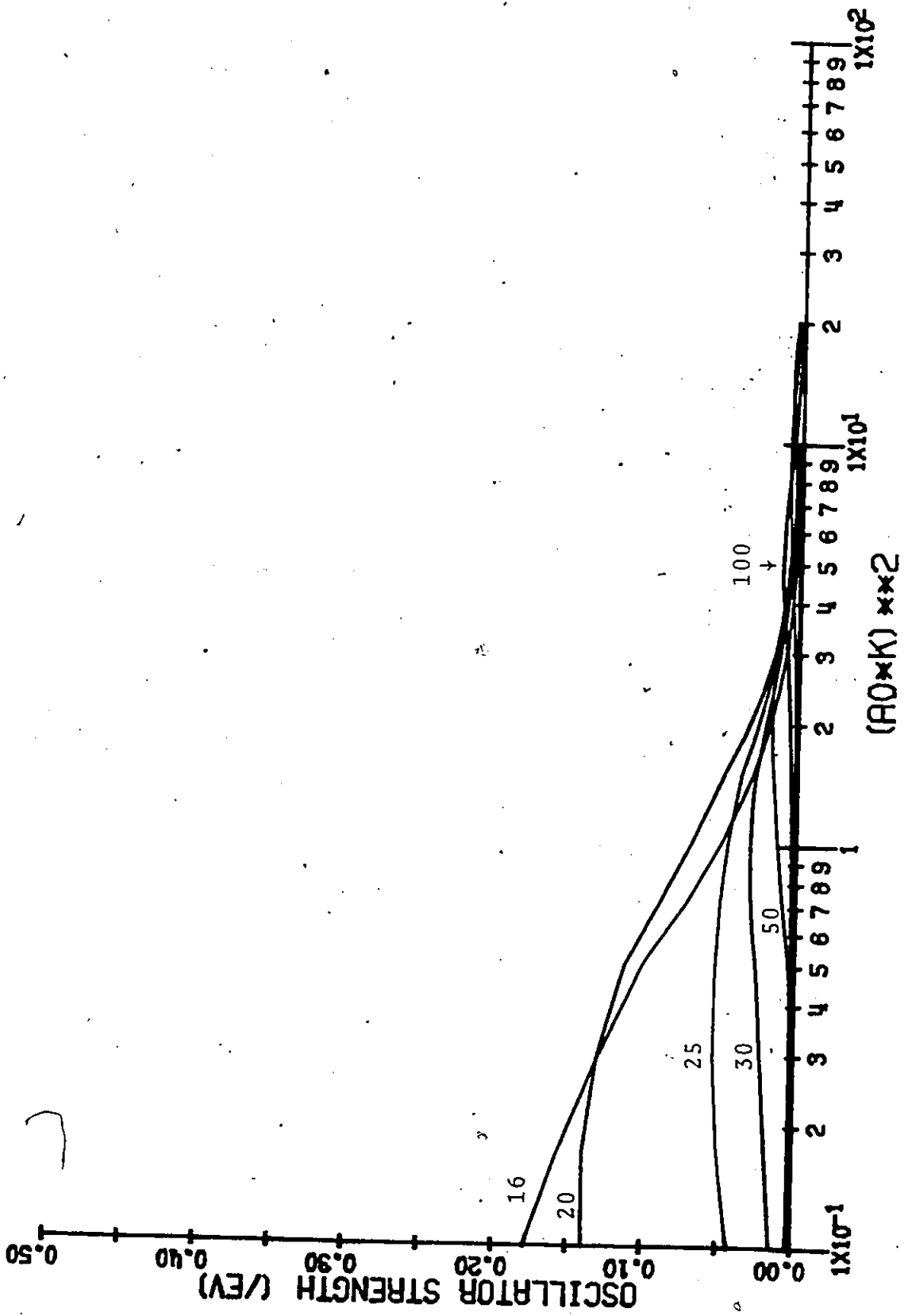
Figure VI-6: Electron Energy = 10 MeV.

124

$$\Delta[\ln(a_o K)^2] \approx (\frac{B}{W})^{1/2}$$

For small energy loss, relative to the binding energy
of the atomic electron, the Bethe ridge disappears and
the oscillator strength becomes a much more sensitive func-
tion of the wavefunction of the atomic electron. Compar-
ing Figures VI-2 through VI-6 it is apparent that the os-
cillator strength, and thus the total cross section, de-
creases with increasing incident electron energy. At
about 1 MeV, however, this trend reverses and the oscil-
lator strength increases again. This effect is called the
"relativistic rise" and is due to the interaction between
the incident electron and the atomic electron, through the
emission and reabsorption of virtual photons. As shown by
Fano[48,44] and by Rose[45], the Coulomb interaction, a matrix
element of $e^2/|\vec{r}_1 - \vec{r}_2|$, exerts a force parallel to the
momentum transfer vector, $\vec{K}$, and hence is called longitudinal
whereas the virtual photon interaction acts through "trans-
verse" photon fields perpendicular to $\vec{K}$. Emission of a
photon of momentum $\vec{K}$ by the incident electron and absorp-
tion of the same photon by the atomic electron is repre-
sented by the $\vec{\alpha}_1 \cdot \vec{\alpha}_2$ term in the Møller interaction de-
scribed previously. In the region of the relativistic
rise, the cross section does not continue to increase in-
definitely, but, rather, starts to decrease again as the
"density effect"[43,46], which involves the polarization
by the electron of the atoms of the gas through which it is
moving, becomes important.

The cross sections differential in energy, $\frac{d\sigma}{dW}$, computed using these Bethe surfaces are shown in Figure VI-7. The total ionization cross sections are shown in Figure VI-8 along with the results of some other investigations. The experimental data shown are the non-relativistic results of Van der Wiel, et al.[47], and of Schram, et al.[48], and the relativistic absolute cross sections measured by Rieke and Prepejchal[3]. The cross sections of Salop[49] were computed using Bethe's relativistic formula[6,14] and approximate non-relativistic matrix elements calculated with the projection operator method of Hahn and Watson[50, 51].

The low energy total cross sections calculated here agree very well with the experimental values, while the high energy cross sections differ somewhat from the experimental values. The computed total cross section for an incident electron energy of 10 MeV is 4.5×10^{-17} cm^2, which is about a factor of forty too large. The explanation for this involves the calculation of the relativistic form factor in the limit of small momentum transfer (photoeffect) and should be apparent in the following analysis due to Fano[11].

The total ionization cross section is given in terms of the relativistic form factor by equation (9) of Section II. As discussed by Bethe[5], the relativistic form factor can be approximately related to the non-relativistic form factor $|F(W,Q)|^2$ and the optical dipole matrix element
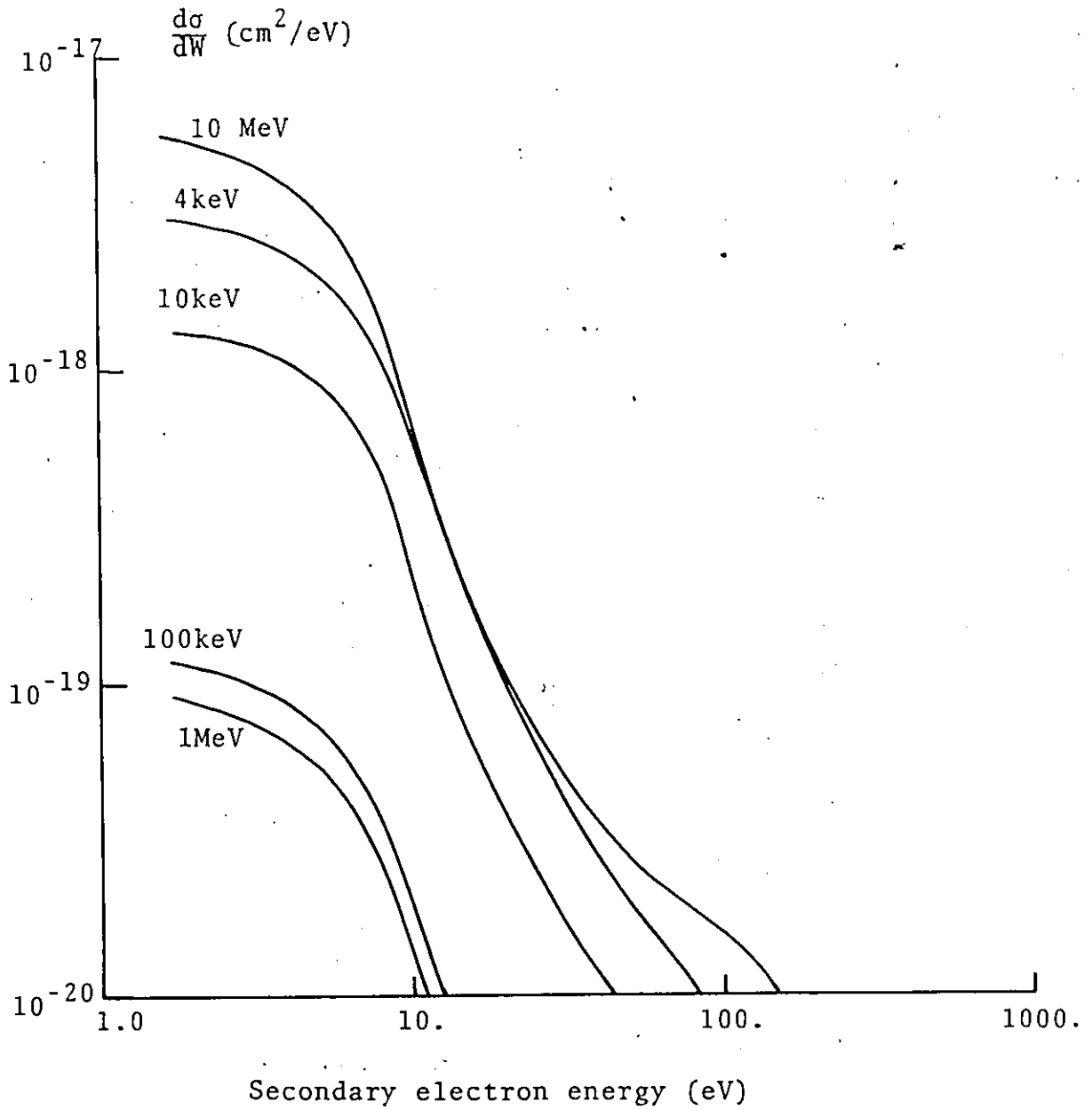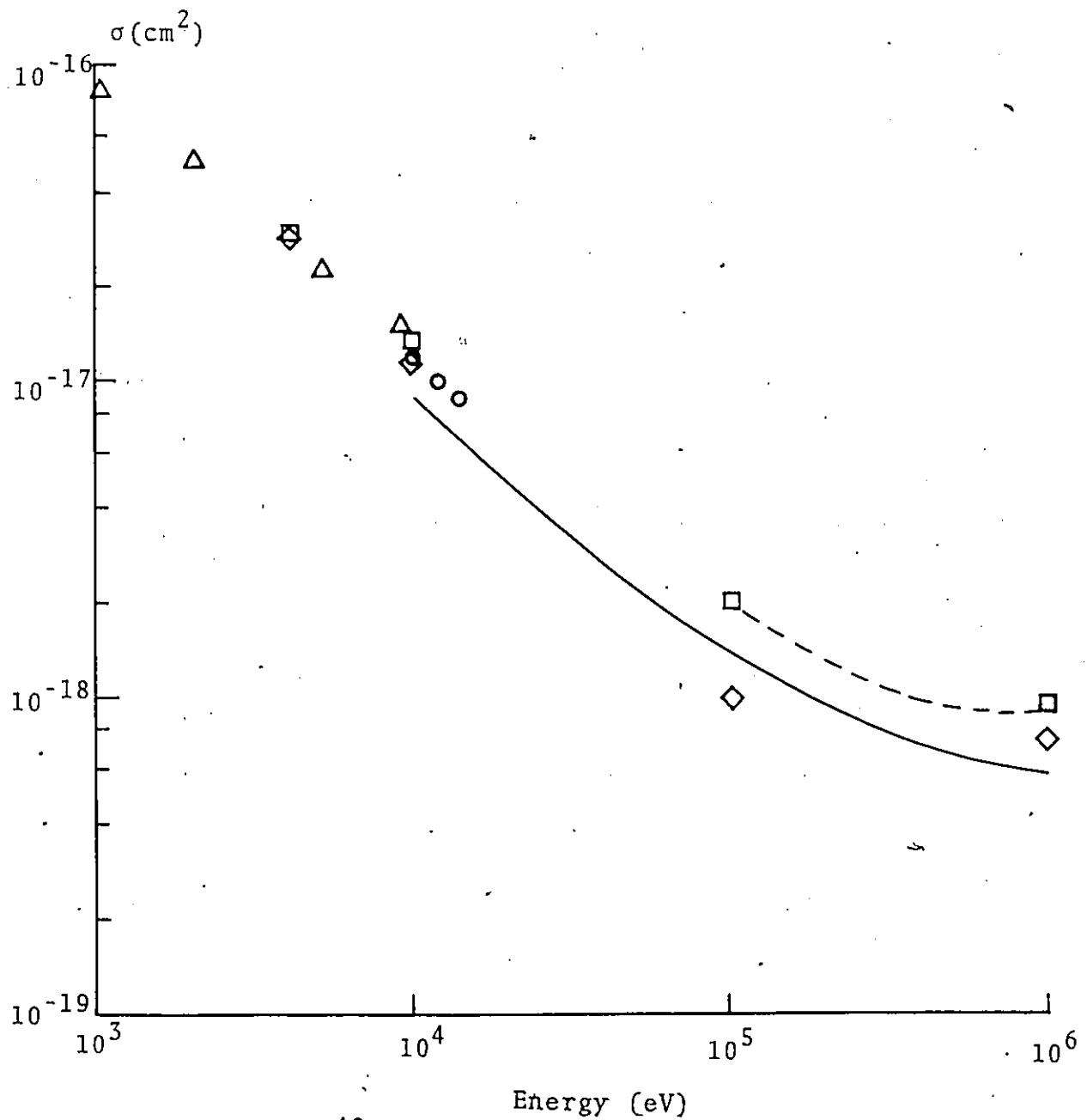
Figure VI-7:   Calculated Cross Section Differential in
Energy Loss for Ionization of Argon M_{III}.

Figure VI-8: Electron Impact Ionization Cross Sections for Argon.

squared, $|x(W)|^2$ by the following:

$$|\eta(W,Q)|^2 \simeq |F(W,Q)|^2 - |X(W)|^2 \frac{W^2(1-\beta^2)}{2mc^2 Ry} \qquad (2)$$

where $R \leq 13.605$ eV, the Rydberg. The integration limits, which are functions of incident electron energy, can be taken as

$$Q \min = \frac{W^2(1-\beta^2)}{2mc^2 Ry}$$

and

$$Q \max \simeq \infty$$

For allowed electric dipole collisions ($Q<<W$), $|F(W,Q)|^2$ has the form

$$|F(W,Q)|^2 \simeq \frac{Q}{Ry} |X(W)|^2$$

If the integration of $|F(W,Q)|^2$ is split into two parts at $Q = \frac{W^2}{2mc^2} << W$ and the integrals over Q of $|X(W)|^2$ are performed the following is obtained

$$\int_{Q\min}^{\infty} |\eta(W,Q)|^2 \frac{dQ}{Q^2} \simeq \frac{|X(W)|^2}{Ry} [\ln\left[\frac{\beta^2}{1-\beta^2}\right] - \beta^2] \qquad (3)$$

$$+ \int_{\frac{W^2}{2mc^2}}^{\infty} |F(W,Q)|^2 \frac{dQ}{Q^2}$$

The total cross section is then just $\frac{2\pi e^4}{\beta^2 mc^2}$ times the integral of (3) over energy loss, W. For low energy collisions, the dominant term in (3) is the integral involving the non-relativistic form factor. As β increases toward the limiting value of unity, however, the contribution from the term involving the optical dipole matrix element

increases and eventually becomes dominant. At relativistic
energies, then, the total cross section becomes sensitive
to the value of $|X(W)|^2$, which is proportional to the photo-
ionization cross section. As we have seen, however, these
form factor calculations are not very accurate in the small
K limit, particularly at the low values of energy loss
that contribute most to the total cross section. This then
explains the inaccuracies in the total cross section at
relativistic energies and in particular at 10 MeV.

As a test of this explanation the total ionization
cross section was calculated using equation (2) and the for
factor for 4 keV electrons computed here and the optical
dipole matrix elements squared from the photoionization
cross section data given by Samson[31]. The 4 keV form factor
was used because it was available from the electron impact
calculations presented above and because it is the most
non-relativistic of the form factors calculated. The re-
sults, also shown on Figure VI-8, can be seen to be much
better. The 10 MeV cross section computed in this manner
is 1.2×10^{-18} cm^2 , a marked improvement
over the 4.5×10^{-17} cm^2 value computed previously. It
thus appears that the best way to compute a relativistic
ionization cross section is to calculate the non-relativis-
tic form factor, obtain experimental photoionization data,
and use the formalism of Fano presented above.

VII. Conclusion

.As pointed out in the introduction, this is, to my knowledge, the first time that a complete relativistic electron impact ionization calculation has been performed using relativistic self-consistent atomic wavefunctions. The Bethe surface so computed reduces to the correct non-relativistic surface at low energy and exhibits the proper behavior due to relativistic effects at high energy. These effects which are due to electron-electron interactions via transverse virtual photons and are responsible for the rise in the cross section at high energy, are implicit in the relativistic theory. They are naturally included via the $\vec{\alpha}\cdot\vec{u}_i\vec{\alpha}\cdot\psi_i$ terms in the Møller interaction which mix large and small components of the wavefunctions. At relativistic energies the small components of plane wavefunctions are large enough for these terms to make a sizeable contribution to the interaction energy. These interactions are not present in the non-relativistic theory so that explicit multiplying factors involving electron velocity must be used when applying non-relativistic matrix elements to relativistic collisions, as in the Fano theory presented above. However, these calculations exhibit the correct relativistic effects qualitatively, but their quantitative accuracy suffers from the problems inherent in small momentum transfer (photoionization limit) calculations. A recent study by Robb et als[52] shows that even in the relatively simple case of helium,

130

correlation effects in both the initial and final states have a large effect on the photoionization cross-section. The correct treatment in this case, which would involve consideration of many body effects, is not a simple matter in the relativistic theory because, as has been pointed out previously, there is no known method of dealing with many body interactions in the relativistic quantum theory in closed form. In this sense, these calculations are difficult to improve upon. The relativistic calculation described here works reasonably well up to about 1 MeV incident electron energy, but then begins to break down due to an inadequate representation of the photoionization cross-section near threshold. The best approach above 1 MeV appears to be the semi-empirical method which incorporates the experimental photoionization cross section near the threshold as described at the end of the preceding section. They could be expanded, however, to investigate other relativistic effects such as spin flip by the incident electron due to the spin-orbit interaction, which is automatically included in the relativistic theory.

It would be interesting and useful to apply this scattering calculation to the ionization of, say, the K-shell of a heavy atom, where the relativistic nature of the inner shell atomic electron is particularly important. This calculation has never been performed, but as has been pointed out by others[4,52], would be desirable.

References

1. W. L. Morgan, "A Study of the Plasma Chemistry of the Argon Oxide Laser," RIES Report #75-109, Wayne State University (October 1975).

2. L. R. Peterson and J. E. Allen, J. Chem Phys, $\underline{56}$, 6068 (1972).

3. F. F. Rieke and W. Prepejchal, Phys. Rev., $\underline{A6}$, 1507 (1972).

4. M. Inokuti, Rev. Mod. Phys., $\underline{43}$, 297 (1971).

5. H. Bethe, in "Handbuch der Physik," ed. H. Geiger and K. Scheel, $\underline{24/1}$, 273 (Springer, Berlin, 1933).

6. L. I. Schiff, "Quantum Mechanics," (McGraw-Hill, New York, 1968).

7. A. I. Akhiezer and V. B. Berestetskii, "Quantum Electrodynamics" (Wiley Interscience, New York, 1965).

8. C. Møller, Z. Phys., $\underline{70}$, 786 (1931); Ann. Phys., $\underline{14}$, 531 (1932).

9. L. Armstrong and S. Feneville, "Relativistic Effects in the Many Electron Atom," in Advances in Atomic and Molecular Physics, ed. D. R. Bates, $\underline{10}$, 1 (Academic Press, New York, 1974).

10. H. S. Perlman, Proc. Phys. Soc., $\underline{76}$, 623 (1960).

11. U. Fano, Phys. Rev., $\underline{95}$, 1198 (1954).

12. W. F. Miller and R. I. Platzman, Proc. Phys. Soc. (London), $\underline{A70}$, 299 (1957).

13. U. Fano and J. W. Cooper, Rev. Mod. Phys., $\underline{40}$, 441 (1968).

14. A. Messiah, "Quantum Mechanics," Vol. II (Wiley, New York, 1968).

15. D. M. Brink and G. R. Satchler, "Angular Momentum" (Clarendon Press, Oxford, 1968).

16. Note that the $f(r)$ defined here is the negative of that used in reference (7).

17. Dr. Chien-ping Lin private communication.

18. D. R. Hartree, "The Calculation of Atomic Structures" (Wiley, New York, 1957).

19. J. C. Slater, "Quantum Theory of Atomic Structures," Vol. II (McGraw-Hill, New York, 1960).

20. F. Herman and S. Skillman, "Atomic Structure Calculations" (Prentice-Hall, Englewood Cliffs, N.J., 1963).

21. I. P. Grant, Advances in Physics, $\underline{19}$, 747 (1970).

22. S. Cohen, Phys. Rev., $\underline{118}$, 489 (1960).

23. D. A. Liberman, D. T. Cromer, J. T. Waber, Comp. Phys. Comm., $\underline{2}$, 107 (1971).

24. T. C. Tucker, et al., Phys. Rev., $\underline{178}$, 998 (1969).

25. J. A. Bearden and A. F. Burr, Rev. Mod. Phys., $\underline{45}$, 273 (1973).

26. IBM Scientific Subroutine Package.

27. J. W. Cooper, Phys. Rev., $\underline{128}$, 681 (1962).

28. R. H. Pratt, A. Ron, H. K. Tseng, Rev. Mod. Phys., $\underline{45}$, 273 (1973).

29. J. J. Sakurai, "Advanced Quantum Mechanics" (Addison-Wesley, Reading, Mass., 1967).

30. S. T. Manson, Phys. Rev., $\underline{A5}$, 668 (1972).

31. J. A. R. Samson, "The Measurement of Photoionization Cross Sections of Atomic Gases," in Advances in Atomic and Molecular Physics, ed. D. R. Bates, $\underline{2}$, (Academic Press, N.Y., 1966).

32. J. W. Cooper, Phys. Rev. Lett., $\underline{13}$, 762 (1964).

33. E. J. McGuire, Phys. Rev., $\underline{175}$, 20 (1968).

34. S. T. Manson and J. W. Cooper, Phys. Rev., $\underline{165}$, 126 (1968).

35. W. Brandt, L. Eder, S. Lundquist, J.Q.S.R.T., $\underline{1}$, 185 (1967).

36. M. Y. Amus'ya, et al., Phys. Lett., $\underline{24A}$, 394 (1967).

37. M. Y. Amus'ya, et al., Phys. Lett., $\underline{24A}$, 541 (1967).

38. I. P. Grant, J. Phys. B., $\underline{7}$, 1458 (1974).

39. V. V. Afrosimov, et al., Sov. Phys. JETP, $\underline{28}$, 821 (1969).

40. N. F. Mott and H. S. W. Massey, "The Theory of Atomic Collisions" (Clarendon Press, Oxford, 1965).

41. M. R. H. Rudge, Rev. Mod. Phys., $\underline{40}$, 564 (1968).

42. M. Y. Amus'ya, et al., Sov. Phys. JETP, $\underline{31}$, 332 (1970).

43. U. Fano, Phys. Rev., $\underline{102}$, 385 (1956).

44. U. Fano, Ann. Rev. Nucl. Sci., $\underline{13}$, 1 (1963).

45. M. E. Rose, "Relativistic Electron Theory" (Wiley, N.Y., 1961).

46. J. D. Jackson, "Classical Electrodynamics" (Wiley, N.Y., 1962).

47. M. J. Van der Wiel, et al., Physica, $\underline{42}$, 411 (1969).

48. B. L. Schram, et al., Physica, $\underline{31}$, 94 (1964).

49. A. Salop, Phys. Rev., $\underline{A9}$, 2496 (1974).

50. Y. Hahn and K. M. Watson, Phys. Rev., $\underline{A6}$, 548 (1972).

51. Y. Hahn and K. M. Watson, Phys. Rev., $\underline{A2}$, 491 (1973).

52. W. D. Robb, S. P. Rountree and T. Burnett, Phys. Rev., $\underline{A11}$, 1193 (1975).

53. C. B. O. Mohr, "Relativistic Inner Shell Ionization," in Advances in Atomic and Molecular Physics, Vol. 4, ed. D. R. Bates (Academic Press, New York, 1968).

<center>Vita Auctoris</center>

<center>William Lowell Morgan</center>

Born: September 27, 1946

Education

1964:   Clarence M. Kimball High School, Royal Oak, Michigan.

1969:   B.S.E. (Physics) and B.S.E. (Science Engineering),
        The University of Michigan, Ann Arbor, Michigan.

1972:   M.A. (Physics), Wayne State University, Detroit,
        Michigan.

1976:   Ph.D. (Physics), The University of Windsor, Windsor,
        Ontario, Canada.

Employment

1968-1974:   Research Assistant, The University of Michigan
             Institute of Science and Technology, Willow
             Run Laboratories.

1972-1976:   Research Assistant, Research Institute for
             Engineering Sciences, College of Engineering,
             Wayne State University.

Summer,   Physicist, University of California, Lawrence
1973-1974   Livermore Laboratory, Laser Fusion Division.

1975-1976:   Teaching Assistant, The University of Windsor,
             Department of Physics.

Professional and Honorary Societies

American Physical Society

Sigma Xi

<center>135</center>